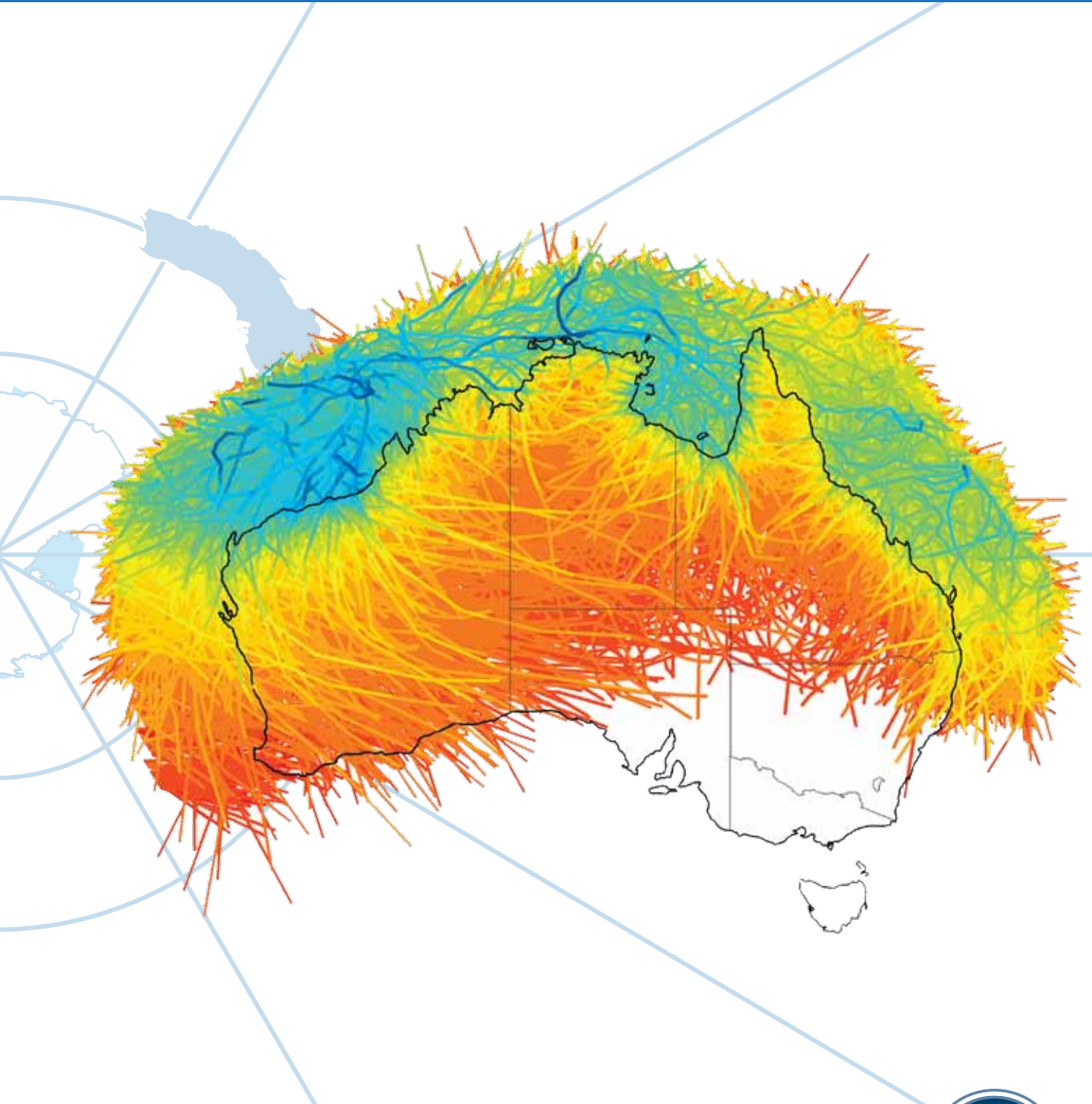


TECHNICAL REPORT

Estimating present day extreme total water level exceedance probabilities around the coastline of Australia



Prepared by Ivan D. Haigh, E.M.S. Wijeratne, Leigh R. MacPherson, Matthew S. Mason, Charitha B. Pattiaratchi, Ryan P. Crompton, S George Antarctic Climate and Ecosystems Cooperative Research Centre 2012

ANTARCTIC CLIMATE
& ECOSYSTEMS CRC

Technical Report: Estimating Present Day Extreme Total Water Level Exceedance Probabilities Around the Australian Coastline

Prepared by: Ivan D Haigh^{1,2}, E M S Wijeratne¹, Leigh R MacPherson¹, Matthew S Mason³, Charitha B Pattiaratchi¹, Ryan P Crompton³, S George⁴

¹School of Environmental Systems Engineering and UWA Oceans Institute, The University of Western Australia, M470, 35 Stirling Highway, Crawley, WA 6009, Australia

²National Oceanography Centre, University of Southampton, Waterfront Campus, European Way, Southampton, SO16 3HZ, UK.

³Risk Frontiers, National Hazards Research Centre, Macquarie University, NSW 2109, Australia.

⁴Antarctic Climate and Ecosystems Cooperative Research Centre, University of Tasmania, Private Bag 80, Hobart, Tasmania 7001, Australia

ISBN: 978-0-9871939-2-6

TR_STM05_120620



THE UNIVERSITY OF
WESTERN AUSTRALIA
Achieving International Excellence



While the Antarctic Climate & Ecosystems Cooperative Research Centre (ACE) takes reasonable steps to ensure that the information in this document is correct, ACE provides no warranty, guarantee or representation that information provided on this document is accurate, complete or up-to-date. In particular, to the maximum extent permitted by law, no warranty regarding non-infringement, security accuracy, fitness for a particular purpose or freedom from errors is given in relation to this report and its contents. The use of this report is entirely at your own risk.

To the maximum extent permitted by law ACE, its officers, employees, contractors and agents exclude all liability for any loss, damage, liability, costs or expenses whatsoever whether direct, indirect, or consequential including loss of profits, opportunity or loss suffered by you or claims against you in connection with the use of this report.

Before relying on material contained on this report, users should carefully evaluate its accuracy, currency, completeness and relevance for their purposes, and should obtain any appropriate professional advice relevant to their particular circumstances. ACE does not accept any responsibility or liability for any actions taken as a result of, or in reliance on, information in this report.

© Antarctic Climate & Ecosystems Cooperative Research Centre 2012

This work is copyright. It may be reproduced in whole or in part for study or training purposes subject to the inclusion of an acknowledgement of the source, but not for commercial sale or use. Reproduction for purposes other than those listed above requires the written permission of the Antarctic Climate & Ecosystems Cooperative Research Centre.

Citation: Haigh ID, Wijeratne EMS, MacPherson LR, Mason MS, Pattiaratchi CB, Crompton RP & George S 2012, Estimating Present Day Extreme Total Water Level Exceedance Probabilities Around the Coastline of Australia, Antarctic Climate & Ecosystems Cooperative Research Centre, Hobart, Tasmania.

Requests and enquiries concerning reproduction rights should be addressed to:

Ms Miranda Harman
Media and Communications Manager
Antarctic Climate & Ecosystems
Cooperative Research Centre
Private Bag 80
Hobart Tasmania 7001
Tel: +61 3 6226 7888
Fax: +61 3 6226 2440
Email: enquiries@acecrc.org.au
www.acecrc.org.au

Established and supported under the Australian Government's Cooperative Research Centres Program

Additional funding support gratefully acknowledged from:



ANTARCTIC CLIMATE
& ECOSYSTEMS CRC



An Australian Government Initiative



Australian Government
Department of Climate Change
and Energy Efficiency



Government of Western Australia
Department of Transport



Australian Government
Department of Sustainability, Environment,
Water, Population and Communities
Australian Antarctic Division



Australian Government
Department of Climate Change
and Energy Efficiency

NIWA
Taihoro Nukurangi



The ACE CRC is a unique collaboration between its core partners the Australian Antarctic Division; CSIRO; University of Tasmania; the Australian Government's Department of Climate Change and Energy Efficiency; the Alfred Wegener Institute for Polar and Marine Research (Germany); and the National Institute of Water and Atmospheric Research Limited (New Zealand) and a consortium of supporting partners.

Table of contents

| | |
|--|-----------|
| Table of contents | 1 |
| List of figures | 3 |
| List of tables | 5 |
| Summary | 6 |
| | |
| 1 Introduction | 8 |
| | |
| 2 Background | 9 |
| | |
| 3 Stage 1: Tides, extra-tropical surges and mean sea level | 14 |
| 3.1 <i>Model configuration</i> | 14 |
| 3.2 <i>Model validation</i> | 16 |
| 3.2.1 Tidal component | 18 |
| 3.2.2 Storm surge component | 18 |
| 3.2.3 Mean sea level component | 20 |
| 3.2.4 Total water levels | 23 |
| 3.3 <i>Water level exceedance probabilities</i> | 23 |
| | |
| 4 Stage 2: Tropical cyclone-induced surges | 28 |
| 4.1 <i>Analysis of tide-gauge observations</i> | 28 |
| 4.2 <i>Model validation and sensitivity tests</i> | 29 |
| 4.2.1 Event selection | 29 |
| 4.2.2 Wind field model description and validation | 30 |
| 4.2.3 Storm surge validation | 31 |
| 4.2.4 Sensitivity testing | 32 |
| 4.3 <i>Storm surge simulation of 10,000 years of synthetic tropical cyclones</i> | 33 |
| 4.3.1 Synthetic tropical cyclone database | 33 |
| 4.3.2 Hydrodynamic simulations | 36 |
| 4.4 <i>Water level exceedance probabilities</i> | 37 |

| | | |
|----------|---------------------------|-----------|
| 5 | Concluding remarks | 40 |
| 6 | Acknowledgments | 44 |
| 7 | References | 45 |
| | Tables | 54 |
| | Figures | 62 |

List of figures

| | |
|--|----|
| Figure 1: Location of tide gauge sites around the coastline of Australia with high frequency (at least hourly) water level records longer than 30 years. Note: Milner Bay does not have 30 years of data but has been included so that there is a validation site in the Gulf of Carpentaria. | 63 |
| Figure 2: Hydrodynamic model grid and bathymetry configured in Mike21 FM. | 63 |
| Figure 3: NCEP/NCAR mean sea level pressure fields and 10 m wind vectors every 12 hours for a large extra-tropical storm event in May 2003. | 64 |
| Figure 4: Comparison of the measured and predicted amplitudes of the 8 main tidal constituents for the 30 validation sites for 1995. | 65 |
| Figure 5: Comparison of the measured and predicted phases of the 8 main tidal constituents for the 30 validation sites for 1995. | 66 |
| Figure 6: Comparison of the measured (blue) and predicted (red) surge component for 1995 at select sites around southern Australia. | 67 |
| Figure 7: Comparison of the measured (blue) and predicted (red) surge component at Thevenard for the period 1995 to 1999. | 68 |
| Figure 8: Time-series of the annual root mean square error (RMSE), standard deviation error (STD) and correlation coefficient (Corr Coef) between the measured and predicted storm surge component at Fremantle over the 61-year hindcast period. | 69 |
| Figure 9: (a) Mean range in the seasonal mean sea level cycle; and (b) Month during which the seasonal mean sea level cycle is largest. | 70 |
| Figure 10: Comparison of the measured (blue) and predicted (red) total water level (a) frequency distribution and (b) cumulative frequency distribution curves for Albany, Port Lincoln, Burnie and Newcastle. | 71 |
| Figure 11: Comparison of the measured (blue) and predicted (red) return period curves for 2010 (relative to AHD) at the 30 validation sites estimated using the AMM fitted to a GEV distribution. | 72 |
| Figure 12: Return period curves for 2010 (relative to AHD) estimated using the AMM fitted to a GUM and GEV distribution and the RLM fitted to a GEV distribution, derived from the measured sea level data at (a) Geraldton and (b) Fort Denison. The maximum-recorded water level has been plotted against the length of the record (i.e. 40 years) and is shown as a green square. | 73 |
| Figure 13: 100-year total water return levels for 2010 (relative to m AHD) at the model coastal grid points estimated using the AMM fitted to a GUM distribution. The estimates from the tide gauge records are also shown (circles). | 74 |
| Figure 14: The tracks of the ten largest tropical cyclone-induced surge events that made it into the top 100 largest surge events identified at each study tide gauge site. | 75 |
| Figure 15: Measured and predicted wind speed, direction and atmospheric pressure time-series for (top to bottom) Arlington Reef, Flinders Reef, Lucinda Point and Townsville meteorological stations during the passage of tropical cyclone Yasi in Feb 2011. | 76 |
| Figure 16: Tropical cyclone tracks for Althea, Rosita and Yasi. | 77 |

-
- Figure 17: Comparisons between the measured (blue) and predicted (red) surge time-series at (a) Townsville for cyclone Althea and (b) Broome for cyclone Rosita. 77
- Figure 18: Comparisons between the measured (blue) and predicted (red) surge time-series for cyclone Yasi at four tide gauges in Queensland. Each time series has been arbitrary offset for presentation purposes. 78
- Figure 19: Tide-surge interaction at Townsville associated with tropical cyclone Althea. (a) Total water levels for the four different tidal states; (b) surge levels for the four different tidal states and surge only simulation; (c) surge levels for the four different tidal states and surge only simulation, but re-adjusted for the time offset. 79
- Figure 20: Tide-surge interaction at Broome associated with tropical cyclone Rosita. (a) Total water levels for the four different tidal states; (b) surge levels for the four different tidal states and surge only simulation; (c) surge levels for the four different tidal states and surge only simulation, but re-adjusted for the time offset. 80
- Figure 21: Synthetic tropical cyclone tracking (hatched) and genesis and tracking (cross-hatched) domains. Wind statistics validation locations also shown. 81
- Figure 22: Measured (dot) and predicted (line) wind speed return period curves for 2010 at select locations around the Australian coastline. Local wind speed adjustments are applied to the predicted data. 82
- Figure 23: (a) Observed tropical cyclone tracks for the 39 year period between 1970 and 2008; (b) Synthetic tropical cyclone tracks for a 39-year period; and (c) Synthetic tropical cyclone tracks for a 1,000 year period. 83
- Figure 24: 1,000-year surge return levels for 2010 (relative to AHD) at the model coastal grid points estimated in (a) stage 1 and (b) stage 2 (tropical cyclones). 84
- Figure 25: Return periods (years) at which the tropical cyclone generated surges are larger than the extra-tropical generated surges at the model coastal grid points. 85
- Figure 26: 1,000-year total water return levels for 2010 (relative to AHD) at the model coastal grid points estimated in (a) stage 1 and (b) stage 2 (i.e. tropical cyclones). 86
- Figure 27: Comparison of the return period curves for 2010 (relative to AHD) for stage 1 (blue) and stage 2 (red) at the 30 validation sites. 87
- Figure 28: Return periods (years) at which the tropical cyclone generated total water levels are larger than the extra-tropical generated total water levels at the model coastal grid points. 88
- Figure 29: Combined (from stages 1 and stage 2) 1,000-year total water return levels for 2010 (relative to m AHD) at the model coastal grid points. 89

List of tables

| | |
|---|----|
| Table 1: Key parameterizations used in the Mike21 model. | 55 |
| Table 2: Details of the tide gauge records used for model validation. | 56 |
| Table 3: Mean absolute amplitude and phase errors of the main eight tidal constituents, estimated from the measured and predicted datasets, for the 30 validation sites. The numbers in brackets are the mean absolute differences between the measured and TPOX7.2 global ocean tidal model for the 30 validation sites. | 57 |
| Table 4: Root mean square errors (RMSE), mean standard deviation errors (STD) and correlation coefficients for the hourly mean sea level (MSL), astronomical tide, surge and total water levels for 1995, at the 30 validation sites. | 58 |
| Table 5: Comparison of the 10-, 50- and 100-year measured and predicted return levels for 2010 (relative to m AHD) estimated using the AMM fitted to the GEV distribution, at the 30 validation sites. | 59 |
| Table 6: Largest recorded storm surge events, ranked in order of surge height, resulting from a tropical cyclone at 17 of the study tide-gauge sites. | 60 |
| Table 7: Details of the tropical cyclones used for model validation. | 61 |

Summary

The occurrence of extreme water level events along low-lying, highly populated and/or developed coastlines can lead to devastating impacts on coastal infrastructure. Therefore it is very important that the probabilities of extreme water levels are accurately evaluated to inform flood and coastal management and for future planning. The aim of this study was to provide estimates of present day extreme total water level exceedance probabilities around the whole coastline of Australia, arising from combinations of mean sea level, astronomical tide and storm surges generated by both extra-tropical and tropical storms, but exclusive of surface gravity waves.

The study has been undertaken in two main stages. In the first stage, a high-resolution (~10 km along the coast) hydrodynamic depth averaged model has been configured for the whole coastline of Australia using the Danish Hydraulics Institute's Mike21 modelling suite of tools. The model has been forced with astronomical tidal levels, derived from the TPX07.2 global tidal model, and meteorological fields, from the US National Center for Environmental Prediction's global reanalysis, to generate a 61-year (1949 to 2009) hindcast of water levels. This model output has been validated against measurements from 30 tide gauge sites around Australia with long records. At each of the model grid points located around the coast, time series of annual maxima and the several highest water levels for each year were derived from the multi-decadal water level hindcast and have been fitted to extreme value distributions to estimate exceedance probabilities.

Stage 1 provided a reliable estimate of the present day total water level exceedance probabilities around southern Australia, which is mainly impacted by extra-tropical storms. However, as the meteorological fields used to force the hydrodynamic model only weakly include the effects of tropical cyclones the resultant water levels exceedance probabilities were underestimated around western, northern and north-eastern Australia at higher return periods. Even if the resolution of the meteorological forcing was adequate to represent tropical cyclone-induced surges, multi-decadal periods yielded insufficient instances of tropical cyclones to enable the use of traditional extreme value extrapolation techniques. Therefore, in the second stage of the study, a statistical model of tropical cyclone tracks and central pressures was developed using historic observations. This model was then used

to generate synthetic events that represented 10,000 years of cyclone activity for the Australia region, with characteristics based on the observed tropical cyclones over the last ~40 years. Wind and pressure fields, derived from these synthetic events using analytical profile models, were used to drive the hydrodynamic model to predict the associated storm surge response. A random time period was chosen, during the tropical cyclone season, and astronomical tidal forcing for this period was included to account for non-linear interactions between the tidal and surge components. For each model grid point around the coast, annual maximum total levels for these synthetic events were calculated and these were used to estimate exceedance probabilities. The exceedance probabilities from stages 1 and 2 were then combined to provide a single estimate of present day extreme water level probabilities around the whole coastline of Australia.

1 Introduction

The occurrence of extreme water level events along low-lying, highly populated and/or developed coastlines can lead to devastating impacts on coastal infrastructure (Lowe et al., 2010). The incidence of major storm surges in the last decade (i.e. those arising from hurricanes Katrina, Sidr, Nargis and Irene, or in the case of Australia, cyclone Yasi), have dramatically emphasized the destructive capabilities of extreme water level events (Menéndez and Woodworth, 2010).

Throughout history, coastal settlers have had to adapt to periodic coastal flooding. However, as a society we have become increasingly vulnerable to extreme water level events as our cities and our patterns of coastal development become more intricate, populated and interdependent (Pugh, 2004; Nicholls et al., 2007). In addition to this, there is now a real and growing concern about rising sea levels. Over the last 150 years, global sea levels have on average risen by about 25 cm (Bindoff et al., 2007) and it is predicted that this rise will continue over the 21st century (and beyond) at an accelerated rate (Meehl et al., 2007). With rises in sea level, given water levels will be exceeded more and more frequently as progressively less severe storm conditions are required to achieve that water level (Haigh et al., 2011a). In some coastal regions, extreme water levels could be amplified further by changes in storminess, such as more intense tropical cyclones, although there are still significant uncertainties regarding possible future changes in tropical and extra-tropical storm activity (Meehl et al., 2007; Seneviratne et al, 2012).

Therefore it is very important that the exceedance probabilities of extreme water levels are accurately evaluated to inform flood and erosion risk-based management and for future planning. This report describes a study aimed at estimating present day extreme sea level exceedance probabilities due to tides, storm surges, tides and mean sea level (but exclusive of wind-waves) around the whole coastline of Australia.

2 Background

In coastal flood and erosion risk management, the concepts of average recurrence intervals (ARI) or annual exceedance probabilities (AEP) are commonly used to convey information on the likelihood of rare events such as extreme water levels (Coles, 2001). ARI, also known as return periods, are an estimate of the average interval of time between events of a certain magnitude. The AEP is the probability that an event of a certain magnitude will occur in a particular year. These statistical concepts are often used to define design conditions for flood defences and other coastal and offshore structures. Ensuring they are accurately estimated is important to prevent catastrophic structure failures due to under-design or expensive wastes due to over-design.

Traditionally, ARI and AEP for high water levels have been calculated from tide-gauge measurements. However, there are two problems with this approach: (i) as a minimum ~30 years of measurements are required to produce accurate estimates using the conventional extreme value analysis statistical methods (Haigh et al., 2010a); and, (ii) the probabilities of extreme water levels caused by large tropical cyclones (which influence the western, northern and north-eastern coastline of Australia) cannot be estimated solely on the basis of tide gauge records (Harper et al., 2001).

In regards to the first issue, there are currently only 29 tide-gauge sites around Australia, the locations of which are shown in **Figure 1**, with records 30 years or longer. Extreme water levels arise as a combination of three main factors: mean sea level, astronomical tide and storm surge (Pugh, 2004) (Wind-waves can further elevate coastal sea levels (see O'Grady and McInnes, 2010) but their effect has not been considered in this study). The characteristics of these components vary significantly around the Australian coastline and hence the way in which they combine to generate high water levels differs for different parts of the coast. For example, the mean tidal range varies between about 0.5 and 10 m and the form (i.e. diurnal/semi-diurnal) of the tide also changes considerably around the coast (Pattiaratchi et al., in prep). In addition, the Australian coastline is subject to both tropical and extra-tropical cyclones. Further, the seasonal and inter-annual variations in mean sea level are large (up to 1 m) around parts of the coast and thus strongly influence the timing and magnitude of extreme events. Therefore, a simple interpolation of ARI

between the existing network of 29 tide-gauges will not accurately capture the spatial variation in extreme total water levels around the coast. More recent extreme value statistical methods have been introduced (see Haigh et al., 2010a) that allow water level ARI to be calculated using shorter tide-gauge records. However, even considering all of the shorter records from tide gauges located around the country would still not provide an adequate and uniform spatial map of water level ARI for the whole coastline of Australia.

The second issue is that the probabilities of extreme water levels caused by large tropical cyclones cannot be estimated solely on the basis of tide gauge records. In tide gauge records, even those covering many decades to a century, there are often only a few observations of large tropical-cyclone-induced water levels. It is relatively rare that a tropical cyclone will pass close to a tide gauge site to generate a significant extreme water level and in addition, the response of the generated high water level is complex, localized and dependent on the timing of the astronomical tide (Harper et al., 2001). Further, when a severe cyclone makes landfall near to the tide gauge station, the recorded water level can often be significantly higher than any other water level recorded in the past. Therefore, using the observational record only to make extrapolation to very low probabilities of occurrence is inadequate (McInnes et al., 2009).

Hydrodynamic numerical models can be used to overcome the first issue (i.e. poor spatial coverage of long observational data sets). Following the success of operational tide-surge modelling in many regions (Flather, 2000), hydrodynamic models have been used to improve understanding of water level characteristics. Until recently, majority of studies simulated water levels over a particular storm event or for a few tidal cycles (von Storch and Woth, 2008). It is only over the last decade that hydrodynamic models have been used to construct multi-decadal time series of historic total water levels (Lowe et al., 2010). Flather (1987) and Flather et al. (1998) were the first to estimate ARI continuously around a coastline (the UK), using individual simulations of several large storms and then multi-decadal hindcasts of water levels, respectively, created by driving a barotropic (two-dimensional depth averaged models) hydrodynamic model, validated against tide gauge measurements, with meteorological fields. Several other studies have produced multi-decadal hindcasts of water levels (i.e. Langenberg et al. (1999) and Weisse and Plüß (2006) for the North Sea; Bernier and Thompson (2006) for the North Atlantic; Sebastiao

et al. (2008) for the Atlantic coast of Europe; and, McMillan et al. (2011) for the British Isles) and the method has recently been applied to estimate extreme water level probabilities around southeast Australia (McInnes et al., 2009; McInnes et al., 2011a) and Tasmania (McInnes et al., 2011b). Hydrodynamic models have also been driven with meteorological fields from global climate models for past/present and future periods to examine the impact of anthropogenic climate change on the frequency of water level extremes for different regions (i.e. Flather and Smith, 1998; Langenberg et al., 1999; Lowe et al., 2001; Debernard et al., 2002; Lowe and Gregory, 2005; Woth, 2005; Woth et al., 2006; Unnikrishnan et al., 2006) and this was done for parts of Australia by McInnes et al. (2009, 2011a, b) and Colberg and McInnes (2012).

With respect to the second issue (i.e. estimating probabilities of extreme water level arising from tropical cyclones); the meteorological fields (usually from global reanalyses or climate models) that are currently used to force hydrodynamic models are too coarse spatially and temporally to adequately resolve tropical cyclones and thus significantly underestimate the likely storm surge. Even if the resolution was adequate to represent tropical cyclone-induced surges, the problem still remains that multi-decadal periods yield insufficient instances to enable the use of traditional extrapolation techniques (McInnes et al., 2009). To put it another way, whilst multi-decadal records reasonably sample the full population of extra-tropical storm events, much longer periods are required to adequately sample the population of tropical cyclone events, because by comparison they are rare and more localised. The approach that tends to be used is to develop statistical models of the tracks and central pressures of tropical cyclones from observations for specific areas (Harper et al., 2001). The statistical model is then used to generate synthetic events that represent many thousands of years of tropical cyclone activity (e.g. McInnes et al., 2003; James and Mason, 2005). Wind and pressure fields, derived from these synthetic events using analytical profile models (e.g. Holland, 1980), can then be used to drive hydrodynamic models to predict the associated surge response. The surges predicted for these synthetic events can be randomly combined with different tidal states and the generated time-series can be fitted to extreme value distributions to estimate extreme water level AEP. This approach has been used in many studies around Australia, particularly for the Queensland coast (see Harper et al. 2009).

The best available information on extreme total water levels is required for effective flood and erosion risk-based management (McMillan et al., 2011). In the context of Australia, the majority of past studies that have estimated water level AEP have done so on local or regional scales and hence the current information is not up to date and consistent around the country. Further, a wide range of different approaches has been used on different spatial resolutions. In addition to this, the coastline of Australia, similar to that of the US east coast (Zhang et al., 1997, 2000), is subject to both extra-tropical and tropical storms. Few, if any past studies in Australia (and elsewhere to our knowledge) have jointly estimated the probabilities of extreme total water levels arising from both extra-tropical and tropical storms. Not surprisingly, the studies (listed above) that have produced multi-decadal hindcasts of water levels have all been undertaken for regions without tropical cyclone influence. Therefore, the overall aim of this current study was to provide a coherent and up to date estimate of present day extreme total water level AEP around the whole coastline of Australia, arising from combinations of mean sea level, astronomical tide and storm surges generated by both extra-tropical and tropical storms.

The study was undertaken in two main stages. In the first stage, described in Section 3, a hydrodynamic model has been configured (Section 3.1) and used to generate a 61-year time-series of historic water levels around Australia. This predicted dataset has been validated against measurements from tide gauge sites around Australia with long records (Section 3.2) and then used to estimate exceedance probabilities around the entire coastline (Section 3.3). The second stage of the study, described in Section 4, is aimed at more accurately including tropical cyclone-induced surges in the estimation of extreme total water level probabilities. First, an analysis of tide gauge records has been undertaken in order to briefly assess the characteristics of tropical cyclone-induced surges around Australia (Section 4.1). Selected events have been modelled and validated against measurements (Section 4.2). A statistical model of the tracks and central pressures of tropical cyclones has been developed and used to generate synthetic events that represent the equivalent of 10,000 years of tropical cyclone activity with characteristics based on the tropical cyclones observed over the last about 40 years, for the Australian region (Section 4.3). Wind and pressure fields derived for these synthetic events were then used to drive the hydrodynamic model. Annual maximum total levels for these synthetic events have been calculated and these have been used to estimate exceedance probabilities around the

coastline (Section 4.4). The exceedance probabilities calculated in stage 1 and 2 have then been combined to give a single estimate of current extreme water level probabilities around the whole coastline of Australia. Finally, conclusions and recommendations are given in Section 5.

3 Stage 1: Tides, extra-tropical surges and mean sea level

This section describes the first stage of the study in which a hydrodynamic model has been configured (Section 3.1) and validated against measurements (Section 3.2) and used to generate a multi-decadal time-series of historic total water levels around Australia. This predicted dataset has then been used to estimate exceedance probabilities around the entire coastline (Section 3.3).

3.1 Model configuration

A depth-averaged barotropic hydrodynamic model has been configured for the entire Australian coastline using the Danish Hydraulic Institute's Mike21 FM (flexible mesh) suite of modelling tools. The Mike21 FM modelling system is based on the numerical solution of the incompressible Reynolds averaged Navier-Stokes equations invoking the assumptions of Boussinesq and hydrostatic pressure. The spatial discretization of the primitive equations, over the flexible mesh, is performed using a cell-centred finite volume method (see DHI, 2010).

The model grid that was configured is shown in **Figure 2**. It has a resolution of between about $1/3^{\text{rd}}$ and $1/5^{\text{th}}$ of a degree (~ 20 and 80 km) at the open tidal boundaries, increasing to $1/12^{\text{th}}$ of a degree (~ 10 km) along the entire coastline of mainland Australia, Tasmania and surrounding Islands. The grid was configured using the National Oceanic and Atmospheric Administration's (NOAA) medium resolution (1:70,000) coastline (obtained from http://www.ngdc.noaa.gov/mgg_coastline/). The bathymetric data, interpolated onto the model grid, was obtained from the Geoscience Australia 9 arc second (~ 250 m) dataset (Webster and Petkovic, 2005). The minimum model depth was set to -4 m.

In order to generate the astronomical tidal component of sea levels, the open model boundaries were driven with tidal levels derived from TPXO7.2 global ocean model (Egbert et al. 1994; Egbert and Erofeeva, 2002). TPXO7.2 is based on OTIS (Oregon State University Tidal Inversion Software) and incorporates data from the TOPEX/Poseidon and Jason altimetry missions. The tides are provided for eight primary (M_2 , S_2 , N_2 , K_2 , K_1 , O_1 , P_1 , Q_1), two long period (M_f , M_m) and three non-linear (M_4 , MS_4 , MN_4) harmonic constituents, on a $1/4^{\text{th}}$ of a degree resolution full global grid. The harmonic constituents

for the global grid were downloaded from the OTIS web site (<http://volkov.oce.orst.edu/tides/>). The harmonic constituents were extracted from this database and the astronomical tide was predicted, for each boundary grid point, using the Tidal Model Driver (TMD) MATLAB toolbox, created by scientists at Earth Space Research (http://polaris.esr.org/ptm_index.html). TMD includes standard satellite modulation corrections based on equilibrium tide expectations and hence the 4.4-year cycle of lunar perigean influence and the 18.6-year lunar nodal cycle (see Haigh et al., 2011b) are accounted for in the predictions. TMD also incorporates 16 other minor constituents, inferred using the eight major constituents.

In many numerical studies of coastal regions, tidal forcing is primarily provided through the open boundary tidal forcing (i.e. similar to that described in the paragraph above). This generally neglects the tide generated specifically in a basin or on a shelf sea by direct gravitational tidal forcing and motion of the solid Earth. Direct gravitational forced tides are the result of the gravitational forces of the Moon and Sun on the water in a particular shelf sea itself, whereas co-oscillating tides represent tides which propagate in and out of the shelf sea from the adjacent ocean through the open boundaries. Incorporating direct gravitational tidal forcing terms into the model equations of motion allows the model to capture both the tide generated specifically in the basin or shelf sea and the free tidal response. We accounted for direct gravitation forcing in the model simulations by including the ‘tidal potential’ forcing incorporated into Mike21. We found that this significantly improved prediction of the astronomical tide, particularly in Bass Strait, a region in which several authors have found it difficult to accurately model tides in the past (i.e. McIntosh and Bennett, 1984; Fandry et al., 1985; McInnes and Hubbert, 2003). A detailed description of direct gravitation forcing and the effect of including this in the hydrodynamic model simulations around Australia, in particular in Bass Strait, are given in Wijeratne et al. (in review).

To generate the storm surge component of water levels, the model has been forced with mean sea level pressure fields and u and v components of 10 m wind fields, obtained from the US National Center for Environmental Prediction’s/National Center for Atmospheric Research’s (NCEP/NCAR) global reanalysis (Kalnay et al., 1996; Kistler et al., 2001). These meteorological fields are available every 6 hours from 1948 to present and have a

horizontal resolution of 2.5° . The data was downloaded directly from the reanalysis web page (<http://www.cdc.noaa.gov/cdc/reanalysis/reanalysis.shtml>). The NCEP/NCAR mean sea level pressure fields and wind vectors every 12-hours between 15 and 20 May 2003 are shown in **Figure 3**. This extra-tropical storm generated a large storm surge along much of the coastline of southern Australia and resulted in the highest recorded total water levels at Fremantle since 1897. The spatial and temporal resolution of the NCEP/NCAR forcing is adequate for predicting storm surges associated with large extra-tropical storms such as these, but is too coarse to accurately predict the more intense and localised tropical cyclone-induced storm surge events.

The tide-surge model was run for the 61-year period from 1949 to 2009. Each year was run separately with a five day warm up period included. Results were outputted for each model grid cell every hour. By running the model with both tides and meteorological forcing, non-linear interactions between the tide and surge components are included (Horsburgh and Wilson, 2007). The key parameterisations used in our Mike21 model are listed in **Table 1**.

3.2 Model validation

The model has been validated, in several stages, against measurements from the 30 tide-gauge sites shown in **Figure 1**, which with the exception of Milner Bay all have at least 30 years of records (**Table 2**). Milner Bay was included so that there was a validation site in the Gulf of Carpentaria. The tide-gauge records were obtained from the Australian National Tidal Centre (NTC). The records were converted into the same format and referenced in universal time + 0 h and Australian Height Datum (AHD). Where higher frequency data was available these have been sub-sampled to hourly values. The data has been rigorously checked for common errors such as data spikes and spurious values have been excluded. At each site, annual values of mean sea level were calculated for years where the records were at least 75% complete. A trend was then fitted to these mean sea level time-series using linear regression and this was used to de-trend the hourly measurements relative to a base year, in this case 2010.

Sixty-one year long time-series of predicted water levels were extracted from the hydrodynamic model results at the grid points closest to the corresponding tide gauges. The de-trended water level measurements and predicted model time-series at each site were then separated into seasonal and inter-annual mean sea level, tidal and surge components (Pugh, 1987). Each of these three components were validated separately, before a comparison of the measured and predicted total water levels was undertaken.

A consistent method was used to separate both the de-trended measured and predicted water level time-series into the three component parts. The mean sea level component was derived using a 30-day running mean of the hourly time-series. The tidal component was estimated using the Matlab T-Tide harmonic analysis software (Pawlowicz et al., 2002). A separate tidal analysis was undertaken for each calendar year with the standard set of 67 tidal constituents. The surge component was then calculated by subtracting the mean sea level and tidal component from the total water level time-series.

A range of different methods were used to assess the performance of the hydrodynamic model in reproducing these three separate water level components and the combined total levels at each of the 30 validation sites. To determine how accurately the model predicts the astronomical tidal component, the amplitude and phase of the eight main tidal constituents, extracted from both the measured and predicted water levels using the T-Tide package, were compared. In addition, three error measures were used to quantify the model skill for the hourly tides, surges, mean sea level and total water levels. For each of the four time-series, the absolute difference between each hourly measured and predicted value was computed. The mean (i.e. equivalent to root mean square error (RMSE)) and standard deviation of the absolute hourly differences were then calculated, for each year and the total 61-year time-series. Correlation coefficients between the measured and predicted hourly time-series were also derived for each year and the complete time-series. In the following four sub-sections, the differences between the measured and predicted tide, surge and mean sea level components are described and then the total levels are considered, respectively.

3.2.1 Tidal component

A comparison of the amplitude and phase of the eight main tidal constituents, estimated from the measured and predicted datasets, at each of the validation sites are shown in **Figure 4** and **Figure 5**, respectively for the year 1995. We focus on the year 1995, because the measured records for this year were at least 90% complete at all tide gauge sites. There is relatively good agreement for each of the tidal constituents. The mean absolute difference between the amplitude and phase of each of the eight tidal constituents across the 30 sites are listed in **Table 3**. The mean amplitude differences are less than 11 cm and the mean phase differences are less than 12 degrees. For comparison, the amplitude and phase of the measured tidal constituents were compared to the amplitude and phase of the constituents from the TPXO7.2 global ocean tidal model, which are used to force the open boundaries of the model. These are also listed in **Table 3**. As expected, the higher resolution Australian model does a much better job of predicting tidal characteristics around the coast compared to the lower resolution global model.

The three error measures used to quantify the difference between the measured and predicted hourly tidal time-series are listed in **Table 4**, for 1995. The largest RMSE is at MacKay (0.45 m) and the smallest are at Geraldton, Albany and Esperance (0.04 m). The average (across all the validation sites) mean and standard deviation errors were 0.14 and 0.10 m, respectively. The mean correlation coefficient was 0.94. The errors for the complete 61-year time-series (not shown) were of similar magnitude. Overall, these results demonstrated that the model reproduces the observed characteristics of tides around the Australian coastline.

3.2.2 Storm surge component

A comparison of the measured and predicted surge component for 1995, at selected sites around southern Australia are shown in **Figure 6**. It can be seen that the model accurately captures the characteristics of surges throughout the year around southern Australia, a region dominated by extra-tropical storm events. The model tends to slightly underestimate the peak of the large storm surge events. This is probably because of the relatively coarse temporal (6 hourly) and spatial (2.5°) scale of the meteorological forcing.

The three error measures used to quantify the difference between the measured and predicted surge time series, for 1995 are listed in **Table 4**. The average (across the 30 validation sites) mean and standard deviation errors are 0.05 m and 0.04 m, respectively. The average correlation coefficient is 0.75. For just the southern sites, the correlation coefficients are relatively high (>0.8). However, the correlation coefficients are lower for the northern regions, which experience tropical storms. This is not surprising, considering that the relatively coarse meteorological forcing used only weakly includes the effects of tropical storms and cyclones.

The measured and predicted storm surge component for the 5-year period from 1995 to 1999 at Thevenard (South Australia) are shown in **Figure 7**. This demonstrates how well the model reproduces the surge characteristics over a longer time scale, but how does the model perform over multi-decadal periods? Time-series of the three annual error measures are shown in **Figure 8** for the storm surge component at Fremantle over the 61-year hindcast period. The other sites show similar findings. Interestingly, the performance of the model improves slightly with time, although the overall improvement is relatively small. There is an increase in performance from 1949 to about 1970 and then a small increase from around 1970 to about the start of 1980. Between about 1980 and 2009 the model accuracy is fairly consistent. This improvement in recent decades is not evident in the tidal time series, indicating that it arises from the meteorological forcing and not the quality of the tide-gauge measurements. This suggests there could be small inhomogeneities in the NCEP/NCAR meteorological fields used to drive the model. Reanalysis are prone to inhomogeneities due to changes in the observing system (Kristler et al., 2001). With the introduction of satellites, the amount of observations has increased enormously in recent decades. Sterl (2004) compared the European Centre for Medium-Range Weather Forecasts' (ECMWF) so called ERA-40 dataset (Uppala et al, 2005) with the NCEP/NCAR reanalysis and found several inhomogeneities in the Southern Hemisphere before 1980. The density of observational data was sufficient to constrain the reanalysis models in the North Hemisphere but not in the Southern Hemisphere. While the increase in model performance over time is of scientific interest, the improvement is relatively small and hence unlikely to significantly influence the estimation of current extreme total water level exceedance probabilities.

3.2.3 Mean sea level component

As previously mentioned, extreme water levels arise as a combination of three main factors: mean sea level, astronomical tide and storm surge (Pugh, 1987, 2004). The latter two have been discussed above, now we focus on mean sea level. In many parts of the world, including the areas for which the previous multi-decadal hindcasts were produced (i.e. North Sea (Langenberg et al., 1999; Weisse and Plüß, 2006); North Atlantic (Bernier and Thompson, 2006); the Atlantic coast of Europe (Sebastiao et al., 2008); the British Isles (McMillan et al., 2011); and in Australia, Victoria (McInnes et al., 2009, 2011a) and Tasmania (McInnes et al., 2011b)), seasonal and inter-annual variations in mean sea level are relatively small, and so it is the combination of surge and tide that dominates the generation of extreme total water level events, hence the term ‘storm tide’. However, around parts of the Australian coastline, the seasonal and inter-annual mean sea level variations are relatively large and can strongly influence the timing and magnitude of extreme events, particularly in areas such as the Gulf of Carpentaria, where the seasonal cycle is very large, or in southwest Australia where the tidal range is relatively small in comparison (Pattiaratchi et al., in prep). Eliot (2012) recently showed how both seasonal and inter-annual mean sea level variations strongly influence extreme water levels and coastal flooding at Fremantle, Western Australia. Therefore, for parts of the Australian coastline, it is particularly important that we accurately model variations in mean sea level in order to correctly capture the observed characteristics of total water levels around the coast.

Seasonal and inter-annual variations in mean sea level arise from both barotropic and baroclinic effects. Depth averaged hydrodynamic models only reproduce the barotropic, and not baroclinic variations in mean sea level. Most of the previous studies that have generated multi-decadal hindcasts, used depth averaged models. This was appropriate because both the barotropic and the baroclinic variations in mean sea level were relatively small in the areas assessed and did not have a marked effect on total water levels. The alternative is to run full three-dimensional baroclinic models, but this is generally avoided because they are considerably more computationally expensive to run. From our perspective, it was desirable not to have to run a baroclinic model given the relatively large domain being modelled. Therefore, we conducted a detailed analysis of mean sea level variation around Australia using tide gauge and altimetry records. We examined the

relative barotropic and baroclinic contributions and determined how well the model reproduces the barotropic component. The estimated baroclinic signal was compared with steric heights derived from temperature and salinity climatology obtained from the World Ocean Atlas (WOA-09). This is described in detail in Wijeratne et al. (in prep) and summarized briefly here.

Monthly mean tide gauge and satellite altimetry records were obtained from the websites of the Permanent Service for Mean Sea Level (PSMSL) (<http://www.psmsl.org/>) and the Archiving, Validation, and Interpretation of Satellite Oceanographic Data (AVISO) (<http://www.aviso.oceanobs.com/>), respectively. A simple approach was used to decompose the monthly sea level records into seasonal and inter-annual components at each site. First the monthly sea level records were de-trended using linear regression. Then a 12-month running mean was applied to generate the inter-annual component. The inter-annual component was then subtracted from the de-trended monthly sea level records to generate the seasonal component.

The mean range in the seasonal component around Australia is shown in **Figure 9a**. In the Gulf of Carpentaria, the seasonal cycle in mean sea level has a range of up to about 1 m, which is one of the biggest seasonal variations in mean sea level in the world. The average month during which the seasonal cycle is largest is shown in **Figure 9b**. Hypothetically, for a storm to generate a given total water level in the Gulf of Carpentaria, the associated surge would have to be 1 m higher in June to generate the same total water level in January. In southwestern Australia the range of the seasonal mean sea level cycle is large (~0.3 m) compared to the relatively small mean tidal range in the region (~0.4 m).

The inter-annual component (results not shown) has a maximum range of up to 0.3 m around northern and western Australia and is much smaller (>0.1 m) around southern and eastern Australia. Around northern, western and southern Australia the inter-annual variability is highly correlated with the Southern Oscillation Index (SOI), a descriptor of the El Niño-Southern Oscillation (ENSO) and a large part of the variability is coherent between sites (see Haigh et al., 2011c). Along this part of the coast, years with low annual mean sea level values (i.e. 1997/98) are associated with El Niño episodes and hence

sustained negative values of the SOI, whereas years with high annual mean sea level values (i.e. 1999/2000) are associated with La Niña events and hence positive SOI values.

Having established the general characteristics of the seasonal and inter-annual variations in mean sea level around the coast, we then attempted to determine the relative barotropic and baroclinic contributions around Australia. For the 10-year period from 2000 to 2010, we derived monthly mean values from the model hindcast (i.e. the barotropic component) over the whole model domain and subtracted this from monthly mean values from the altimetry data, to estimate the baroclinic signal. In areas where the mean sea level variability is large, we found that the barotropic component accounted for a large part of the overall signal and was generally well reproduced by the model. The barotropic signal in the Gulf of Carpentaria accounts for more than 80% of the large variability in this region. However, to accurately model this variability, which arises as a result of monsoonal wind setup, we had to extend the model domain to cover the Java, Banda and Arafura Seas around Indonesia. Where the mean sea level variability was smaller, the baroclinic component accounted for more of the variability, and hence our model underestimated the variability in these regions. However, because the overall mean sea level variability is smaller in these regions, it has less influence on the total water levels.

Finally, at each of the 30 study sites we compared the observed mean sea level component (derived using a 30-day running mean of the de-trended hourly time-series; see Section 3.2 above) with the predicted barotropic component (derived in the same way). At each site the model underestimated mean sea level, because the model does not predict the baroclinic component. However, overall the differences were still relatively small, because the barotropic component is generally a large component of the overall variability where the mean sea level variability is large. The three performance measures at each of the validation sites for 1995 are listed in **Table 4**. The average (across all the validation sites) mean and standard deviation errors are 0.07 m and 0.04 m, respectively. The average correlation coefficient is 0.78. The errors for the complete 61-year time-series (not shown) are of similar magnitude.

3.2.4 Total water levels

It is clear from the above three sections that the predicted tide, surge and mean sea level components accurately reproduce the measured tide, surge and mean sea level variations at the 30 validation sites. Hence, it is reasonable to assume that the combined predicted tide, surge and mean sea level components will accurately reproduce the de-trended measured total water levels. A comparison of measured and predicted total water level frequency and cumulative frequency distribution curves are shown in **Figure 10** for four selected sites (Albany, Port Lincoln, Burnie and Newcastle). There is good agreement at each of these sites and the other 26 validation sites not shown. The three performance measures are listed in **Table 4** for the total water levels at each of the validation sites for 1995. The average (across all the validation sites) mean and standard deviation errors are 0.18 m and 0.12 m, respectively. The average correlation coefficient is 0.92.

Overall, the model does a very good job in accurately reproducing total water levels and its component parts. The differences between the measured and predicted time series are of a similar magnitude, or lower on average to that reported in similar studies undertaken for different areas of the world and parts of Australia.

3.3 Water level exceedance probabilities

In this section the AEP estimated from the de-trended measured total water levels (with the datum adjusted so that the levels related to the middle of the base year 2010) and the predicted total water levels are compared at the 30 validation sites. Following that, the procedure used to estimate the AEP at all of the coastal model grid points is described.

Over the last 50 years, several different methods have been developed and refined for estimating probabilities of extreme water level, but there is currently no universally accepted method (Haigh et al., 2010). In this paper, we perform extremal analyses using the classic annual maxima method (AMM), fitted to both Gumbel (GUM) and Generalized Extreme Value (GEV) distributions, and compare estimates to those obtained using the related r-largest method (RLM). An overview of these statistical methods is given in Haigh et al. (2010) and the literature referenced within can be consulted for the mathematical detail. These two methods, along with the peaks over threshold Method (POT), are called

direct methods as they analyze the extremes of the observed water level (we choose not to use the POT method because a separate threshold must be selected for each site and threshold selection is somewhat subjective due to considerable temporal and spatial water level variability; whereas, both the AMM and RLM are robust to temporal and spatial variations as they rely upon a relative definition of what constitutes an extreme event (Butler et al., 2007)). There are two main objections to using the traditional relatively simple direct extreme analysis methods. First, water level is made up of a complex combination of tide-driven (deterministic) and mean and storm-driven (stochastic) components that have strong seasonal patterns. Hence, the naive assumptions leading to the GUM or GEV family for block maxima are somewhat unrealistic. Second, the direct methods, particularly the AMM, are inefficient in their use of data. More sophisticated indirect (i.e. the astronomical tidal and non-tidal components are modelled separately and the extremes of sea level are inferred) extreme analysis methods, such as the joint probability method (JPM) (Pugh and Vassie, 1979, 1980) and the revised joint probability method (RJPM) (Tawn and Vassie, 1989) have been developed to address these limitations (see Haigh et al., 2010). However, we did not consider these two methods as they are very sensitive to timing errors (see Pugh, 1987 p. 53-58), which are particularly prevalent in early parts of many of the tide-gauge records around Australia. Correcting for this is a particularly arduous and time-consuming exercise and beyond the scope of the study. Recently the state-of-the art skew surge joint probability method (SSJPM) was introduced by McMillan et al. (2011). This new technique builds on the JPM and RJPM method and has the considerable advantage over the other two indirect methods that it is relatively robust to timing errors and does not require non-linear interactions between the surge and tide to be accounted for. In the future we hope to update the estimates presented below using this new more sophisticated method, but in the meantime focus on the AMM and RLM.

The extremal analyses were undertaken using the *ismev* package (Coles, 2001) implemented in the statistical language R (<http://www.r-project.org/>). This computes the maximum likelihood estimation of the exceedance distribution and its upper and lower 95% confidence limits. Annual maxima and the several largest levels each year were derived, in both the measured and predicted datasets, using a clustering algorithm. Each level was required to be separated by at least 72 hours, to ensure distinct extreme events

were identified. AEP were then estimated using the annual maxima time-series fitted to (i) a GEV distribution; (ii) a GUM distribution, and (iii) the r -largest time-series fitted to a GEV distribution. In regards to the latter, sensitivity tests were undertaken using r -values ranging from two to 15, with five largest values per year found to give a stable estimate.

First we compare the measured and predicted AEP estimated using the AMM fitted to a GEV distribution. The return period curves for the base year 2010, derived from both the measured and predicted time-series, are shown in **Figure 11** for the validation sites. The predicted levels have been artificially adjusted so that the 1-year return period levels exactly match those of the measured estimates at each site. This was done because the predicted water levels are relative to MSL, whereas the measured levels are relative to AHD. Around mainland Australia, AHD was defined using MSL records between 1966 and 1968 at 30 sites around the coast of the Australia and hence differs from present day MSL. Around Tasmania, AHD was defined using two records from 1972. The agreement between the measured and predicted AEP is reasonable at most sites. In general, the predicted curves under estimate the return levels, at higher return periods, for the sites that are strongly influenced by tropical cyclones (i.e. Mackay around to Carnarvon), particularly Port Hedland. The measured and predicted 10-, 50- and 100-year return levels are listed in **Table 5**. The absolute difference between the measured and predicted return levels is also listed for each site. The average difference across the 30 validation sites for the 10-, 50- and 100-year return levels is 0.06 m, 0.1 m and 0.15 m, respectively. Similar magnitudes of differences were obtained for the estimates obtained using annual maxima time-series fitted to a GUM distribution and the r -largest ($r=5$) time-series fitted to a GEV distribution.

It is interesting now to briefly compare estimates obtained from the three different approaches we used to estimate AEP. Return period curves calculated using the three approaches are shown in **Figure 12** for the measured data at Geraldton and Fort Denison. The majority of the other validation sites showed similar characteristics. At the lower return periods ($< \sim 20$ years) the three estimates agree well. However, at the long return periods ($\sim > 20$ years) the AMM and RLM fitted to GEV distributions tend to flatten off more rapidly than the estimates from the AMM fitted to GUM distributions. As a result the difference between the 100- and 1,000-year return level is relatively small (typically < 0.1

m) at most sites. The performance of the three estimates can be assessed, using a simple approach suggested by Dixon and Tawn (1999), by comparing the difference between the estimated return periods of the observed maximum water level at each site with the corresponding data length. At both locations shown in **Figure 12**, the respective maximum recorded water level has been plotted against the length of the respective record (i.e. 45 and 96 years) and this is shown as a green square. For both Geraldton and Fort Denison it can be seen to agree closely with the estimate calculated using the AMM fitted to the GUM distribution. At almost all sites (results not shown), the AMM fitted to the GUM distribution has the lowest so called ‘prediction errors’. This indicates that the AMM and RLM fitted to GEV distributions tend to underestimate the return levels (or overestimate the return periods) at high return periods. Based on these results, we focus here onwards on the estimates derived using the AMM fitted to a GUM distribution. This also has the added advantage that the estimates are more conservative.

Dixon and Tawn (1999) and Haigh et al. (2010) compared different direct and indirect methods using tide gauge records around the UK and also showed that the direct methods, fitted to GEV distributions, tend to underestimate return levels for return periods of 20 years or more at UK sites where the surge variation is small in comparison with the variation in astronomical tidal levels. Dixon and Tawn (1999) suggested that the reason the direct methods tend to underestimate the long period return levels is most likely due the key assumption in the AMM and RLM, that the maximum or r -largest values over a year behaves like a maximum of a stationary process. The sequence of water level would be approximately stationary and the assumption correct, if the tidal variations and seasonality were negligible compared with the surge variability. However, if the variability of the surge component is negligible relative to that of the tide, then because of the deterministic nature of the tide, the maximum level over an 18.6-year nodal cycle will be approximately a degenerate random variable equal to the highest astronomical tide. When this is the case, the extrapolation to long return periods will be poor when using the direct methods. As Haigh et al. (2010) point out, the differences between the indirect methods and direct methods are small for return periods less than 18 years, confirming this point. Without undertaking a more detailed comparison of different methods, it is difficult to say with certainty whether this holds true for Australia, but most likely this is the case. We think therefore, that it would be beneficial to conduct a much more detail comparison in the

future, similar to that undertaken for UK sites by Haigh et al. (2010), of the different extreme value methods around Australia, including the SSJPM that has recently become available, to better understand observed differences.

In order to estimate AEP around the entire coastline of Australia, 61-year annual maxima time-series were derived for the 2,440 model grid points located at $1/12^{\text{th}}$ of a degree (~ 10 km) intervals around the mainland Australian and Tasmanian coastlines. At each coastal point, AEP were estimated using the AMM fitted to a GUM distribution. The offset between the measured and predicted 1-year return level at each of the 30 validation sites was linearly interpolated onto all of the coastal model grid points. The interpolated value at each coastal grid point was then used to adjust the estimated AEP at that corresponding point. The AEP values were then linearly interpolated to $1/60^{\text{th}}$ of a degree (~ 2 km) intervals around the coast. The 100-year return water levels for each of the coastal model grid points is shown in **Figure 13** for the base year 2010. The corresponding 100-year levels, estimate from the tide-gauge records, are also shown on **Figure 13** as circles.

It is important to emphasize that whilst the results shown in **Figure 13** provide a reliable estimate of current total water level recurrence intervals around southern Australia, which is mainly impacted by extra-tropical storms, the resultant water level recurrence intervals are underestimated at this stage around western, northern and north-eastern Australia at higher return periods. This is because the meteorological fields used to force the hydrodynamic model only weakly include the effects of tropical cyclones, but, even if the resolution of the meteorological forcing was adequate to represent tropical cyclone-induced surges, multi-decadal periods yield insufficient instances of tropical cyclones to enable the use of traditional extreme value extrapolation techniques. This brings us to stage 2 of the study, which has been undertaken to address these issues.

4 Stage 2: Tropical cyclone-induced surges

The aim of the second stage of the study, which is described in this section, is to more accurately include tropical cyclone-induced surges in the estimation of extreme total water level probabilities. Here, an analysis of tide gauge records was undertaken in order to assess the characteristics of tropical cyclone-induced surges around Australia (Section 4.1) and select events which could be simulated and validated against measurements (Section 4.2). A stochastic tropical cyclone model was developed and used to generate a synthetic event set (10,000 years) statistically representative of tropical cyclone activity (1969-2008) in the Australian region (Section 4.3). Wind and pressure fields, derived for these synthetic events, were used to drive the hydrodynamic model. Annual maximum total levels for these synthetic events were calculated and used to estimate exceedance probabilities around the coastline (Section 4.4). The exceedance probabilities calculated in stages 1 and 2 were then combined to provide a single estimate of the current extreme water level probabilities around the whole coastline of Australia.

4.1 Analysis of tide-gauge observations

As a first step, an analysis of tide gauge records has been undertaken in order to: (i) briefly assess the characteristics of tropical cyclone-induced surges around Australia; and (ii) select events suitable for validating the hydrodynamic model for tropical cyclones. The analysis focused on the storm surge component of the tide gauge records at the 30 validation sites (**Figure 1**). For each site, the 100 largest storm surge events between 1970 and 2008 were identified from the derived surge component. Each storm surge event was required to be separated from the subsequent event by at least 72 hours to ensure distinct storm events were identified, rather than double counting of the same event. The dates of these events were then compared to the dates and tracks of cyclones obtained from the Australian Bureau of Meteorology's (BOM) tropical cyclone database (downloaded from the following web site: <http://www.bom.gov.au/cyclone/history/index.shtml>). Although BOM's database extends back to 1907, we focused on the post 1969 'satellite era'. Our analysis was restricted up until 2008, because the database only contained cyclone information up until this year at the time of analysis. Of the 30 tide gauge sites, only Milner Bay and Brisbane didn't have records spanning the complete 1970 to 2008 period; the Milner Bay record started in 1993 and the Brisbane record in 1977.

Seventeen of the 30 tide gauge records were found to have tropical cyclone-induced surge events within the 100 highest surge events recorded at each site between 1970 and 2008. The tracks of the tropical cyclones responsible for the ten largest cyclone-induced surge events that made it into the top 100 largest surge events identified at each site, are shown in **Figure 14**. For Esperance and Albany, only one tropical cyclone (Alby in 1978) generated a storm surge that was within the top 100 events identified at each site, implying therefore that the other 99 largest events were generated by extra-tropical or tropical (but not classified as cyclone) storms. In contrast, for more northern sites, an increasing number of tropical cyclone-induced storm surge events feature in the top 100 surge events. For most of the sites, shown in **Figure 14**, the largest cyclone-induced storm surges were generated by cyclones tracking to the left of the site. This is expected given that onshore winds are generated to the right of the cyclone along the Northern Australia coastline.

The largest tropical cyclone-induced surges at each of the 17 sites, in order of storm surge height, are listed in **Table 6**. The largest recorded surge, over the period 1970 to 2008 at the tide gauges analysed, was 2.84 m at Townsville, resulting from tropical cyclone Althea in 1971. This event also resulted in the highest total water levels recorded at this location over the analysis period (2.53 m), despite the fact that the peak of the surge occurred around the time of low water (tidal height was -0.31 m). The second largest recorded surge was 2.26 m at Broome, resulting from tropical cyclone Rosita in 2000. This event only generated the 45th highest recorded total water levels at Broome. The peak of the event occurred only two hours after high water, but because the tidal range is very large at this site (~10 m), it did not generate a particularly extreme total water level.

4.2 Model validation and sensitivity tests

4.2.1 Event selection

The next stage involved a validation exercise to determine the accuracy of tropical cyclone-induced storm surge events that could be simulated using the 2D hydrodynamic model. Based on the tide-gauge analysis described above, and in particular the large events listed in **Table 6**, we selected nine events to validate the model, ensuring that these covered different regions of the cyclone affected part of the Australian coastline. These

chosen events are listed in **Table 7**. In addition, we considered Cyclone Yasi, a category 5 system which occurred recently in February 2011. During this event a maximum storm surge of 5.5 m was recorded at the Cardwell tide gauge, located midway between Cairns and Townsville. Water level measurements were obtained for this period for the Cairns and Townsville tide gauges and three additional gauges located along that stretch of coastline.

4.2.2 Wind field model description and validation

For each of the selected events, gradient level wind and pressure fields, necessary to force the hydrodynamic model, were derived using the analytical double vortex model proposed by Cardone et al (1994). As in McConochie et al. (1999), a secondary vortex was included to flatten the decay profile moving away from the storm, not to generate a distinctive second peak. This model overcomes the observed limitation of an overly rapid decay with the standard Holland (1980) model and affords better agreement with observed wind records at large radii (McConochie et al. 1999). We implemented the wind speed dependent surface reduction (notionally to an elevation of 10 m), inflow angle and asymmetry regimes outlined in McConochie et al. (2004), which are based on Harper (2001). The only variation to these models was the random selection of the location of maximum wind speed, chosen to reside between 20° and 135° anti-clockwise from the direction of storm motion, in line with surface wind observations presented in Uhlhorn et al. (2007). No synoptic winds were included.

The basic wind field model has previously undergone validation for Coral Sea and, notionally, Indian Ocean tropical cyclones (McConochie et al. 2004), but is again validated for the current implementation. The BOM tropical cyclone database does not record all required model parameters (i.e. radius to maximum winds (primary and secondary vortex), location of maximum winds and Holland B parameters). Therefore, these were estimated for a number of historic events by randomly sampling possible variable combinations and minimising simulation least-squares error in wind speed, direction and surface pressure, where these data were available, along with some visual refinement to arrive at optimal event parameters. Using these values, predicted wind speed and surface pressure time histories were extracted for each event. Model performance is exemplified in **Figure 15** which compares predicted wind, direction and surface pressure results with those recorded during the passage of tropical cyclone Yasi in 2011 at several locations. Localised

adjustment factors were used to transform the predicted wind speed to an equivalent 10-minute mean with the surface characteristics of the site. The relative error seen in this figure is representative of that found for other predicted events.

For inputting wind and pressure fields to the hydrodynamic model, a 0.1° rectilinear grid was built throughout the domain. For the 100 km zone buffering land, the grid was refined to 0.05° to better resolve the flow in the near-shore region. For grid points within 20 km of land, an additional wind speed adjustment was applied to account for the increased surface roughness in the coastal zone. Variable factors for on- and off-shore winds as well as near- (<10 km) and deep-coastal (10-20 km) regions were applied based on generic surface roughness transition arguments (Simiu and Scanlan 1986; Harper et al. 2009). Assumed surface roughness values in the four regions were: on-shore deep-coastal $z_0 = 0.01$ m; on-shore near-coastal $z_0 = 0.015$ m; off-shore deep-coastal $z_0 = 0.02$ m; off-shore near-coastal $z_0 = 0.07$ m. All fields were parsed at a temporal resolution of 1 hour.

4.2.3 Storm surge validation

The validated gradient wind and pressure fields for each event were then used to force the same hydrodynamic model described in Section 3.1 (i.e. using the full grid shown in **Figure 2**) and the results were compared to water level measurements. Rather than presenting results for all 10 events, we focus briefly on the three largest events, namely tropical cyclones Althea and Rosita, which generated the largest two recorded surges between 1970 and 2005 at the sites analysed (Section 4.1), and Yasi. The tracks of these three cyclones are shown in **Figure 16**.

As non-linear interactions between the tide and surge are shown to be important along certain stretches of the Australian coastline (see Section 4.2.4 below), tidal forcing was included at the open boundary using levels derived from the TPXO7.2 global ocean model (see Section 3.1). For each event, a tide only run was also undertaken. The results from this were subtracted from the tide plus surge run to obtain the predicted storm surge component.

Comparisons between the measured and predicted storm surge at Townsville, for cyclone Althea, and Broome, for cyclone Rosita, are shown in **Figure 17**. Generally, the hydrodynamic model reproduces the storm surge profile at each site. The model predicts

the maximum surge at Townsville for cyclone Althea to within 5 cm and the maximum surge at Broome for cyclone Rosita to within 1 cm. Comparisons between the measured and predicted storm surge are shown in **Figure 18** for cyclone Yasi, across four tide gauges in Queensland. Again, the model reproduces the observed storm surge at each site and predicts the maximum storm surge at the Cardwell tide gauge to within 8 cm, but with less accuracy at the other three sites.

4.2.4 Sensitivity testing

Tests were then carried out to examine the sensitivity of the simulated surge to tidal state. In many parts of the world, non-linear interactions occur between the tide and surge components of water level. This process, known as tide-surge interaction, has been most studied in the southern North Sea where it tends to result in surge maxima occurring on the rising tide, which significantly influences extreme total water levels (see Horsburgh and Wilson, 2007, and references within). In other parts of the world, tide-surge interactions are generally strongest over broad and shallow continental shelves, where the retarding effect of bottom friction more effectively influences the currents induced by tides and surges (McInnes et al., 2011a).

Generally, in modelling studies the preferred and most efficient approach is to model the storm surges separately from the tide and statistically combine the two to evaluate extreme total water levels (Harper et al., 2001). However, where tide-surge interactions are strong, the total water level heights obtained from the combined tide and storm surge does not equal the height of the tide and surge simulations separately, and subsequently summed together (McInnes et al., 2011a). Therefore, to determine the importance of non-linear effects around Australia, two sets of simulations were undertaken for tropical cyclones Althea and Rosita. For both cyclones, an initial run was undertaken in which the model was driven only with meteorological forcing. Then for both cyclones, four additional runs were undertaken in which the model was driven with both tidal forcing and meteorological forcing, but the timing of the meteorological forcing was artificially adjusted so that the peak of the surge occurred around the time of low water, on the rising tide, high water and on the ebb tide.

Non-linear tide-surge interactions were apparent both at Townsville for cyclone Rosita (**Figure 19**) and at Broome for cyclone Althea (**Figure 20**), but the non-linear interactions were much larger at Broome where the tidal range is ~10 m, compared to Townsville where the tidal range is ~1 m. The predicted total water levels (i.e. tide + surge runs) for both Townsville and Broome are shown in **Figure 19a** and **Figure 20a**, respectively, for the four different tidal states. The storm surge components associated with these four simulations and the storm surge from the storm surge only run are shown in **Figure 19b** and **Figure 20b**. The same information is shown in **Figure 19c** and **Figure 20c**, but the timing of the storm surge curves has been readjusted for the time offset previously applied, so that the time-series can be compared directly. At Townsville, the differences between the surges for the four tidal states are small (<0.3 m) (**Figure 19c**). This implies that the surge could be predicted independently of the tide in this region, and this is the approach followed in many of the previous cyclone storm surge studies for Queensland (Harper et al., 2001). However, there is more than a 1 m difference between the storm surges for the four different tidal states at Broome (**Figure 20c**), with the largest storm surge being produced around peak ebb and the smallest around peak flood. Not only does the maximum height of the event change with tidal state, but the duration and shape also varies. Therefore, it is clear that the surge should not be predicted independently of the tide on the North West Shelf of Australia. Hence, we decided to include the tide in all the simulations.

4.3 Storm surge simulation of 10,000 years of synthetic tropical cyclones

In the previous section, we demonstrated the ability of our hydrodynamic model to accurately simulate the storm surges associated with observed tropical cyclone events. The objective now is to predict storm surges associated with 10,000 years of synthetic cyclone events representative of current climate cyclonic activity (1969-2008), and use these long time-series to more accurately estimate total water level exceedance probabilities in tropical cyclone prone areas.

4.3.1 Synthetic tropical cyclone database

A 10,000 year synthetic tropical cyclone database was developed using tropical cyclone observations held by the BOM. Considering data limitations in records prior to the implementation of satellite tracking (Holland 1980; Harper et al. 2008), only the period

following its inception was used to develop baseline climatological statistics. Thus, the database is built upon data from the 1969/70 to 2008/09 tropical cyclone seasons and should only be considered representative of this period (and any variability within it). The tropical cyclone wind model generates and tracks synthetic activity within approximately 600 km of the Australian coastline from 30°S (Coffs Harbour, NSW) on the east coast to 35°S (Augusta, WA) on the west (**Figure 21**). In all areas the domain extends beyond the continental shelf. The analysis grid used for parsing data to the hydrodynamic model is temporally and spatially identical to that described in Section 4.2.2.

Tropical cyclone genesis: Event genesis can occur either within the genesis region of the model domain (cross-hatched in **Figure 21**) or upon one of a series of approximately 200 km gates that follow the outer domain boundary. Those events generated on a gate simulate cyclones that form outside the model domain but track into it during their lifetime (James and Mason 2005). For each of the 10,000 simulated years, a Poisson sampling process generates an appropriate number of events based on historically observed annual event frequencies at each gate or within each of the genesis domain sub-regions (9 cells in total). Given event occurrence at some gates is limited, averaging between gates is necessary in some locations. The cell genesis region extends from 22° S on the east coast to 20° S on the west (**Figure 21**), while gate events can occur anywhere along the outer boundary of the domain. Monte-Carlo sampling of probability distributions is used to assign each synthetic event an initial ambient pressure, central pressure, forward speed, direction and radius of maximum winds (Hardy et al. 2003).

Storm tracking: Following genesis, autoregressive techniques model subsequent forward speed, direction and central pressure values (Vickery et al. 2000). Autoregressive constants were derived using multivariate regression within 14 domain sub-regions of similar storm behaviour. The path of each tropical cyclone is generated as a series of straight lines, each representing 6 hours of elapsed time (linearly interpolated to 1 hour). Whilst over the ocean, the central pressure is limited by the Maximum Potential Intensity at each location and when an event moves over land the central pressure decays using a calibrated exponential decay function similar to that proposed by Kaplan and DeMaria (1995).

Wind and pressure field models: Wind and pressure field models are for the most part identical to those discussed in Section 4.2.2. Primary vortex Holland B parameter values were sampled from a distribution about the central pressure using the B relationship set out in Harper and Holland (1999). The slightly different version of this relationship described in McConochie et al. (2004) was tested but found not to perform as well when compared with long term measured wind statistics. Initial primary vortex radiuses to maximum winds were sampled about the mean relationship with central pressure given in Hardy et al. (2003).

For simplicity, the outer vortex characteristics were held constant with $B2 = 1$ and $R2 = 200$ km (Hardy et al. 2003). Two additional wind field models, Kepert (2001) and Georgiou et al. (1983), were also tested but found not to perform as well when compared with the aforementioned wind statistics. In saying this, however, there were instances where a calibrated Kepert model performed better than the current wind field model when compared with individual events. The main reason for its discrepancy with long-term statistics appear to be linked with the arguably too rapid decay of wind speed when moving away from the cyclone core, given that the majority of these data were recorded at a reasonable distance from the storm.

Validation of wind statistics: Model output has been validated against observations from 27 automatic weather stations at a number of locations around the Australian coastline and at reef/island sites, all with meteorological records longer than 30 years. The predicted and measured wind speed return period curves are shown in **Figure 22** at eight selected stations, the locations of which are shown in **Figure 21**, with all return periods estimated using the Gringorten modification to a standard Gumbel procedure (Holmes, 2001, p32). Historic wind data were determined to be tropical cyclone generated when a tropical cyclone tracked within 500 km of that site at the time of record. Again, for comparison with historic data, model output is locally adjusted to be representative of site conditions. Excellent agreement is seen for the majority of sites, but an over prediction of wind speeds is evident in the region around Broome (not shown) and Townsville. Townsville comparisons improve somewhat when looking at gust wind speed data. Coast crossing frequency and central pressure distributions have also been crosschecked and validated against historic coast crossing statistics.

The historic tropical cyclone tracks from the BOM database between 1970 and 2008 and an equivalent period (i.e. 39 years) from the synthetic predicted dataset, are shown in **Figure 23a** and **b**, respectively. Generally, the two show similar characteristics. Synthetic cyclone tracks for a 1,000-year period are shown in **Figure 23c** (and the report cover image).

4.3.2 Hydrodynamic simulations

For each of the synthetic tropical cyclone events (about 75,000 in total; mean of 7.5 per year) that represent the equivalent of 10,000 of years of cyclone activity, the profile model described in Section 4.2.2 was used to generate gradient wind and atmospheric pressure fields every hour. This was then used to force the hydrodynamic model. Each tropical cyclone was modelled separately. Each event was assigned a random tide. First a year was chosen at random, from a 19-year period between 1990 and 2009. This time period corresponds to a complete 18.6-year lunar nodal cycle. Once a year was chosen at random, a particular hour in that year was also chosen at random. However, a weighting was applied based on observations from the BOM dataset to account for the cyclone-surge season. The model was then initiated at the chosen hour and run for the duration of the event. Tidal forcing for this period was included. However, to avoid having to warm-up the model from a flat and stationary water surface, which typically requires at least a two-day simulation period, a simulation was run with tide forcing only for the 19-year period and water levels and u and v current velocities were saved every hour. For the randomly chosen hour, these fields were then used as initial conditions for the simulation, which then only required a few hours of warm up. This considerably reduced combined model run times.

For each event, predicted total water levels (i.e. tide + surge) were output for each model grid cell every hour. To output just the surge component, the tidal levels predicted from the simulation run with tide forcing only, for the 19-year period, were subtracted from these results. For each event, the maximum total and surge levels over the duration of the event were calculated and stored.

4.4 Water level exceedance probabilities

First we examine exceedance probabilities for just the surge component of the tropical cyclone simulations. For each year, of the 10,000-year period, the maximum surge levels were calculated for each of the 2,440 coastal model grid points. Annual maxima were then ranked in order of size and the return periods were estimated by taking 1 over the rank divided by the total number of years (e.g. for the second highest predicted surge level at a given location over the 10,000 year simulation period we get a return period of 5,000 years; i.e. $1/(2/10,000)$). A normal kernel function was used to smooth the distribution and give return levels at specified return periods. The 1,000-year surge level is shown in **Figure 24b** for the entire coastline. For comparison, the corresponding estimates (using the AMM fitted to a GUM distribution) from the first stage of the study are shown in **Figure 24a**. It is interesting to see at what return periods the tropical cyclone-induced surges exceed the extra-tropical generated surges. This is shown in **Figure 25**. For the Pilbara coastline (around Port Hedland) the tropical cyclone generated surge return levels are larger than the extra-tropical generated surge return levels between the 0.1-1 year return period. Elsewhere along most of the northern coastline the tropical cyclone generated surge return levels are larger between the 1-10 year return period. Typically, as you move south the return period beyond which the tropical cyclones are larger increases. Along all of the south and southeast part of the coastline the tropical-cyclone-induced surge return levels do not exceed the extra-tropical generated surge level below the 10,000-year return period, as expected.

Now we consider total water level exceedance probabilities. Each of the 75,000 cyclonic events were modelled separately with a random tidal state, hence the predicted levels are a combination of surge and tide. For each event, the maximum water level was extracted for each of the 2,440 coastal model grid points. However, before deriving annual maximum total levels and estimating recurrence intervals, it was necessary to artificially add a random mean sea level state to the maximum levels for each event to get a total water level (i.e. combined mean sea level, tide and surge). As we showed in Section 3.2.2, seasonal mean sea level variations, particularly in the Gulf of Carpentaria, can be very large (up to 1 m). Each cyclone event typically lasted only a matter of days, and the model was only forced with the gradient level wind and pressure fields derived for that particular cyclone.

Hence, the seasonal and inter-annual mean sea level variability observed around Australia is not captured over this short period, as it is caused by longer-term (>month) synoptic pressure and wind changes which were not accounted for in the model. By comparison, these long-term mean sea level changes are reproduced reasonably well in the 61-year hindcast. Hence, for each of the modelled 75,000 cyclone events, a random year, within the 61-year hindcast period from stage 1 was selected and a random hour within that year (weighted for cyclone season) was again chosen. The height of mean sea level component (for each of the 2,440 coastal grid point) at that randomly selected hour was extracted from the 61-year hindcast generated in stage 1 and added to the predicted (tide and surge) values. Following this the maximum total water levels were calculated for each of the 2,440 coastal model grid points for each year, of the 10,000-year simulated period. Again, the annual maxima total levels were ranked and analysed using a probability density estimate based on the normal kernel function to give exceedance probabilities.

The 1,000-year total level is shown in **Figure 26b**. For comparison, the corresponding estimates from the first stage of the study are shown in **Figure 26a**. The total predicted water level return period curves from stage 1 and 2 are shown in **Figure 27** for the grid cells nearest to the 30 validation sites. Again it is interesting to consider at what return periods the tropical cyclone-induced total water levels exceed the extra-tropical generated total water levels. From Albany to Newcastle, the extreme total water levels are completely dominated by extra-tropical storm events. However, for the northern sites the upper return periods are dominated by tropical cyclones. The return periods at which the tropical cyclone-induced total water levels exceed the extra-tropical generated total water levels are shown in **Figure 28** for the entire coastline. Comparing **Figure 25** with **Figure 28**, it is clear that for total water levels the north to south crossover is not as uniform as for the storm surge levels alone. This is expected given that the tidal range varies considerably around Australia. An interesting feature occurs around Fremantle to Bunbury for total water levels, indicating the importance of coastline topography. At Fremantle the tropical-cyclone-induced total return levels do not exceed the extra-tropical generated levels below the 10,000-year return period, whereas further south at Bunbury they do. This is most likely because surges are enhanced in Geographe Bay, whereas the continental shelf is relatively narrow offshore of Fremantle.

To create a final dataset, suitable for coastal engineers and managers, we combined the results for stages 1 and 2. We did this by simply taking whichever return level was higher, from either stage 1 or 2, for different return periods. These values were then linearly interpolated to $1/60^{\text{th}}$ of a degree (~ 2 km) intervals around the coast. The combined 1,000-year total water level is shown in **Figure 29**.

5 Concluding remarks

This study, for the first time, has provided estimates of present day extreme total water level exceedance probabilities around the whole coastline of Australia, arising from combinations of mean sea level, astronomical tide and storm surges generated by both extra-tropical and tropical storms, but exclusive of surface gravity waves. A high-resolution depth averaged hydrodynamic model was configured for the whole coastline of Australia and was used to generate a 61-year time-series of historic water levels around Australia. This predicted dataset was validated against measurements from tide gauge sites around Australia with long records and then used to estimate exceedance probabilities around the entire coastline. To more accurately include tropical cyclone-induced surges in the estimation of extreme total water level probabilities, which are underestimated in the multi-decadal hindcast because of the coarse meteorological forcing used, a statistical model of the tracks and central pressures of tropical cyclones was developed. This was then used to generate 10,000 years of synthetic tropical cyclone events in the Australian region, based on characteristics of tropical cyclone activity over about the last 40 years. Wind and pressure fields were derived for these synthetic events and were used to drive the hydrodynamic model. Annual maximum total levels for these synthetic events were calculated and these were used to estimate exceedance probabilities around the coastline. The exceedance probabilities calculated from the hindcast and synthetic tropical cyclone simulations were then combined to give a single estimate of present extreme water level probabilities around the whole coastline of Australia.

In the first part of the study, a 61-year hindcast of water levels for the Australian continental shelf region was generated. The multi-decadal hindcast generated was then used to estimate current extreme water level AEP around the entire coastline of Australia. However, the long time-series of historic water levels could be used for a wide range of other purposes. For example, the long historic water levels simulated by Flather et al. (1998) for the UK were used by: Butler et al. (2007) to assess decadal variations in storm surges in the North Sea; Wakelin et al. (2003), Tsimplis et al. (2005) and Woodworth et al. (2007) to examine the influence of large scale climate variability, represented by the North Atlantic Oscillation, on sea level; and Woodworth et al. (2009) to remove variability in time-series of annual mean sea level in order to improve longer-term sea-level rise trend

estimates. McMillan et al. (2011) used their long predicted historic water level dataset for the British Isles to create design storm surges around the UK. These can be used in various engineering applications. These examples demonstrate the usefulness of these predicted multi-decadal water level datasets and it is hoped this dataset will be more widely used in the future. In the future we hope to improve the hindcast by: incorporating higher resolution bathymetric data onto the model grid; validating the model with water level measurements from a greater number of tide-gauge sites; and running the model using longer (i.e. Compo et al., 2011) or higher resolution (Saha et al., 2010) meteorological reanalysis, that have recently become available.

The present day extreme total water level exceedance probabilities, estimated in this study, are freely available for coastal engineers and managers via a web-based tool (www.sealevelrise.info). To ensure this information is best used it is important to emphasize several key points:

1. The hydrodynamic modelling was undertaken on grid with a resolution of $1/12^{\text{th}}$ of a degree (~ 10 km) around the coasts (**Figure 2**) and the results were then interpolated down to $1/60^{\text{th}}$ of a degree (~ 2 km) intervals along the whole coastline. The current model resolution accurately predicts water levels along open stretches of coastline and in large bays and inlets, but is not likely to resolve water level propagation in narrow bays, inlets and estuaries (e.g. the Swan or Peel Harvey Estuaries in Western Australia). In these regions, much higher resolution (in many cases <100 m) models are needed to adequately capture the water level propagation into and through the system (see MacPherson et al., 2011).
2. Surface gravity wave effects have been neglected in this study. Higher than normal water levels can occur at the coast during storm events through wave setup and wave runup, but the relative contribution of these to extremes in a given area depends on a number of factors including: continental shelf width; coastal orientation with respect to the prevailing winds during storm events; and coastal features such as headlands, bays and estuaries which can either shelter the coast or amplify extreme sea levels (O'Grady and McInnes, 2010). An Australia wide assessment of wave setup and runup is needed and would enhance the result of this current study.

3. The study focused on estimating present day extreme water level exceedance probabilities. There is strong observation evidence that mean sea levels are rising (Church and White, 2011) and that extreme events are increasing as a result (Lowe et al., 2010). This must be taken into account when estimating future exceedance probabilities. This point is discussed in more detail below.
4. We recognise that several studies were undertaken prior to this current study that have estimated extreme water level recurrence intervals on local and regional scales around Australia. In the future we hope to conduct a detailed comparison of the estimates between these different studies and our study.

Finally, we now briefly review how the exceedance probabilities of extreme water levels around Australia might alter in the future with climate change. Over the 20th century, tide-gauge observations show that global mean sea level on average rose by 17 cm (i.e. 1.7 mm/year) as a result of climate-change-related processes including the melting of land-based ice and the thermal expansion of sea water (Bindoff et al., 2007). One of the most certain consequences of anthropogenic climate change, according to all of the Intergovernmental Panel on Climate Change's (IPCC) assessments (i.e. Meehl et al., 2007; Seneviratne, 2012), is that the global average rate of rise will very likely accelerate over the 21st century and beyond. The IPCC's Fourth Assessment Report (AR4) projected a global mean sea level rise of 0.18 to 0.79 m from 1990 to the 2090's, if 0.2 m is added to the upper limit to account for processes involving land ice in Greenland and Antarctica that were not fully included in the models for this period (Meehl et al. 2007). The lower end of the range is approximately consistent with the continuation of the average rate of rise observed by tide gauges over the 20th century, whilst the upper value represents a significant increase on 20th century rates. Since the publication of the AR4 in 2007, the subject of mean sea level rise has received considerable attention, and there is a view that larger rises (>1m) are possible (Rahmstorf, 2007; Horton et al., 2008; Grinsted et al., 2010; Vermeer and Rahmsdorf, 2009; Jevrejeva et al., 2010; Nicholls et al., 2011).

As Haigh et al. (2011a) point out; changes in mean sea level affect extreme sea levels in two ways:

- (a) Directly: a rise (or fall) in mean sea level will result in a lower (or higher) surge elevation at high tide being necessary to produce a sea level high enough to cause flooding;
- (b) Indirectly: changes in mean sea level alter water depths and hence modify the propagation and dissipation of the astronomical tide and surge components of sea level.

In addition, extreme sea levels can change as a result of variations in the strength and tracks of weather systems which alter the magnitude, duration and intensity of storm surges. Two quasi-global assessments (Woodworth and Blackman, 2004; Menendez and Woodworth; 2010) of past changes in extreme sea levels have found that extremes have increased at most locations around the world over the last century, but largely as a result of changes in mean sea level (i.e. direct changes), and the results of several regional studies (see Lowe et al. (2010) for a review) are in agreement. This implies that indirect changes and variations in storminess have been relatively small at most locations over the past century, but there are some locations like in the German Bight (Mudersbach et al., in review) for example, where this appears not to be the case.

Small increases in mean sea level can result in relatively large increases in the frequency of extreme events. McInnes et al. (2011a; 2011b) showed that a mean sea level rise of 0.1 m (the approximate mid-range estimate for sea level rise projected for 2030) increased the frequency of an extreme sea level event by between 5 and 10 times for Victoria and Tasmania, respectively (i.e. a 1-in-100 year event will become a 1-in-10 to 20 year event). For Western Australia, Haigh and Pattiaratchi (2010b) showed that a mean sea level rise of 0.18 m (lower end of the IPCC's AR4 projections for 2100) increased the frequency of extreme sea level events by between 10 and 50 times. Changing weather patterns will also influence return periods of extreme events. These have recently been investigated over southern Australia by Colberg and McInnes (2012). In general, future weather pattern changes were found to decrease extreme (95th percentile) sea levels by up to 0.1 m along the southern Australian coast and by smaller amounts further west. These changes in extreme sea level are comparatively small, compared with the AR4 projected range of sea level changes over the period from 1990 to 2090. Harper et al. (2009) reported on recent studies on the tropical east coast of Australia that, like this study, utilise synthetically

generated tropical cyclones to force a hydrodynamic model. Mean sea level rise was found to produce a larger contribution to changes in future 1-in-100 year sea level extremes than projected changes in tropical cyclone intensity. Bases on these findings, and others for different parts of the world (again see Lowe et al. (2010) for a review), it seems reasonable to assume that increases in mean sea level will dominate changes in the extreme total water level exceedance probabilities for Australia, and that further increases due to changes in storm patterns will be small by comparison.

Hunter (2010) recently developed a technique for combining the uncertainties in existing extreme water levels with the uncertainties in the projections of mean sea level rise. The results are given in the form of exceedance probability curves as a function of still water level. Each curve represents the likelihood of one or more flooding events at a given height and at one location, over a specified period during the 21st century, under conditions of a prescribed emission scenario. More recently, Hunter (2011) described a simple extension of this technique which enables the objective choice of a vertical allowance for mean sea-level rise (i.e. the amount by which coastal assets need to be raised), given the statistics of present extreme water levels and projections of mean sea-level rise. The method preserves the expected frequency of flooding events if this allowance is applied as mean sea-level rises. These techniques have been implemented into the web-based tool mentioned earlier, which uses the results of this current study.

6 Acknowledgments

We would like to thank the Australian National Tidal Centre, Western Australian Department of Transport, Sydney Ports Corporation and Fremantle Ports for supplying the observational tide-gauge datasets, John Hunter and Tessa Jakszewicz for managing the project, and Matthew Eliot for useful discussions regarding the study. We would also like to acknowledge Kathleen McInnes and Robert Nicholls who formally reviewed this report. Their comments and suggestions greatly improved the final report. This study was funded by the Australian Department of Climate Change and Energy Efficiency and the Western Australian Department of Transport, and builds on an earlier study funded by the Western Australian Marine Science Institution.

7 References

- Bernier, N.B., Thompson, K.R., 2006. Predicting the frequency of storm surges and extreme water levels in the northwest Atlantic. *Journal of Geophysical Research-Oceans*, 111, C10009.
- Bindoff, N.L., Willebrand, J., Artale, V., Cazenave, A., Gregory, J., Gulev, S., Hanawa, K., Le Quéré, C., Levitus, S., Nojiri, Y., Shum, C.K., Talley L.D., Unnikrishnan, A., 2007. Observations: Oceanic climate change and sea level. In: *Climate Change 2007: The physical science basis. Contribution of working group I to the Fourth Assessment Report of the Intergovernmental Panel on Climate Change*. Editors: Solomon, S., Qin, D., Manning, M., Chen, Z., Marquis, M., Averyt, K.B., Tignor M., Miller H.L. Cambridge University Press, Cambridge, United Kingdom and New York, NY, USA, pp. 385-432.
- Butler, A., Heffernan, J.E., Tawn, J.A., Flather, R.A., Horsburgh K.J., 2007. Extreme value analysis of long-term variations in storm surges. *Journal of Marine Systems*, 67, 189-200.
- Cardone, V.J., Cox, A.T., Greenwood, J.A, Thompson, E.F., 1994. Upgrade of tropical cyclone surface wind field model. Miscellaneous Paper, CERC-94-14, prepared for U.S. Army Corps of Engineers (101pp.).
- Church, J., White, N., 2011. Sea-Level Rise from the Late 19th to the Early 21st Century, *Surveys in Geophysics*, 32(4), 585-602.
- Colberg, F., McInnes, K.L., 2012. The impact of storminess changes on extreme sea levels over southern Australia. In press *JGR-Oceans*.
- Coles, S., 2001. *An Introduction to Statistical Modelling of Extreme Values*. Springer. (207pp.).
- Compo, G.P., Whitaker, J.S., Sardeshmukh, P.D., Matsui, N., Allan, R.J., Yin, X., Gleason, B.E., Vose, R.S., Rutledge, G., Bessemoulin, P., Brönnimann, S., Brunet, M., Crouthamel, R.I., Grant, A.N., Groisman, P.Y., Jones, P.D., Kruk, M.C., Kruger, A.C., Marshall, G.J., Maugeri, M., Mok, H.Y., Nordli, Ø., Ross, T.F., Trigo, R.M., Wang, X.L., Woodruff, S.D., Worley, S.J., 2011. The Twentieth Century Reanalysis Project. *Quart. J. Roy. Meteor. Soc.*, 137, 1-28. DOI:10.1002/qj.776.
- Danish Hydraulic Institute, 2010. Mike 21 & Mike 3 flow model FM, Hydrodynamic and transport module scientific documentation.

-
- Debernard, J., Saeltra, O., Roed, L.P., 2002. Future wind, wave and storm surge climate in the northern North Atlantic. *Climate Research*, 23(1), 39-49.
- Dixon, M.J., Tawn, J.A., 1999. The Effect of non-stationary on extreme sea-level estimation. *Applied Statistics*, 48 (2), 135-151.
- Egbert, G.D., Bennett, A.F., Foreman, M.G.G., 1994. TOPEX/POSEIDON tides estimated using a global inverse model. *J. Geophys. Res.*, 99(C12), 24821-24852.
- Egbert, G.D., Erofeeva, S.Y., 2002. Efficient Inverse Modeling of Barotropic Ocean Tides. *Journal of Atmospheric and Oceanic Technology*, 19(2), 183-204.
- Eliot, M., 2012. Sea level variability influencing coastal flooding in the Swan River region, Western Australia. *Continental Shelf Research*, 33, 14-28.
- Fandry, C.B., Hubbert, G.D., McIntosh, P.C., 1985. Comparison of predictions of a numerical model and observations of tides in Bass Strait. *Australian Journal of Marine and Freshwater Research*, 36(6) 737–752.
- Flather, R.A., 1987. Estimates of extreme conditions of tide and surges using a numerical model of the North-west European Continental Shelf. *Estuarine, Coastal and Shelf Science*, 24, 69-93.
- Flather R.A., 2000. Existing operational oceanography. *Coastal Eng.*, 41, 13–40.
- Flather, R.A., Smith, J.A., 1998. First estimates of changes in extreme storm surge elevations due to the doubling of CO₂. *Global Atmosphere and Ocean System*, 6 (2), 193-208.
- Flather, R.A., Smith, J.A., Richards, J.D., Bell, C., Blackman, D.L., 1998. Direct estimates of extreme storm surge elevations from a 40-year numerical model simulation and from observations. *The Global Atmosphere and Ocean Systems*, 6, 165-176.
- Georgiou, P.N., Davenport, A.G., Vickery, B.J., 1983. Design wind speeds in regions dominated by tropical cyclones. *Journal of Wind Engineering and Industrial Aerodynamics*, 13, 139-152.
- Grinsted, A., Moore, J.C., Jevrejeva, S., 2010. Reconstructing sea level from paleo and projected temperatures 200 to 2100 ad, *Climate Dynamics*, 34(4), 461-472.
- Haigh, I.D., Nicholls, R.J., Wells, N.C., 2010a. A comparison of the main methods for estimating probabilities of extreme still water levels. *Coastal Engineering*, 57(9), 838-849.

-
- Haigh, I.D., Pattiaratchi, C., 2010b. 21st century changes in extreme sea levels around Western Australia. Proceedings of the 17th National Australian Meteorological & Oceanographic Society Conference, Canberra, Australia.
- Haigh, I.D., Nicholls, R.J., Wells, N.C., 2011a. Rising sea levels in the English Channel 1900 to 2100. Proceedings of ICE Maritime Engineering, 164 (2), 81-92.
- Haigh, I.D., Eliot, M., Pattiaratchi, C., 2011b. Global influences of the 18.61 year nodal cycle and 8.85 year cycle of lunar perigee on high tidal levels, J. Geophys. Res., 116, C06025, doi:10.1029/2010JC006645.
- Haigh, I.D., Eliot, M., Pattiaratchi, C., 2011c. Regional changes in mean sea level around Western Australia between 1897 and 2008. Coasts and Ports Conference, Perth, Australia (28-30 Sep 2010).
- Hardy, T.A., McConochie, J.D., Mason, L.B., 2003. Modeling tropical cyclone wave population of the Great Barrier Reef. Journal of Waterway, Port, Coastal and Ocean Engineering, May/June, 104-113.
- Harper, B.A. (ed), 2001. Queensland climate change and community vulnerability to tropical cyclones— ocean hazards assessment stage 1—review of technical requirements. Report prepared by Systems Engineering Australia Pty Ltd in association with James Cook University Marine Modelling Unit, Queensland Government, 375 pp, March 2001.
- Harper, B.A., Holland, G.J., 1999. An updated parametric model of the tropical cyclone. In 23rd Conference on Hurricanes and Tropical Meteorology, 893-896.
- Harper, B.A., Stroud, S.A., McCormack, M., West, S., 2008. A review of historical tropical cyclone intensity in northwestern Australia and implications for climate change trend analysis. Australian Meteorological Magazine, 57, 121-141.
- Harper, B., Hardy, T., Mason, L., Fryar, R., 2009. Developments in storm tide modelling and risk assessment in the Australian region. Natural Hazards 51, 225-238.
- Holland, G. J., 1980: An Analytic Model of the Wind and Pressure Profiles in Hurricanes. Monthly Weather Review, 108, 1212-1218.
- Holmes, J.D., 2001. Wind Loading of Structures. Spon Press, London, 356 pages.
- Horsburgh, K.L., Wilson, C., 2007. Tide-surge interaction and its role in the distribution of surge residuals in the North Sea. Journal of Geophysical Research, 112, C08003.

-
- Horton, R., Herweijer, C., Rosenzweig, C., Liu, J., Gornitz, V., Ruane, A.C., 2008. Sea level rise projections for current generation CGCMs based on the semi-empirical method. *Geophys. Res. Lett.*, 35(2), L02715.
- Hunter, J., 2010. Estimating sea-level extremes under conditions of uncertain sea-level rise. *Climatic Change*, 99(3), 331-350.
- Hunter, J., 2011. A simple technique for estimating an allowance for uncertain sea-level rise. *Climatic Change*, DOI: 10.1007/s10584-011-0332-1.
- James, M.K., Mason, L.B., 2005. Synthetic tropical cyclone database. *Journal of waterway, port, coastal, and ocean engineering*, 131 (4), 181-192.
- Jevrejeva, S., Moore, J.C., Grinsted, A., 2010. How will sea level respond to changes in natural and anthropogenic forcings by 2100? *Geophys. Res. Lett.*, 37(7), L07703.
- Kalnay, E., Kanamitsu, M., Kistler, R., Collins, W., Deaven, D., Gandin, L. Iredell, M., Saha, S., White, G., Woollen, J., Zhu, Y., Leetmaa, A., Reynolds, R., Chelliah, M., Ebisuzaki, W., Higgins, W., Janowiak, J., Mo, K.C. Ropelewski, C., Wang, J. Jenne, R., Joseph, D., 1996. The NCEP/NCAR 40-year reanalysis project *Bull. Amer. Meteor. Soc.* 77 437-70.
- Kaplan, J., DeMaria, M., 1995. A simple empirical model for predicting the decay of tropical cyclone winds after landfall. *Journal of Applied Meteorology*, 34, 2499-2512.
- Kepert, J., 2001. The dynamics of boundary layer jets within the tropical cyclone core. Part 1: Linear Theory. *Journal of the Atmospheric Sciences*, 58, 2469-2484.
- Kistler, R. Kalnay, E., Collins, W., Saha, S., White, G. Woollen, J. Chelliah, M. Ebisuzaki, W., Kanamitsu, M. Kousky, V., Dool, H., Jenne, R. and Fiorino, M., 2001. The NCEP-NCAR 50-Year Reanalysis: Monthly Means CD ROM and Documentation. *Bulletin of the American Meteorological Society*, 82(2), 247-267.
- Langenberg, H., Pfizenmayer, A., von Storch H., Sündermann, J., 1999. Storm-related sea level variations along the North Sea coast: natural variability and anthropogenic change. *Continental Shelf Research*, 19 (6), 821-842.
- Lowe, J.A., Gregory, J.M., Flather, R.A., 2001. Changes in the occurrence of storm surges around the United Kingdom under a future climate scenario using a dynamic storm surge model driven by the Hadley Centre climate models. *Climate Dynamics*, 18 (3/4), 179- 188.

-
- Lowe, J.A., Gregory, J.M., 2005. The effects of climate change on storm surges around the United Kingdom. *Philosophical Transactions of the Royal Society of London*, A363 (1831), 1313-1328.
- Lowe, J.A., Woodworth, P.L., Knutson, T., McDonald, R.E., McInnes, K., Woth, K., Von Storch, H., Wolf, J., Swail, V., Bernier, N., Gulev, S., Horsburgh, K., Unnikrishnan, A.S., Hunter, J., Weisse, R., 2010. Past and future changes in extreme water levels and waves. In: *Understanding sea-level rise and variability*. (Church, J.A., Woodworth, P.L., Aarup T., Wilson, S. (eds)). Wiley-Blackwell.
- MacPherson, L.R., Haigh, I.D., Pattiaratchi, C., 2011. Coastal flooding in the Peel Harvey Estuary and the effects of mean sea level rise. *Coasts and Ports Conference*, Perth, Australia (28-30 Sep 2011).
- McConochie, J.D., Mason, L.B., Hardy, T.A., 1999. A Coral Sea cyclone wind model intended for wave modelling. In: *Proceedings of 14th Conference on Coastal and Ocean Engineering*, IEAust, Perth, 413-418.
- McConochie, J.D., Hardy, T.A., Mason, L.B., 2004. Modelling tropical cyclone over-water wind and pressure fields. *Ocean Engineering*, 31, 1757-1782.
- McInnes, K.L., Hubbert, G.D., 2003, A numerical modelling study of storm surges in Bass Strait. *Aust. Meteorol. Mag.*, 52, 3, 143–156.
- McInnes K.L., Macadam I., Hubbert, G.D., O'Grady, J. D., 2009. A modelling approach for estimating the frequency of sea level extremes and the impact of climate change in southeast Australia. *Natural Hazards*, 51, 115-37.
- McInnes, K.L., Macadam, I., Hubbert, G.D., O'Grady, J.G., 2011a. An assessment of current and future vulnerability to coastal inundation due to sea level extremes in Victoria, southeast Australia. *Int. J. Clim.* DOI: 10.1002/joc.3405.
- McInnes, K.L., O'Grady, J.G., Hemer, M., Macadam, I., Abbs, D.J., White, C.J., Bennett, J.C., Corney, S.P., Holz, G.K., Grose, M.R., Gaynor, S.M., Bindoff, N.L., 2011b. *Climate future for Tasmania: Extreme tide and sea-level events*. Technical Report, Antarctic Climate and Ecosystems Corporate Research Centre.
- McInnes, K.L., Walsh, K.J.E., Hubbert, G.D., Beer, T., 2003. Impact of Sea-level Rise and Storm Surges on a Coastal Community. *Nat. Haz.* 30(2) 187-207.
- McIntosh, P.C., Bennett, A.F., 1984. Open ocean modeling as an inverse problem: M2 tides in Bass Strait, *J. Phys. Oceanogr.*, 14, 3, 601–614.

-
- McMillan, A., Batstone, C., Worth, D., Tawn, J., Horsburgh, K., Lawless, M., 2011. Coastal flood boundary conditions for UK mainland and islands. Technical Report, Project: SC060064/TR2. [accessed 30/08/2011].
<http://publications.environment-agency.gov.uk/PDF/SCHO0111BTKI-E-E.pdf>
- Meehl, G.A., Stocker, T.F., Collins, W.D., Friedlingstein, P., Gaye, A.T., Gregory, J.M., Kitoh, A., Knutti, R., Murphy, J.M., Noda, A., Raper, S.C.B., Watterson, I.G., Weaver A.J., Zhao, Z.C., 2007. Global climate projections. In: Climate change 2007: The physical science basis. Contribution of working group I to the Fourth Assessment Report of the Intergovernmental Panel on Climate Change. Editors: Solomon, S., Qin, D., Manning, M., Chen, Z., Marquis, M., Averyt, K.B., Tignor M., Miller H.L., Cambridge University Press, Cambridge, United Kingdom and New York, NY, USA, pp. 747-845.
- Menéndez, M., Woodworth, P.L., 2010, Changes in extreme high water levels based on a quasi-global tide-gauge dataset. *J. Geophys. Res.*, 115 (C10), C10011.
- Mudersbach, C., Wahl, T., Haigh, I.D., Jensen, J., in review. Trends in extreme high sea levels along the German North Sea coastline compared to regional mean sea level changes. Submitted to *Continental Shelf Research* in June 2011.
- Nicholls, R.J., Wong, P.P., Burkett, V.R., Codignotto, J.O., Hay, J.E., McLean, R.F., Ragoonaden, S., Woodroffe, C.D., 2007. Coastal systems and low - lying areas, in *Climate Change 2007: Impacts, Adaptation and Vulnerability, Contribution of Working Group II to the Fourth Assessment Report of the Intergovernmental Panel on Climate Change*, edited by M. L. Parry et al., pp. 315–356, Cambridge Univ. Press, Cambridge, U. K.
- Nicholls, R.J., Marinova, N., Lowe, J.A., Brown, S., Vellinga, P., de Gusmao, D., Hinkel, J., Tol, R.S.J., 2011. Sea-level rise and its possible impacts given a ‘beyond 4°C world’ in the twenty-first century. *Philosophical Transactions of the Royal Society A: Mathematical, Physical and Engineering Sciences*, 369(1934), 161-181.
- O’Grady, J.G., McInnes, K.L., 2010. Extreme wind waves and their relationship to storm surges in northeastern Bass Strait. *Australian Meteorology and Oceanography Journal*, 60, 265-275.
- Pattiaratchi, C., Eliot, M., Haigh, I.D., Wijeratne, E.M.S., in prep. Physical Processes controlling tidal and non-tidal sea level variability in Western Australia. Plan to submit to *Continental Shelf Research*.

-
- Pawlowicz, R., Beardsley, B., Lentz, S., 2002. Classical tidal harmonic analysis including error estimates in MATLAB using T_TIDE. *Computers & Geosciences*, 28(8), 929-937.
- Pugh, D.T., 1987. *Tides, surges and mean sea-level. A handbook for engineers and scientists.* Wiley, Chichester, 472pp.
- Pugh, D.T., 2004. *Changing sea levels: effects of tides, weather and climate.* Cambridge University Press, Cambridge, United Kingdom, 280pp.
- Pugh, D.T., Vassie, J.M., 1979. Extreme sea-levels from tide and surge probability. *Proceedings of the Sixteenth Coastal Engineering Conference, Hamburg, German, 27 Aug-3 Sep 1978.* American Society of Civil Engineers, New York, Volume 1, 911–930.
- Pugh, D.T., Vassie, J.M., 1980. Applications of the joint probability method for extreme sea- level computations. *Proceedings of the Institution of Civil Engineers Part 2*, 69, 959-975.
- Rahmstorf, S., 2007. A semi-empirical approach to projecting future sea-level rise, *Science*, 315(5810), 368-370.
- Saha S., Moorthi, S., Wu, X., Wang, J., Nadiga, S., Tripp, P., Pan, H., Behringer, D., Hou, Y., Chuang, H., Iredell, M., Ek, M. Meng, J., Yang, R., Dool, H., Zhang, Q., Wang, W., Chen, M., 2010: The NCEP Climate Forecast System Reanalysis. *Bull. Amer. Meteor. Soc.*, 91, 1015–1057. doi: 10.1175/2010BAMS3001.1
- Sebastiao, P., Soares, C.G., Alvarez, E., 2008. 44 years hindcast of sea level in the Atlantic Coast of Europe. *Coastal Engineering*, 55(11), 843-848.
- Seneviratne, S.I., Nicholls, N., Easterling, D., Goodess, C.M., Kanae, S., Kossin, J., Luo, Y., Marengo, J., McInnes, K., Rahimi, M., Reichstein, M., Sorteberg, A., Vera, C., Zhang, X., 2012. Changes in climate extremes and their impacts on the natural physical environment. In: *Managing the Risks of Extreme Events and Disasters to Advance Climate Change Adaptation* [Field, C.B., Barros, V., Stocker, T.F., Qin, D., Dokken, D.J., Ebi, K.L., Mastrandrea, M.D., Mach, K.J., Plattner, G.K., Allen, S.K., Tignor, M., Midgley, P.M. (eds.)]. A Special Report of Working Groups I and II of the Intergovernmental Panel on Climate Change (IPCC). Cambridge University Press, Cambridge, UK, and New York, NY, USA, pp. 109-230.
- Simiu, E., Scanlan, R.H., 1986. *Wind Effects on Structures*, 2nd Edition, Wiley-Interscience, New York.

-
- Sterl, A., 2004. On the (In)Homogeneity of Reanalysis Products, *Journal of Climate*, 17(19), 3866-3873.
- Tawn, J.A., Vassie, J.M., 1989. Extreme sea-levels: The joint probabilities method revisited and revised. *Proceedings of the Institute of Civil Engineering Part 2*, 87, 249-442.
- Tsimplis, M.N., Woolf, D.K., Osborn, T., Wakelin, S., Woodworth, P., Wolf, J., Flather, R., Blackman, D., Shaw, A.G.P., Pert F., Challenor, P., Yan, Z., 2005. Towards a vulnerability assessment of the UK and northern European coasts: the role of regional climate variability. *Philosophical Transactions of the Royal Society of London*, A363 (1831), 1329-1358.
- Uhlhorn, E.W., Black, P.G., Franklin, J.L., Goodberlet, M., Carswell, J., Goldstein, A.S., 2007. Hurricane surface wind measurements from an operational stepped frequency microwave radiometer. *Monthly Weather Review*, 135, 3070-3085.
- Unnikrishnan, A.S., Rupa Kumar, K., Fernandes, S.E., Michael, G.S., Patwardhan, S.K., 2006. Sea level changes along the Indian coast: Observations and projections. *Current Science*, 90 (3), 362-368.
- Uppala, S.M., Kållberg, P.W., Simmons, A.J., Andrae, U., da Costa Bechtold, V., Fiorino, M., Gibson, J.K., Haseler, J., Hernandez, A., Kelly, G.A., Li, X., Onogi, K., Saarinen, S., Sokka, N., Allan, R.P., Andersson, E., Arpe, K., Balmaseda, M.A., Beljaars, A.C.M., van de Berg, L., Bidlot, J., Bormann, N., Caires, S., Chevallier, F., Dethof, A., Dragosavac, M., Fisher, M., Fuentes, M., Hagemann, S., Hólm, E., Hoskins, B.J., Isaksen, L., Janssen, P.A.E.M., Jenne, R., McNally, A.P., Mahfouf, J.-F., Morcrette, J.-J., Rayner, N.A., Saunders, R.W., Simon, P., Sterl, A., Trenberth, K.E., Untch, A., Vasiljevic, D., Viterbo, P., Woollen, J., 2005. The ERA-40 re-analysis. *Quart. J. R. Meteorol. Soc.*, 131, 2961-3012. doi:10.1256/qj.04.176.
- Vermeer, M., Rahmstorf, S., 2009. Global sea level linked to global temperature. *Proceedings of the National Academy of Sciences*, 106, 21527.
- Vickery, P.J., Skerlj, P.F., Twisdale, L.A., 2000. Simulation of hurricane risk in the U.S. using empirical track model. *Journal of Structural Engineering*, October, 1222-1237.
- von Storch, H., Woth, K., 2008. Storm surges: perspectives and options. *Sustainability Science* 3, 33-43.

-
- Wakelin S.L., Woodworth P.L., Flather, R.A., Williams J.A., 2003. Sea-level dependence on the NAO over the NW European Continental Shelf. *Geophysical Research Letters*, 30 (7), 1403.
- Webster, M.A., Petkovic P., 2005. Australian Bathymetry and Topography Grid, June 2005. Record 2005/12.
- Weisse, R., Plüß, A., 2006. Storm-related sea level variations along the North Sea coast as simulated by a high-resolution model 1958–2002, *Ocean Dynamics*, 56, 16-25.
- Wijeratne, E.M.S., Pattiaratchi, C., Eliot, M., Haigh, I.D., in review. Tidal characteristics in Bass Strait, southeast Australia. Submitted to *Estuarine, Coastal and Shelf Research* in Nov 2011.
- Wijeratne, E.M.S., Pattiaratchi, C., Haigh, I.D., Eliot, M., in prep. The seasonal cycle of sea level around Australia. Plan to submit to *Journal of Geophysical Research Oceans*.
- Woodworth, P. L., Blackman, D.L., 2004. Evidence for systematic changes in extreme high waters since the mid - 1970s. *J. Clim.*, 17(6), 1190–1197.
- Woodworth, P.L., Flather, R.A., Williams, J.A., Wakelin, S.L., Jevrejeva, S., 2007. The dependence of UK extreme water levels and storm surges on the North Atlantic Oscillation. *Continental Shelf Research*, 27, 935-946.
- Woodworth, P.L., Teferle, R.M., Bingley, R.M., Shennan, I., Williams, S.D.P., 2009. Trends in UK mean sea level revisited. *Geophysical Journal International*. 176 (1), 19-30.
- Woth, K., 2005. North Sea storm surge statistics based on projections in a warmer climate: How important are the driving GCM and the chosen emission scenario? *Geophysical Research Letters*, 32, L22708.
- Woth, K., Weisse, R., von Storch, H., 2006. Climate change and North Sea storm surge extremes: An ensemble study of storm surge extremes expected in a changed climate projected by four different Regional Climate Models. *Ocean Dynamics*, 56, 3-15.
- Zhang, K., Douglas, B.C., Leatherman, S.P., 1997. East coast storm surges provide unique climate record. *EOS, Transactions of the American Geophysical Union* 78 (37), 389–397.
- Zhang, K., Douglas, B.C., Leatherman, S.P., 2000. Twentieth-century storm activity along the US east coast. *Journal of Climate* 13, 1748–1761.

TABLES

Table 1: Key parameterizations used in the Mike21 model.

| Parameter | Description |
|------------------------|---|
| Open tidal boundaries | Water level time series derived from eight primary (M_2 , S_2 , N_2 , K_2 , K_1 , O_1 , P_1 , Q_1), two long period (M_f , M_m) and three non-linear (M_4 , MS_4 , MN_4) tidal constituents from the TPXO7.2 global ocean model, plus 16 other minor constituents, inferred using the eight primary constituents. |
| Meteorological forcing | Spatially varying mean sea level pressure and u and v components of 10 m wind field from the US National Center for Environmental Prediction's/National Center for Atmospheric Research's global reanalysis on a $2.5^\circ \times 2.5^\circ$ grid every 6 hours. |
| Bed friction | Manning number, constant value 0.031 (default Mike21 value) |

Table 1: Details of the tide gauge records used for model validation.

| Site Number | Site Name | Latitude (decimal degree) | Longitude (decimal degree) | Period | Number of Years (range) |
|--------------------|-----------------------|----------------------------------|-----------------------------------|---------------|--------------------------------|
| 1 | Point Lonsdale | -38.2933 | 144.6148 | 1962-2009 | 48 (48) |
| 2 | Geelong | -38.0920 | 144.3933 | 1966-2009 | 43 (44) |
| 3 | Williamstown | -37.8657 | 144.9165 | 1966-2009 | 44 (44) |
| 4 | Fort Denison | -33.8500 | 151.2333 | 1914-2009 | 95 (96) |
| 5 | Newcastle | -32.9333 | 151.7833 | 1957-2009 | 46 (54) |
| 6 | Brisbane | -27.3667 | 153.1667 | 1977-2009 | 33 (33) |
| 7 | Bundaberg | -24.7717 | 152.3800 | 1966-2009 | 44 (44) |
| 8 | Mackay | -21.2667 | 149.3167 | 1966-2009 | 38 (44) |
| 9 | Townsville | -19.2500 | 146.8333 | 1959-2009 | 51 (51) |
| 10 | Cairns | -16.9167 | 145.7833 | 1966-2009 | 32 (44) |
| 11 | Milner Bay | -13.8600 | 136.4158 | 1993-2009 | 17 (17) |
| 12 | Darwin | -12.4719 | 130.8458 | 1966-2009 | 44 (44) |
| 13 | Wyndham | -15.4500 | 128.1000 | 1966-2009 | 43 (44) |
| 14 | Broome | -18.0008 | 122.2183 | 1966-2009 | 41 (44) |
| 15 | Port Hedland | -20.3000 | 118.5833 | 1966-2009 | 44 (44) |
| 16 | Carnarvon | -24.8833 | 113.6167 | 1965-2009 | 41 (45) |
| 17 | Geraldton | -28.7833 | 114.5833 | 1965-2009 | 45 (45) |
| 18 | Fremantle | -32.0557 | 115.7373 | 1897-2009 | 108 (113) |
| 19 | Bunbury | -33.3167 | 115.6500 | 1966-2009 | 43 (44) |
| 20 | Albany | -35.0333 | 117.8889 | 1966-2009 | 44 (44) |
| 21 | Esperance | -33.8709 | 121.8954 | 1966-2009 | 44 (44) |
| 22 | Thevenard | -32.1490 | 133.6416 | 1966-2009 | 44 (44) |
| 23 | Port Lincoln | -34.7159 | 135.8701 | 1965-2009 | 45 (45) |
| 24 | Port Pirie | -33.1776 | 138.0117 | 1941-2009 | 69 (69) |
| 25 | Port Adelaide (Outer) | -34.7798 | 138.4807 | 1940-2009 | 70 (70) |
| 26 | Port Adelaide (Inner) | -34.8500 | 138.5000 | 1933-1999 | 47 (67) |
| 27 | Victor Harbour | -35.5625 | 138.6354 | 1965-2009 | 45 (45) |
| 28 | Hobart | -42.8833 | 147.3333 | 1962-2009 | 40 (48) |
| 29 | George Town | -41.1083 | 146.8167 | 1967-1997 | 31 (31) |
| 30 | Burnie | -41.0500 | 145.9147 | 1952-2009 | 43 (58) |

Table 3: Mean absolute amplitude and phase errors of the main eight tidal constituents, estimated from the measured and predicted datasets, for the 30 validation sites. The numbers in brackets are the mean absolute differences between the measured and TPOX7.2 global ocean tidal model for the 30 validation sites.

| Tidal constituent | Mean absolute amplitude error (meters) | Mean absolute phase error (degrees) |
|--------------------------|---|--|
| M₂ | 0.106 (0.181) | 10 (15) |
| S₂ | 0.057 (0.086) | 11 (16) |
| N₂ | 0.017 (0.047) | 12 (15) |
| K₂ | 0.015 (0.032) | 11 (18) |
| K₁ | 0.022 (0.049) | 9 (13) |
| O₁ | 0.030 (0.031) | 6 (13) |
| Q₁ | 0.014 (0.022) | 6 (14) |
| P₁ | 0.007 (0.015) | 9 (18) |

Table 4: Root mean square errors (RMSE), mean standard deviation errors (STD) and correlation coefficients for the hourly mean sea level (MSL), astronomical tide, surge and total water levels for 1995, at the 30 validation sites. Units are in meters.

| Site number | Site name | RMSE | | | | STD | | | | Correlation coefficient | | | |
|-------------|-----------------------|------|------|-------|-------|------|------|-------|-------|-------------------------|------|-------|-------|
| | | MSL | TIDE | SURGE | TOTAL | MSL | TIDE | SURGE | TOTAL | MSL | TIDE | SURGE | TOTAL |
| 1 | Point Lonsdale | 0.06 | 0.24 | 0.04 | 0.25 | 0.04 | 0.14 | 0.03 | 0.15 | 0.39 | 0.79 | 0.90 | 0.75 |
| 2 | Geelong | 0.09 | 0.09 | 0.05 | 0.13 | 0.04 | 0.06 | 0.04 | 0.10 | 0.61 | 0.90 | 0.85 | 0.86 |
| 3 | Williamstown | 0.06 | 0.08 | 0.04 | 0.11 | 0.04 | 0.05 | 0.03 | 0.08 | 0.65 | 0.89 | 0.93 | 0.87 |
| 4 | Fort Denison | 0.05 | 0.05 | 0.05 | 0.09 | 0.05 | 0.03 | 0.04 | 0.07 | 0.25 | 0.99 | 0.68 | 0.97 |
| 5 | Newcastle | 0.04 | 0.05 | 0.05 | 0.08 | 0.02 | 0.04 | 0.04 | 0.06 | 0.28 | 0.99 | 0.69 | 0.97 |
| 6 | Brisbane | 0.05 | 0.32 | 0.06 | 0.33 | 0.04 | 0.17 | 0.05 | 0.19 | 0.40 | 0.77 | 0.38 | 0.76 |
| 7 | Bundaberg | 0.03 | 0.13 | 0.06 | 0.14 | 0.02 | 0.08 | 0.04 | 0.10 | 0.80 | 0.98 | 0.25 | 0.98 |
| 8 | Mackay | 0.04 | 0.45 | 0.06 | 0.45 | 0.01 | 0.27 | 0.05 | 0.28 | 0.94 | 0.93 | 0.55 | 0.93 |
| 9 | Townsville | 0.04 | 0.07 | 0.05 | 0.10 | 0.04 | 0.06 | 0.04 | 0.08 | 0.88 | 0.99 | 0.60 | 0.99 |
| 10 | Cairns | 0.04 | 0.09 | 0.05 | 0.11 | 0.04 | 0.07 | 0.04 | 0.09 | 0.75 | 0.98 | 0.42 | 0.98 |
| 11 | Darwin | 0.08 | 0.11 | 0.05 | 0.14 | 0.05 | 0.07 | 0.05 | 0.11 | 0.98 | 0.90 | 0.79 | 0.91 |
| 12 | Milner Bay | 0.08 | 0.22 | 0.05 | 0.24 | 0.05 | 0.21 | 0.04 | 0.22 | 0.91 | 0.98 | 0.57 | 0.98 |
| 13 | Wyndham | 0.09 | 0.36 | 0.10 | 0.37 | 0.02 | 0.23 | 0.10 | 0.24 | 0.98 | 0.98 | 0.21 | 0.98 |
| 14 | Broome | 0.06 | 0.17 | 0.05 | 0.18 | 0.04 | 0.10 | 0.04 | 0.12 | 0.92 | 1.00 | 0.71 | 1.00 |
| 15 | Port Hedland | 0.04 | 0.18 | 0.04 | 0.19 | 0.03 | 0.15 | 0.03 | 0.15 | 0.86 | 0.99 | 0.78 | 0.99 |
| 16 | Carnarvon | 0.14 | 0.09 | 0.05 | 0.16 | 0.05 | 0.06 | 0.04 | 0.11 | 0.65 | 0.95 | 0.84 | 0.92 |
| 17 | Geraldton | 0.13 | 0.04 | 0.05 | 0.14 | 0.05 | 0.03 | 0.04 | 0.09 | 0.88 | 0.95 | 0.91 | 0.90 |
| 18 | Fremantle | 0.12 | 0.05 | 0.05 | 0.13 | 0.05 | 0.03 | 0.04 | 0.09 | 0.83 | 0.93 | 0.89 | 0.87 |
| 19 | Bunbury | 0.11 | 0.05 | 0.06 | 0.13 | 0.05 | 0.03 | 0.04 | 0.09 | 0.86 | 0.94 | 0.88 | 0.88 |
| 20 | Albany | 0.07 | 0.04 | 0.05 | 0.09 | 0.04 | 0.03 | 0.04 | 0.07 | 0.87 | 0.97 | 0.88 | 0.92 |
| 21 | Esperance | 0.11 | 0.04 | 0.05 | 0.12 | 0.05 | 0.03 | 0.04 | 0.08 | 0.82 | 0.97 | 0.90 | 0.92 |
| 22 | Thevenard | 0.05 | 0.11 | 0.07 | 0.13 | 0.04 | 0.08 | 0.05 | 0.10 | 0.89 | 0.94 | 0.89 | 0.93 |
| 23 | Port Lincoln | 0.13 | 0.08 | 0.05 | 0.15 | 0.04 | 0.06 | 0.04 | 0.10 | 0.92 | 0.96 | 0.92 | 0.94 |
| 24 | Port Pirie | 0.04 | 0.19 | 0.08 | 0.21 | 0.02 | 0.13 | 0.07 | 0.15 | 0.87 | 0.97 | 0.87 | 0.95 |
| 25 | Port Adelaide (Outer) | 0.11 | 0.22 | 0.06 | 0.24 | 0.04 | 0.14 | 0.05 | 0.17 | 0.95 | 0.94 | 0.92 | 0.93 |
| 26 | Port Adelaide (Inner) | 0.05 | 0.20 | 0.06 | 0.22 | 0.03 | 0.13 | 0.05 | 0.14 | 0.96 | 0.94 | 0.93 | 0.94 |
| 27 | Victor Harbour | 0.09 | 0.07 | 0.05 | 0.12 | 0.04 | 0.06 | 0.04 | 0.09 | 0.92 | 0.93 | 0.92 | 0.90 |
| 28 | Hobart | 0.08 | 0.07 | 0.06 | 0.11 | 0.03 | 0.06 | 0.05 | 0.09 | 0.90 | 0.96 | 0.79 | 0.93 |
| 29 | George Town | 0.05 | 0.28 | 0.06 | 0.29 | 0.03 | 0.15 | 0.05 | 0.17 | 0.80 | 0.93 | 0.74 | 0.92 |
| 30 | Burnie | 0.04 | 0.15 | 0.04 | 0.17 | 0.02 | 0.09 | 0.04 | 0.10 | 0.68 | 0.99 | 0.84 | 0.99 |
| All | Mean | 0.07 | 0.14 | 0.05 | 0.18 | 0.04 | 0.10 | 0.04 | 0.12 | 0.78 | 0.94 | 0.75 | 0.92 |

Table 5: Comparison of the 10-, 50- and 100-year measured and predicted return levels for 2010 (m, relative to AHD) estimated using the AMM fitted to the GEV distribution, at the 30 validation sites.

| Site Number | Site Name | 10-year return period | | | 50-year return period | | | 100-year return period | | |
|-------------|-----------------------|-----------------------|-------------|-----------|-----------------------|-------------|-----------|------------------------|-------------|-----------|
| | | Meas. | Mod. | Abs. Dif. | Meas. | Mod. | Abs. Dif. | Meas. | Mod. | Abs. Dif. |
| 1 | Point Lonsdale | 1.18 | 1.18 | 0.00 | 1.27 | 1.31 | 0.04 | 1.32 | 1.43 | 0.11 |
| 2 | Geelong | 1.02 | 1.00 | 0.02 | 1.08 | 1.11 | 0.03 | 1.11 | 1.21 | 0.10 |
| 3 | Williamstown | 1.03 | 1.08 | 0.04 | 1.10 | 1.23 | 0.13 | 1.13 | 1.34 | 0.21 |
| 4 | Fort Denison | 1.35 | 1.31 | 0.04 | 1.46 | 1.37 | 0.09 | 1.55 | 1.41 | 0.14 |
| 5 | Newcastle | 1.25 | 1.20 | 0.04 | 1.34 | 1.26 | 0.08 | 1.42 | 1.30 | 0.11 |
| 6 | Brisbane | 1.65 | 1.61 | 0.04 | 1.69 | 1.64 | 0.05 | 1.70 | 1.65 | 0.05 |
| 7 | Bundaberg | 2.02 | 1.94 | 0.08 | 2.11 | 2.00 | 0.11 | 2.17 | 2.05 | 0.11 |
| 8 | Mackay | 3.75 | 3.67 | 0.08 | 3.96 | 3.79 | 0.17 | 4.12 | 3.86 | 0.26 |
| 9 | Townsville | 2.40 | 2.29 | 0.12 | 2.62 | 2.35 | 0.26 | 2.80 | 2.39 | 0.41 |
| 10 | Cairns | 1.96 | 1.87 | 0.09 | 2.08 | 1.93 | 0.15 | 2.14 | 1.96 | 0.18 |
| 11 | Darwin | 1.66 | 1.60 | 0.06 | 1.92 | 1.82 | 0.09 | 2.13 | 2.02 | 0.11 |
| 12 | Milner Bay | 3.97 | 3.94 | 0.03 | 4.08 | 3.99 | 0.09 | 4.15 | 4.01 | 0.13 |
| 13 | Wyndham | 4.12 | 4.08 | 0.03 | 4.33 | 4.30 | 0.03 | 4.58 | 4.60 | 0.03 |
| 14 | Broome | 5.25 | 5.12 | 0.14 | 5.35 | 5.15 | 0.20 | 5.38 | 5.15 | 0.22 |
| 15 | Port Hedland | 3.76 | 3.64 | 0.12 | 4.04 | 3.75 | 0.29 | 4.30 | 3.83 | 0.47 |
| 16 | Carnarvon | 1.29 | 1.18 | 0.11 | 1.43 | 1.25 | 0.19 | 1.53 | 1.30 | 0.23 |
| 17 | Geraldton | 1.06 | 0.97 | 0.08 | 1.19 | 1.11 | 0.08 | 1.27 | 1.25 | 0.02 |
| 18 | Fremantle | 1.11 | 1.00 | 0.11 | 1.27 | 1.11 | 0.16 | 1.39 | 1.22 | 0.17 |
| 19 | Bunbury | 1.18 | 1.07 | 0.11 | 1.37 | 1.20 | 0.17 | 1.52 | 1.32 | 0.20 |
| 20 | Albany | 1.01 | 0.97 | 0.04 | 1.06 | 1.02 | 0.05 | 1.08 | 1.04 | 0.04 |
| 21 | Esperance | 1.18 | 1.15 | 0.03 | 1.24 | 1.23 | 0.00 | 1.26 | 1.29 | 0.03 |
| 22 | Thevenard | 1.91 | 1.93 | 0.01 | 2.05 | 2.16 | 0.11 | 2.13 | 2.37 | 0.24 |
| 23 | Port Lincoln | 1.67 | 1.57 | 0.10 | 1.86 | 1.76 | 0.09 | 1.99 | 1.98 | 0.00 |
| 24 | Port Pirie | 2.61 | 2.60 | 0.01 | 2.86 | 2.95 | 0.08 | 3.03 | 3.28 | 0.25 |
| 25 | Port Adelaide (Outer) | 2.39 | 2.37 | 0.03 | 2.62 | 2.64 | 0.02 | 2.78 | 2.89 | 0.11 |
| 26 | Port Adelaide (Inner) | 2.26 | 2.23 | 0.02 | 2.44 | 2.49 | 0.05 | 2.56 | 2.73 | 0.17 |
| 27 | Victor Harbour | 1.51 | 1.46 | 0.05 | 1.61 | 1.60 | 0.02 | 1.67 | 1.70 | 0.04 |
| 28 | Hobart | 1.18 | 1.14 | 0.04 | 1.36 | 1.27 | 0.09 | 1.52 | 1.36 | 0.16 |
| 29 | George Town | 1.84 | 1.84 | 0.00 | 1.93 | 1.99 | 0.05 | 1.98 | 2.11 | 0.13 |
| 30 | Burnie | 1.92 | 1.91 | 0.01 | 2.02 | 2.06 | 0.04 | 2.08 | 2.19 | 0.11 |
| All | | | Mean | 0.06 | | Mean | 0.10 | | Mean | 0.15 |

Table 6: Largest recorded storm surge events, ranked in order of surge height, resulting from a tropical cyclone at 17 of the study tide-gauge sites.

| Tide gauge | Analysis period | Date of largest surge | Surge ranking | Surge level (m) | Total water level ranking | Total level (m AHD) | Cyclone |
|-------------------|------------------------|------------------------------|----------------------|------------------------|----------------------------------|----------------------------|----------------|
| Townsville | 1970-2008 | 23/12/1971 | 1 | 2.84 | 1 | 2.53 | Althea |
| Broome | 1970-2008 | 19/04/2000 | 1 | 2.26 | 45 | 4.83 | Rosita |
| Port Headland | 1970-2008 | 21/01/1973 | 1 | 2.06 | 1 | 3.81 | Kerry |
| Bunbury | 1970-2008 | 04/04/1978 | 1 | 1.57 | 1 | 1.76 | Alby |
| Wyndham | 1970-2008 | 29/01/1998 | 1 | 1.47 | 2 | 4.00 | Les |
| Darwin | 1970-2008 | 24/12/1974 | 7 | 1.39 | <100 | 2.43 | Tracy |
| Milner Bay | 1993-2008 | 10/02/2001 | 1 | 1.27 | 1 | 2.02 | Winsome |
| Carnarvon | 1960-2008 | 13/03/1979 | 2 | 1.19 | 1 | 1.65 | Hazel |
| Bundaberg | 1970-2008 | 15/03/1992 | 1 | 0.98 | 11 | 1.87 | Fran |
| Fremantle | 1970-2008 | 04/04/1978 | 1 | 0.84 | 3 | 1.01 | Alby |
| Mackay | 1970-2008 | 28/02/1979 | 11 | 0.78 | <100 | -1.57 | Kerry |
| Cairns | 1970-2008 | 27/02/2000 | 1 | 0.78 | <100 | 0.71 | Steve |
| Geraldton | 1970-2008 | 04/04/1978 | 4 | 0.69 | 32 | 0.71 | Alby |
| Newcastle | 1970-2008 | 04/02/1990 | 8 | 0.47 | <100 | 0.32 | Nancy |
| Albany | 1970-2008 | 04/04/1978 | 10 | 0.43 | <100 | 0.26 | Alby |
| Esperance | 1970-2008 | 04/04/1978 | 87 | 0.42 | <100 | 0.59 | Alby |
| Brisbane | 1977-2008 | 04/02/1990 | 12 | 0.37 | <100 | 0.44 | Nancy |

Table 7: Details of the tropical cyclones used for model validation.

| Name | Season | Maximum surge height (m) | Tide-gauge |
|-------------|---------------|---------------------------------|-------------------|
| Rosita | 1999 | 2.26 | Broome |
| Althea | 1971 | 2.84 | Townsville |
| Tracy | 1974 | 1.39 | Darwin |
| Steve | 1999 | 0.78 | Cairns |
| Les | 1997 | 1.47 | Wyndham |
| John | 1999 | 1.48 | Port Headland |
| Kerry | 1972 | 2.06 | Port Headland |
| Hazel | 1978 | 1.19 | Carnarvon |
| Alby | 1977 | 1.57 | Bunbury |

FIGURES

Figure 1: Location of tide gauge sites around the coastline of Australia with high frequency (at least hourly) water level records longer than 30 years. Note: Milner Bay does not have 30 years of data but has been included so that there is a validation site in the Gulf of Carpentaria.

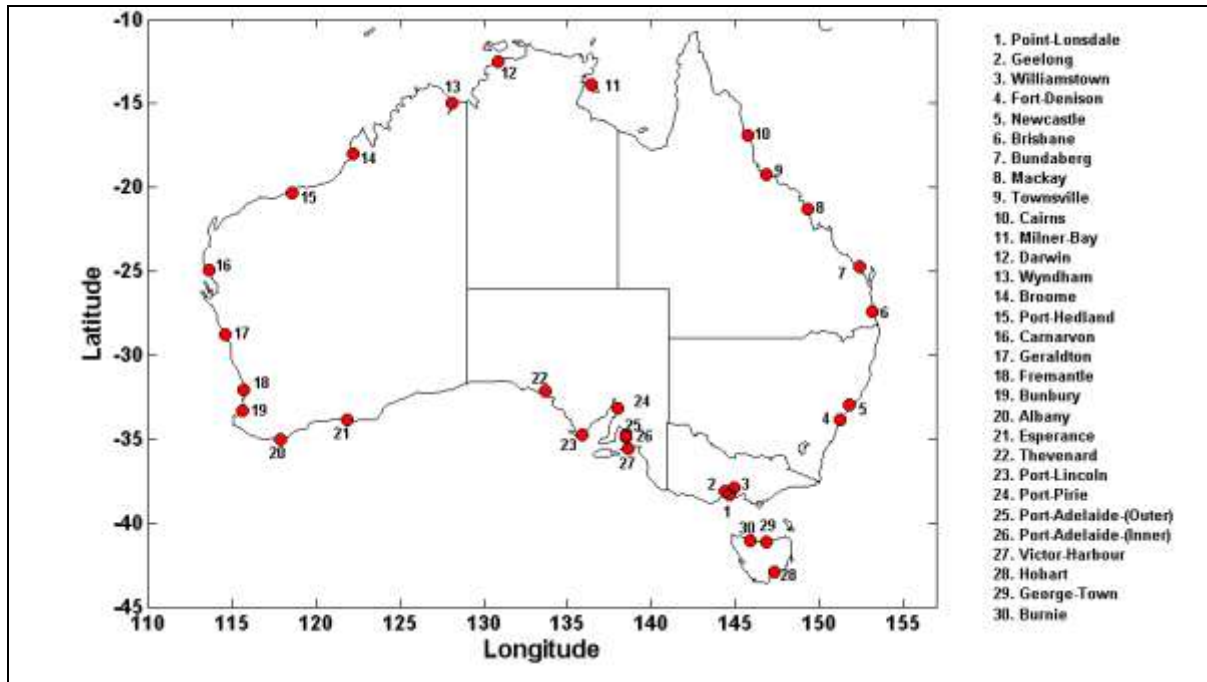


Figure 2: Hydrodynamic model grid and bathymetry configured in Mike21 FM.

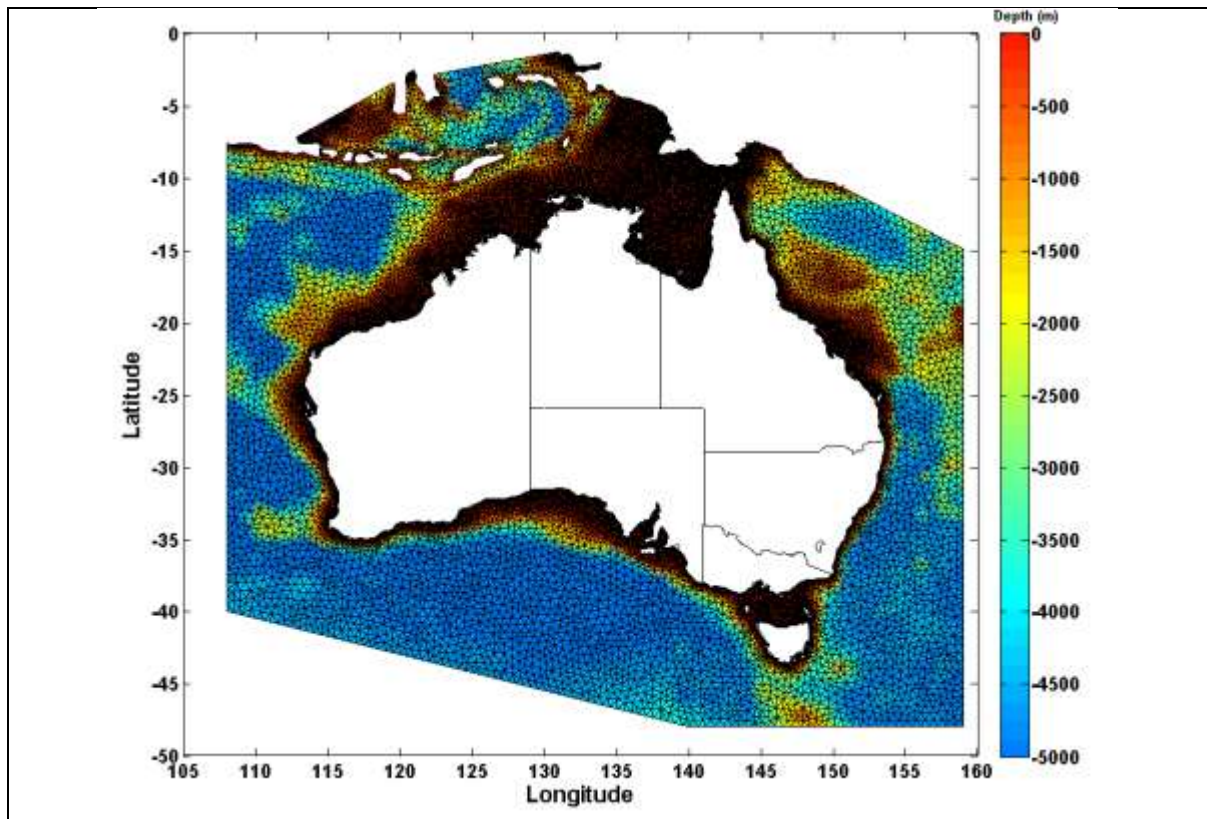


Figure 3: NCEP/NCAR mean sea level pressure fields and 10 m wind vectors every 12 hours for a large extra-tropical storm event in May 2003.

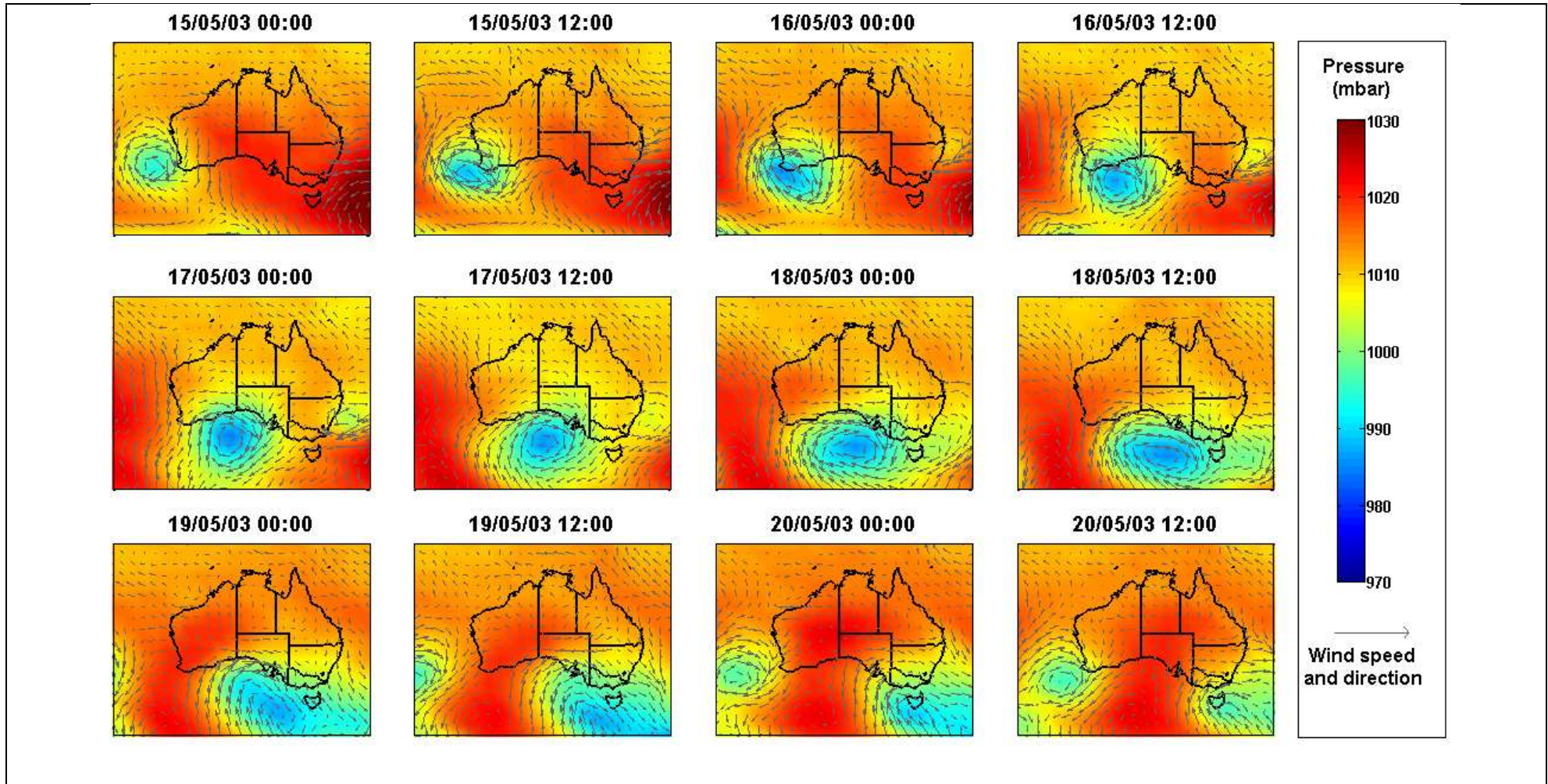


Figure 4: Comparison of the measured and predicted amplitudes of the 8 main tidal constituents for the 30 validation sites for 1995.

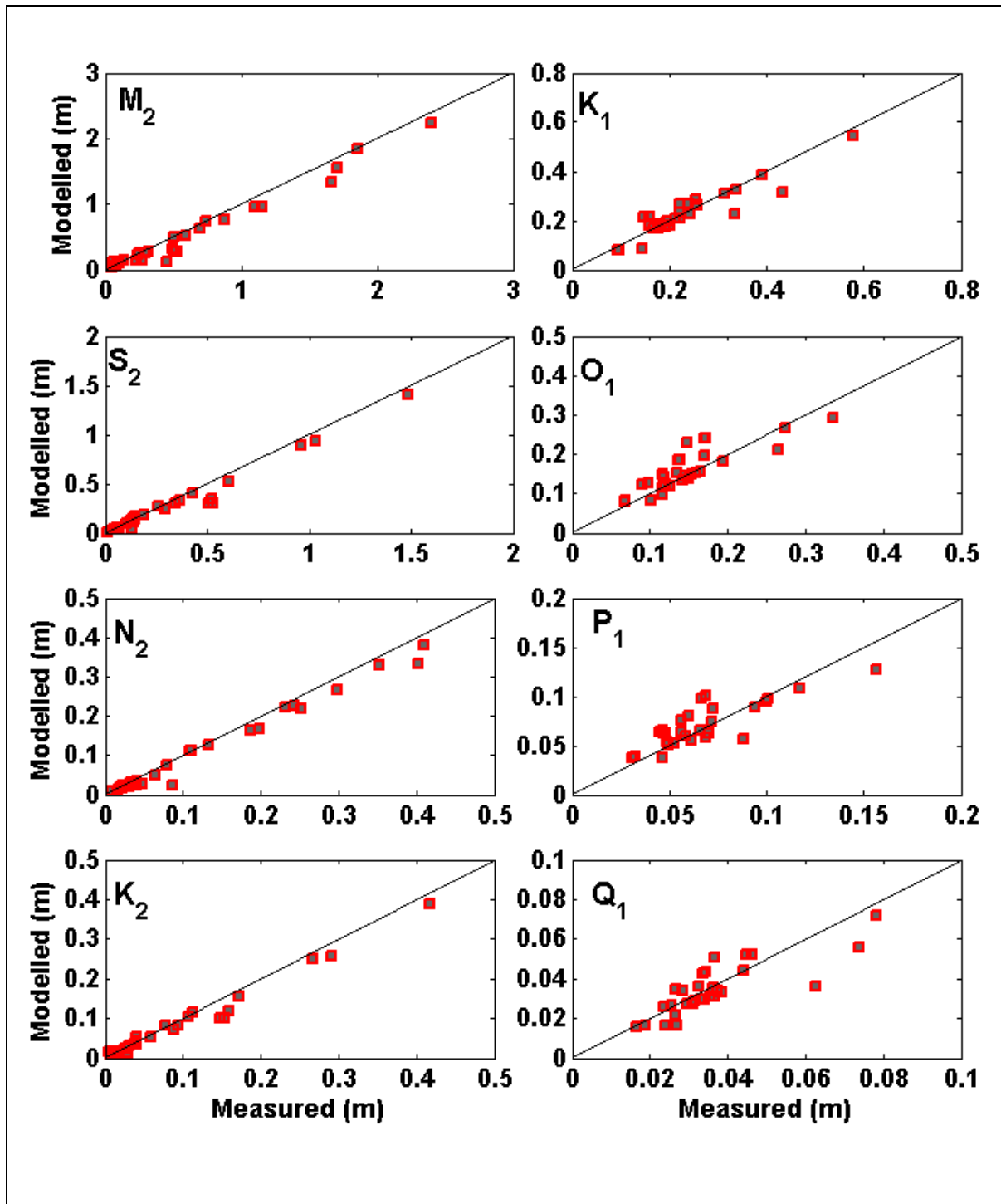


Figure 5: Comparison of the measured and predicted phases of the 8 main tidal constituents for the 30 validation sites for 1995.

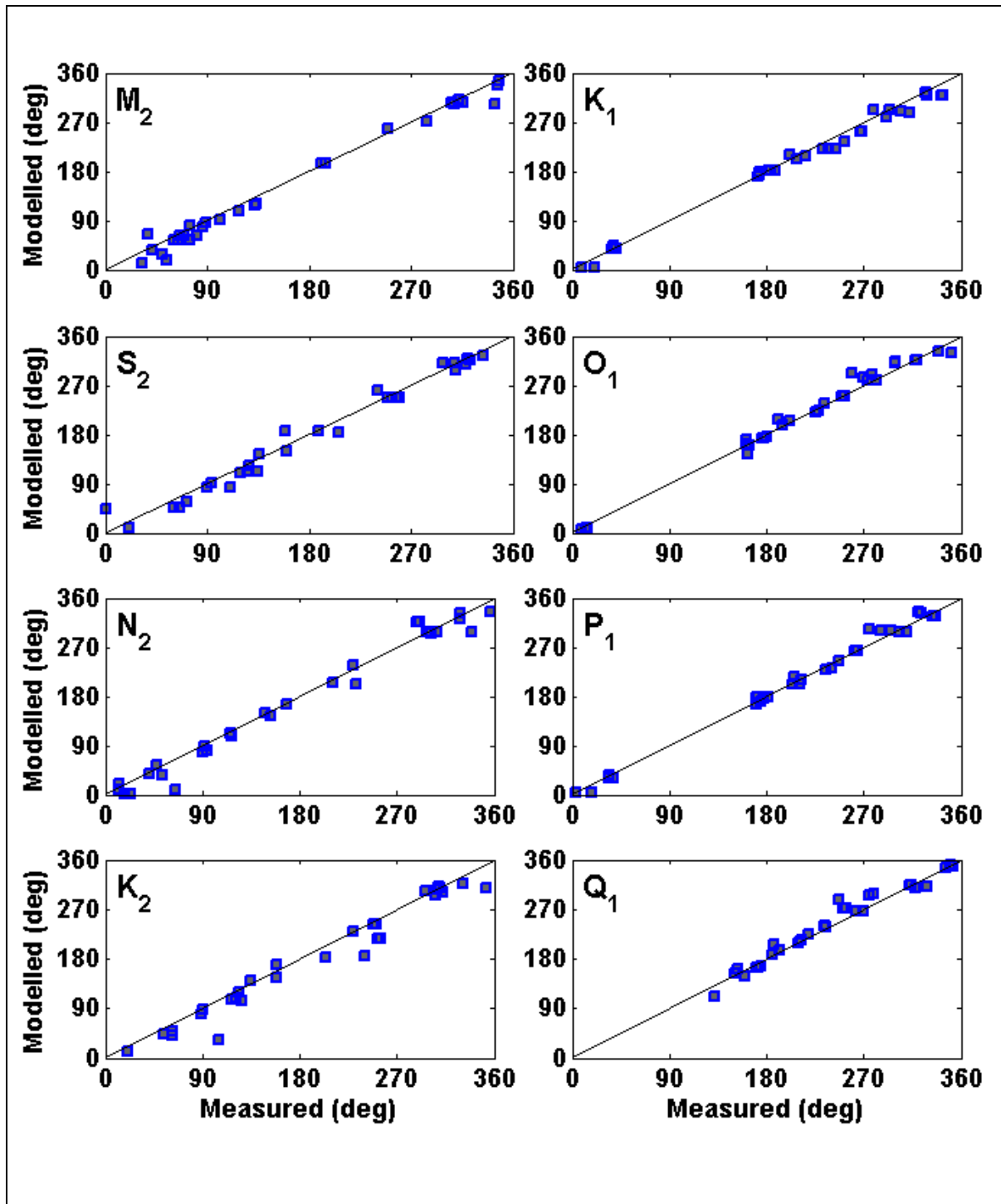


Figure 6: Comparison of the measured (blue) and predicted (red) surge component for 1995 at select sites around southern Australia.

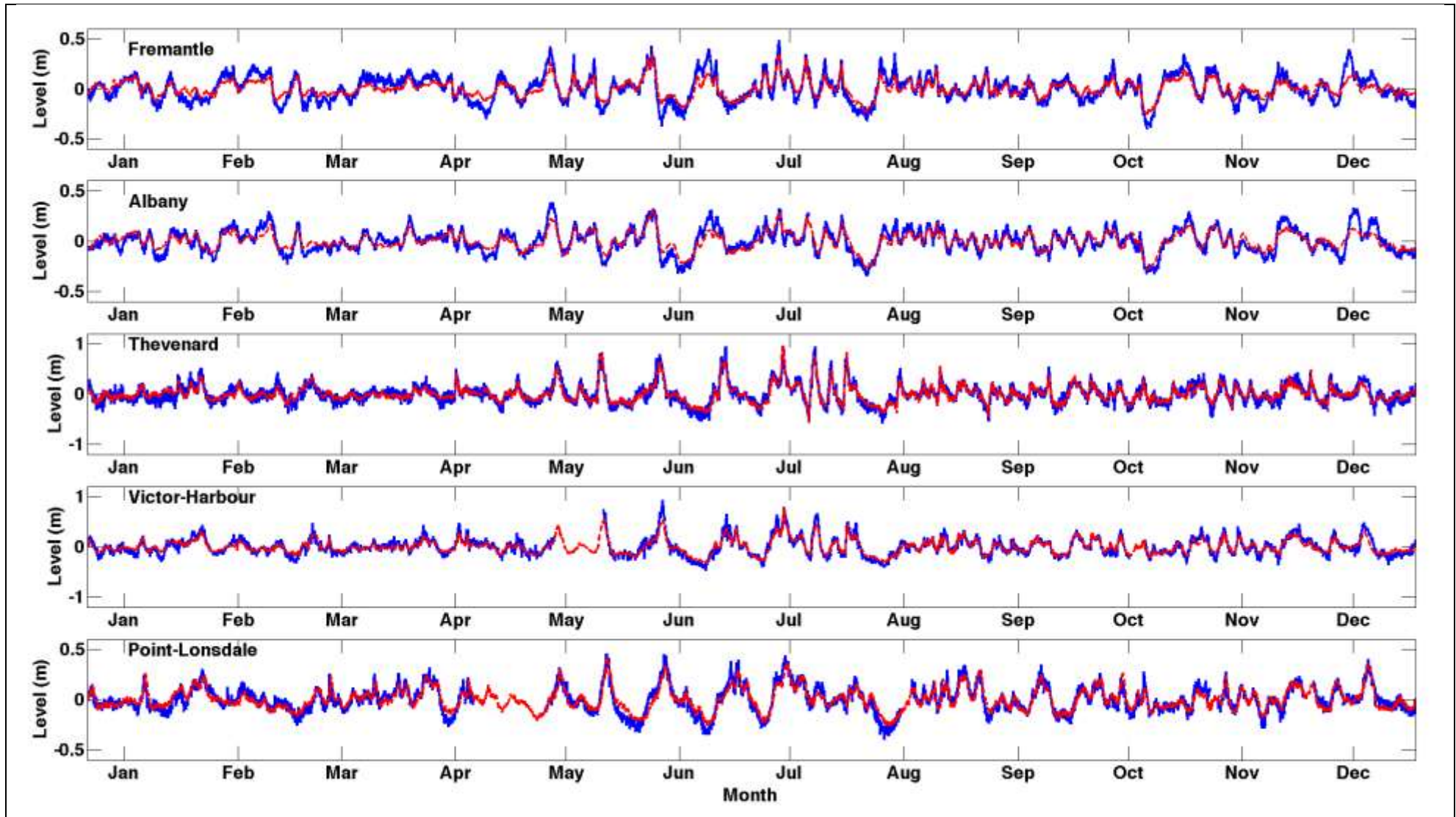


Figure 7: Comparison of the measured (blue) and predicted (red) surge component at Thevenard for the period 1995 to 1999.

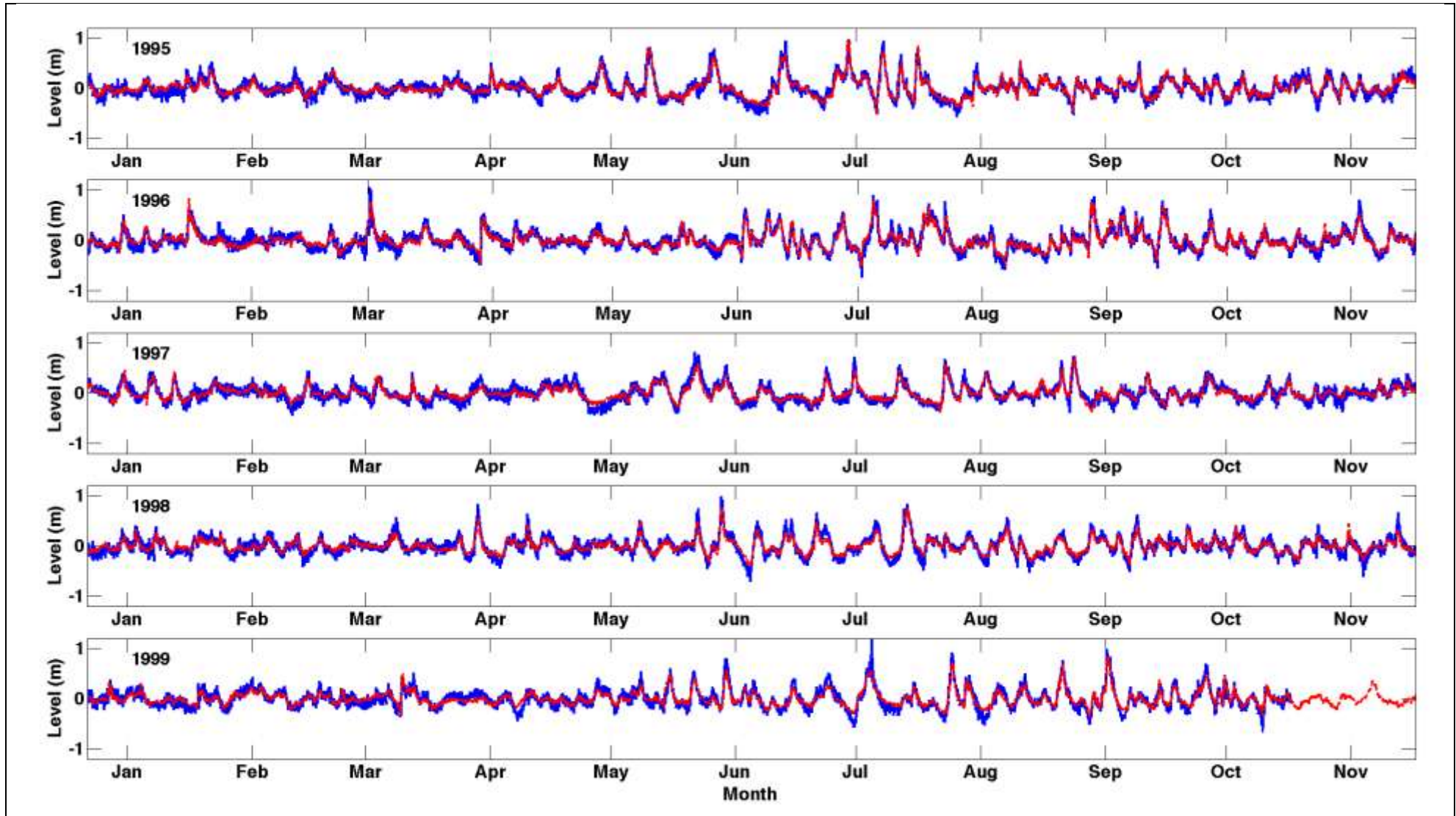


Figure 8: Time-series of the annual root mean square error (RMSE), standard deviation error (STD) and correlation coefficient (Corr Coef) between the measured and predicted storm surge component at Fremantle over the 61-year hindcast period.

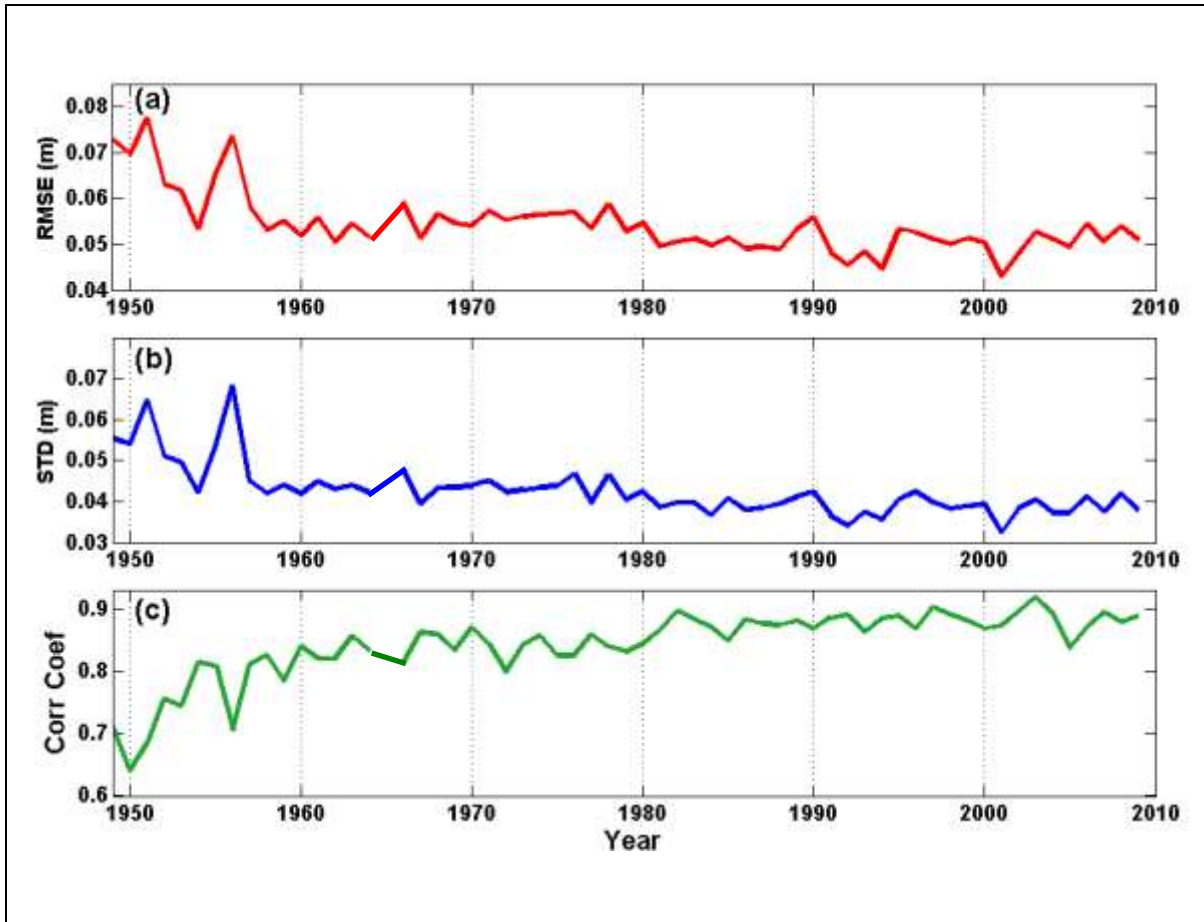


Figure 9: (a) Mean range in the seasonal mean sea level cycle; and (b) Month during which the seasonal mean sea level cycle is largest.

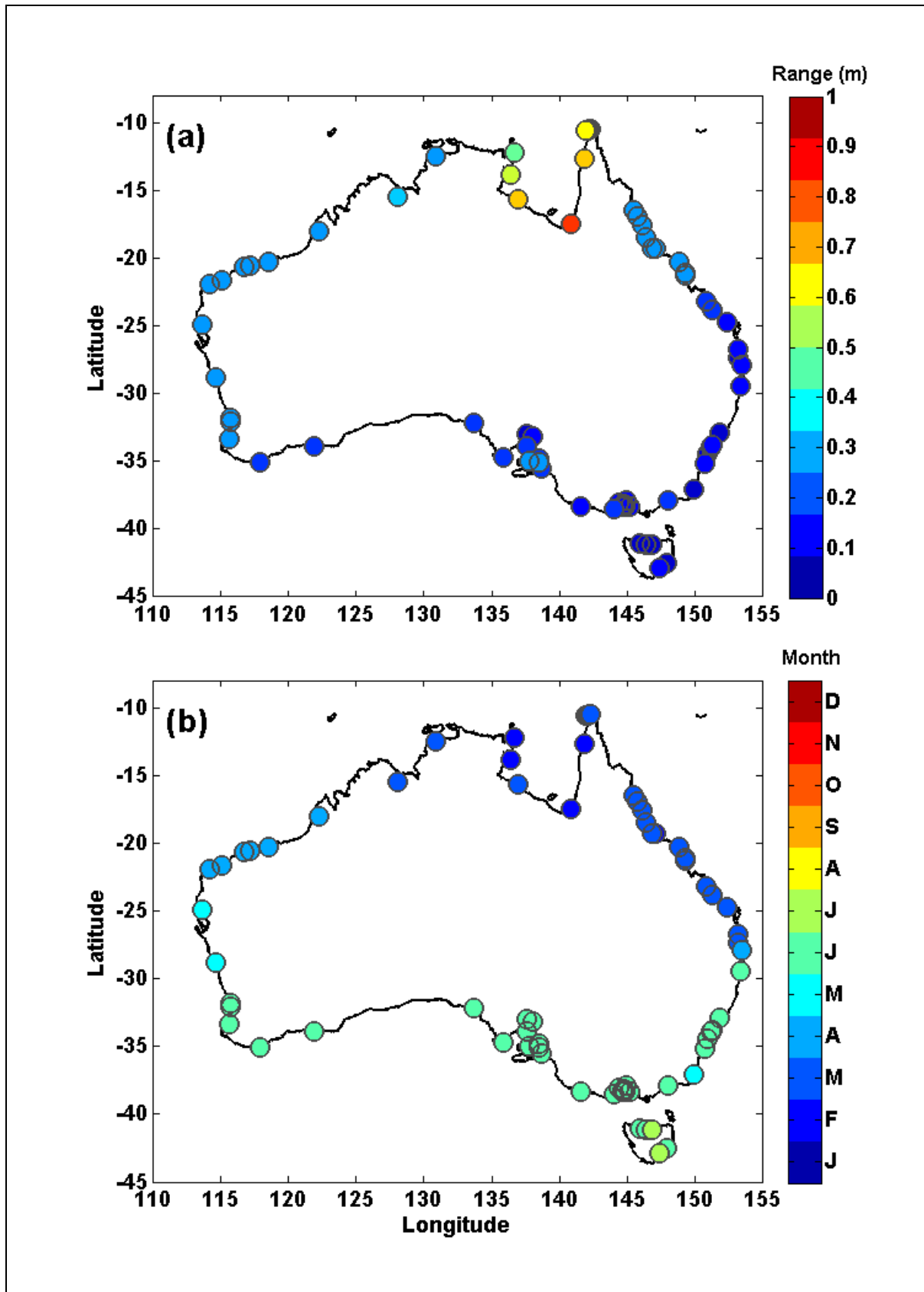


Figure 10: Comparison of the measured (blue) and predicted (red) total water level (a) frequency distribution and (b) cumulative frequency distribution curves for Albany, Port Lincoln, Burnie and Newcastle.

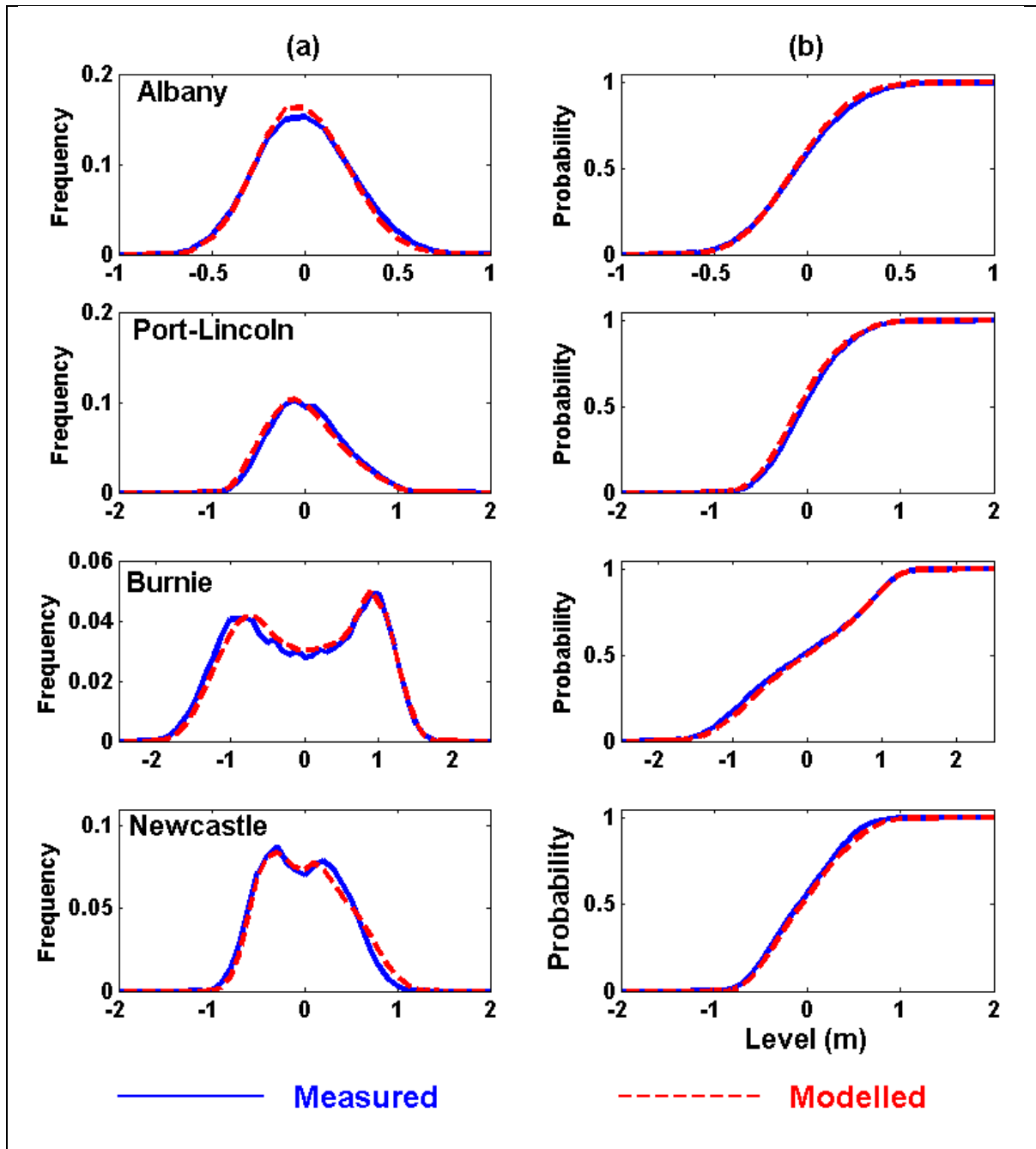


Figure 11: Comparison of the measured (blue) and predicted (red) return period curves for 2010 (relative to AHD) at the 30 validation sites estimated using the AMM fitted to a GEV distribution.

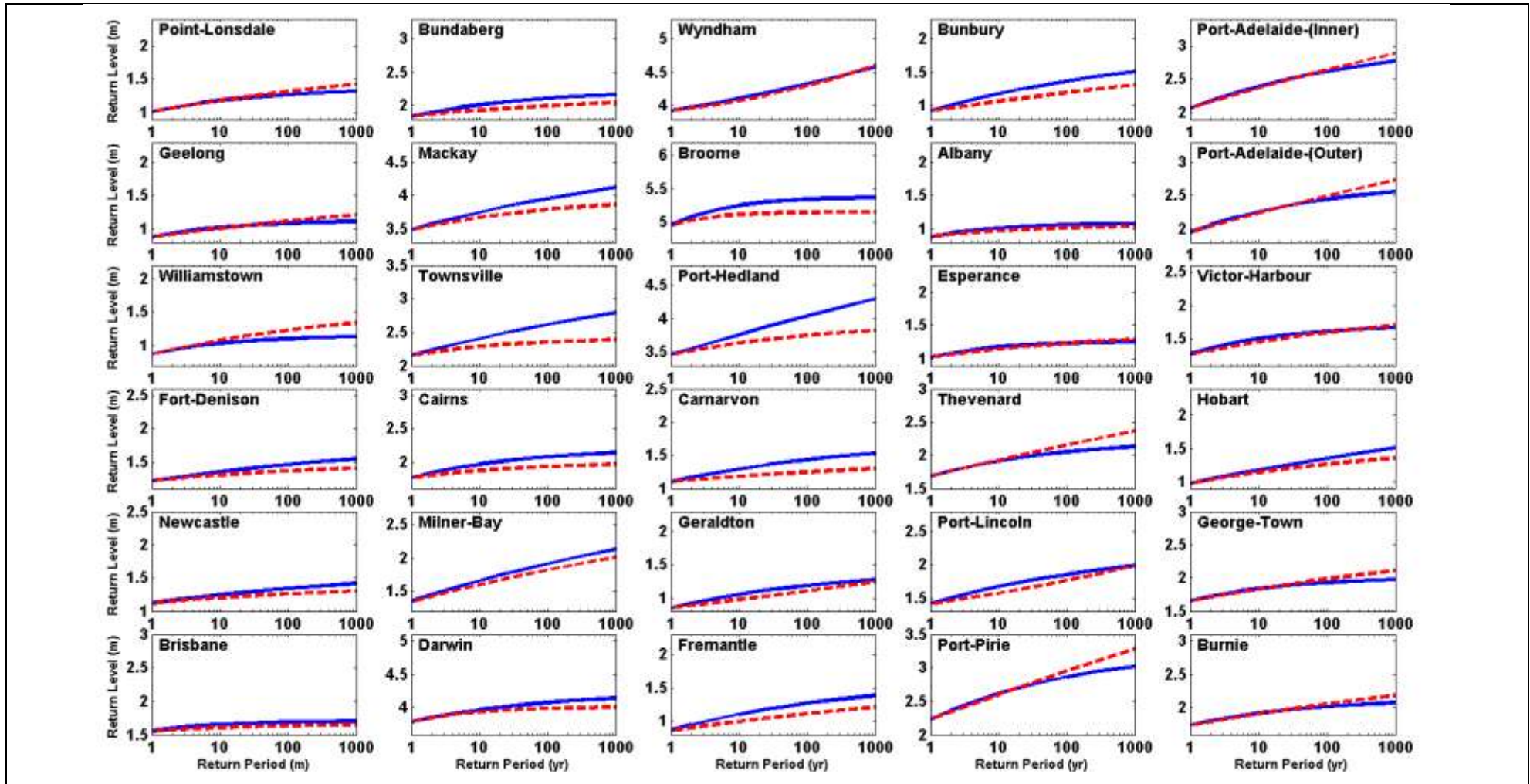


Figure 12: Return period curves for 2010 (relative to AHD) estimated using the AMM fitted to a GUM and GEV distribution and the RLM fitted to a GEV distribution, derived from the measured sea level data at (a) Geraldton and (b) Fort Denison. The maximum-recorded water level has been plotted against the length of the record (i.e. 40 years) and is shown as a green square.

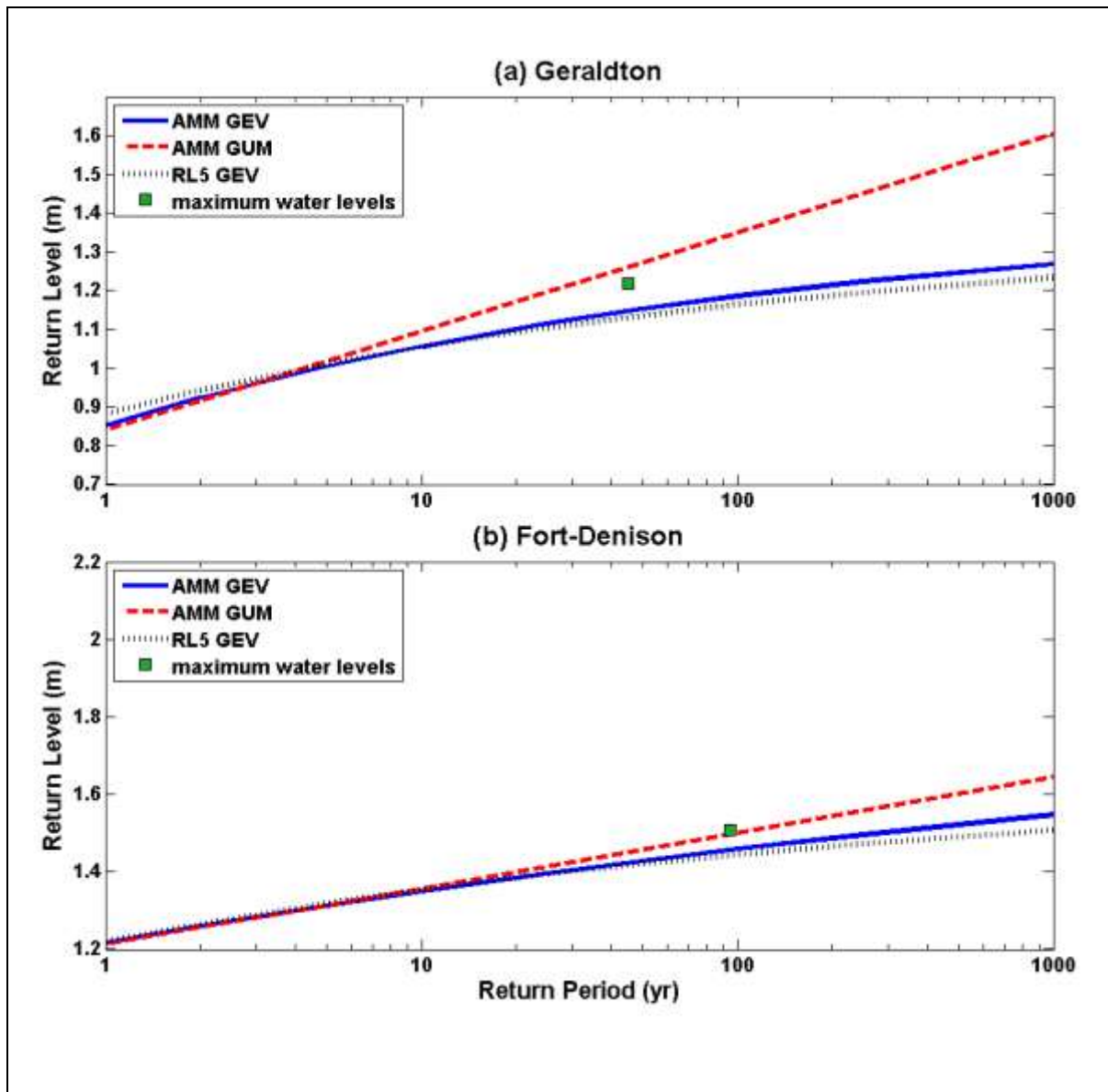


Figure 13: 100-year total water return levels for 2010 (relative to AHD) at the model coastal grid points estimated using the AMM fitted to a GUM distribution. The estimates from the tide gauge records are also shown (circles).

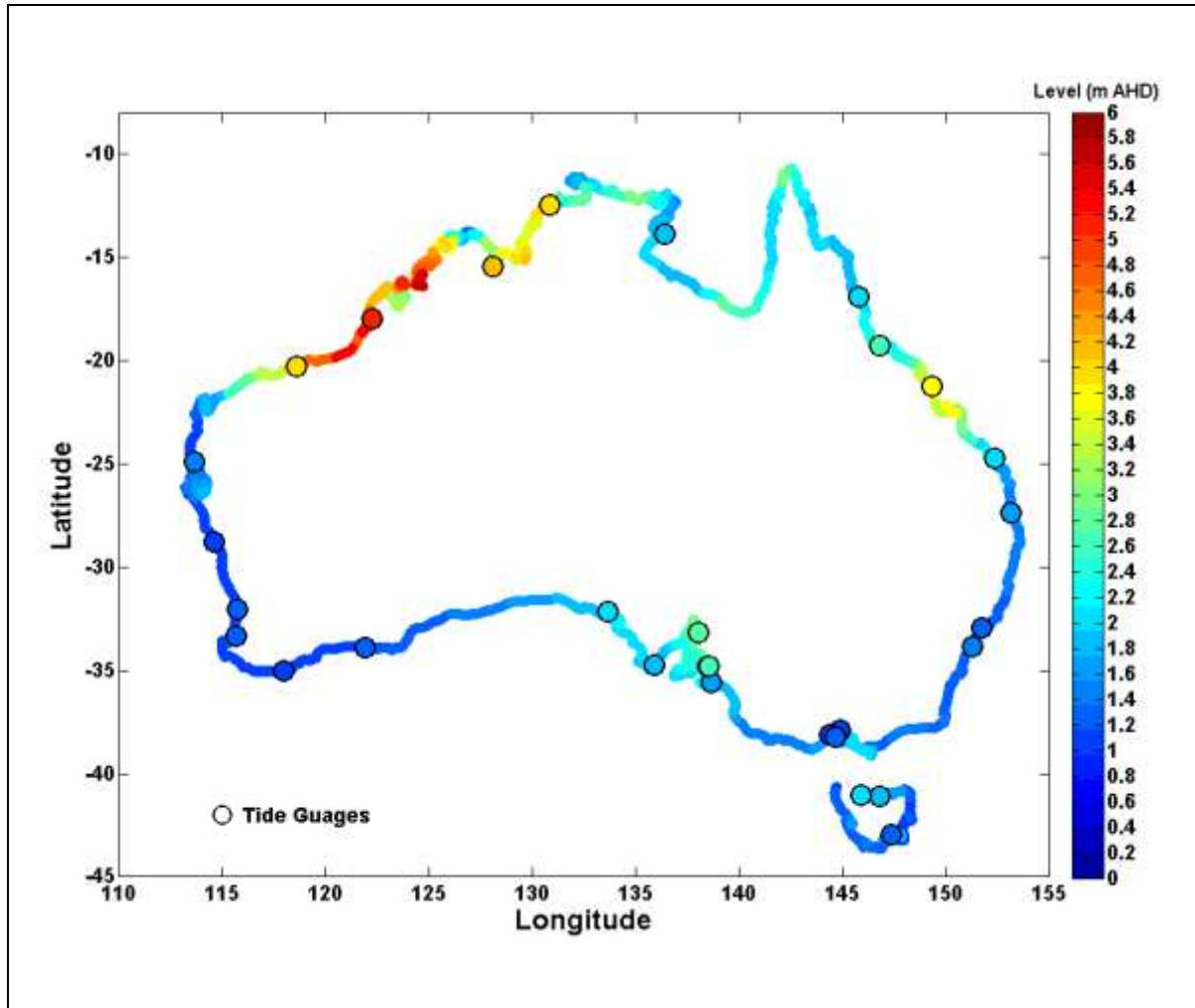


Figure 14: The tracks of the tropical cyclones responsible for the ten largest cyclone-induced surge events that made it into the top 100 largest surge events identified at each study tide gauge site.

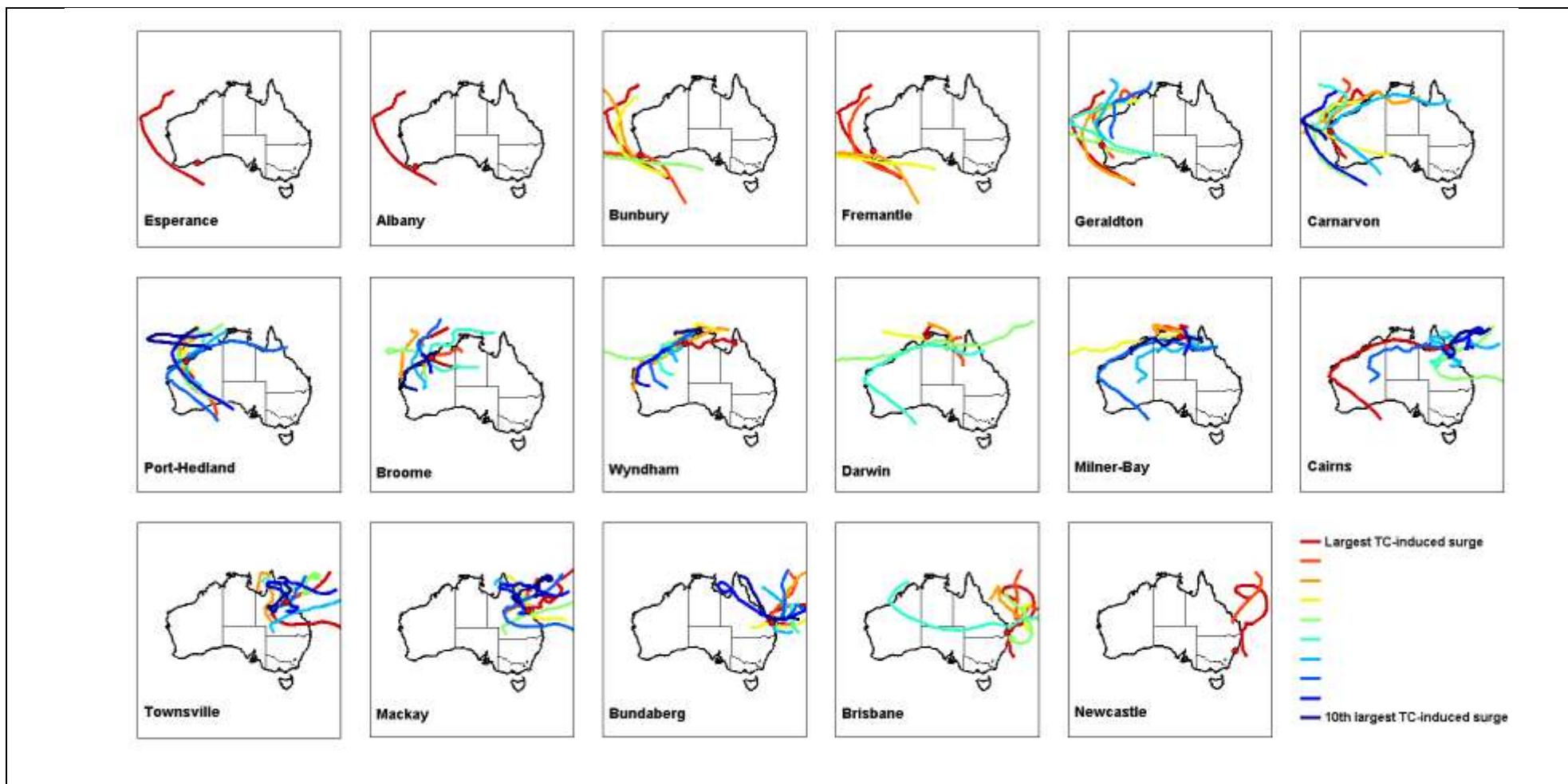


Figure 15: Measured and predicted wind speed, direction and atmospheric pressure time-series for (top to bottom) Arlington Reef, Flinders Reef, Lucinda Point and Townsville meteorological stations during the passage of tropical cyclone Yasi in Feb 2011.

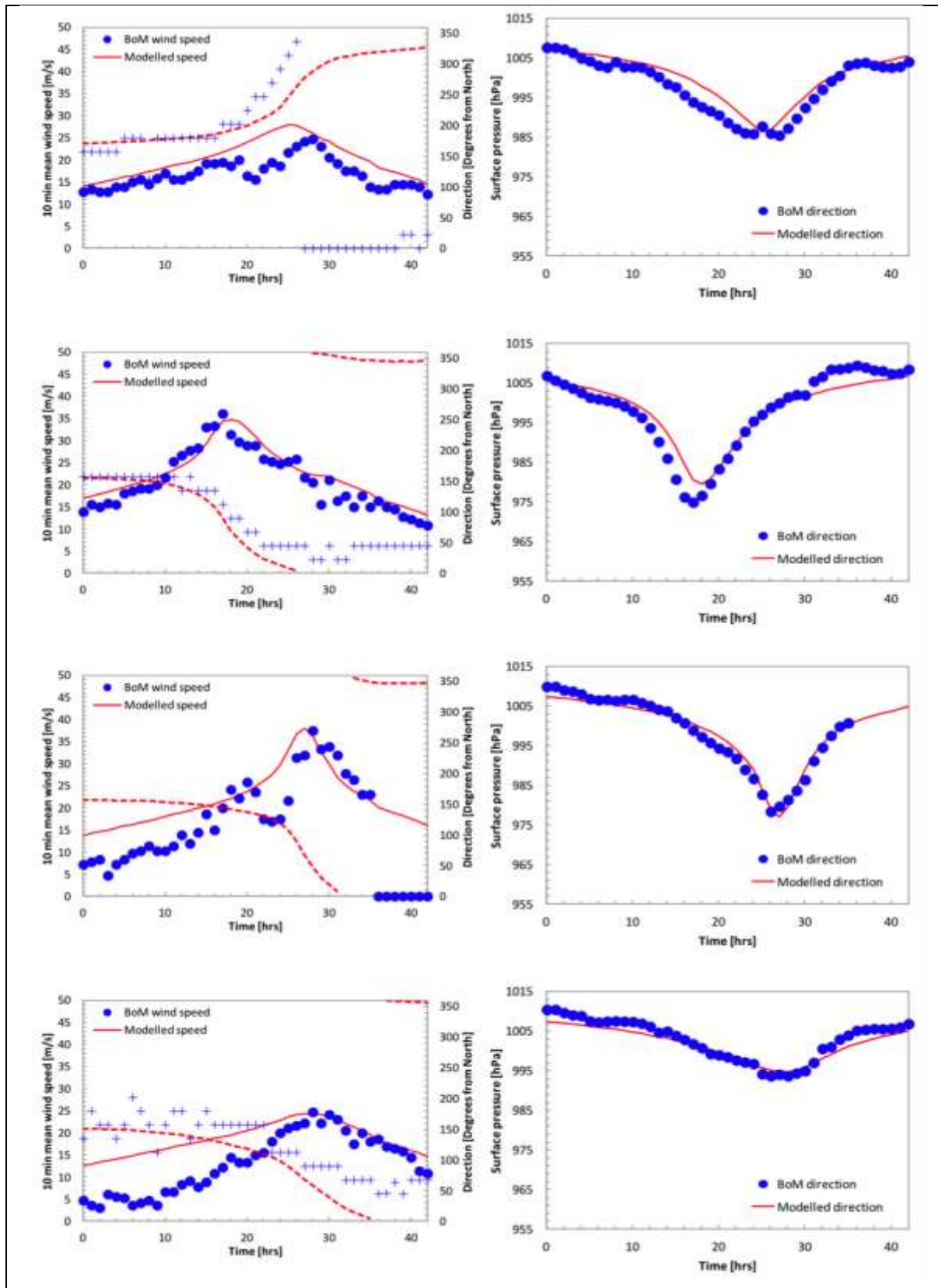


Figure 16: Tropical cyclone tracks for Althea, Rosita and Yasi.

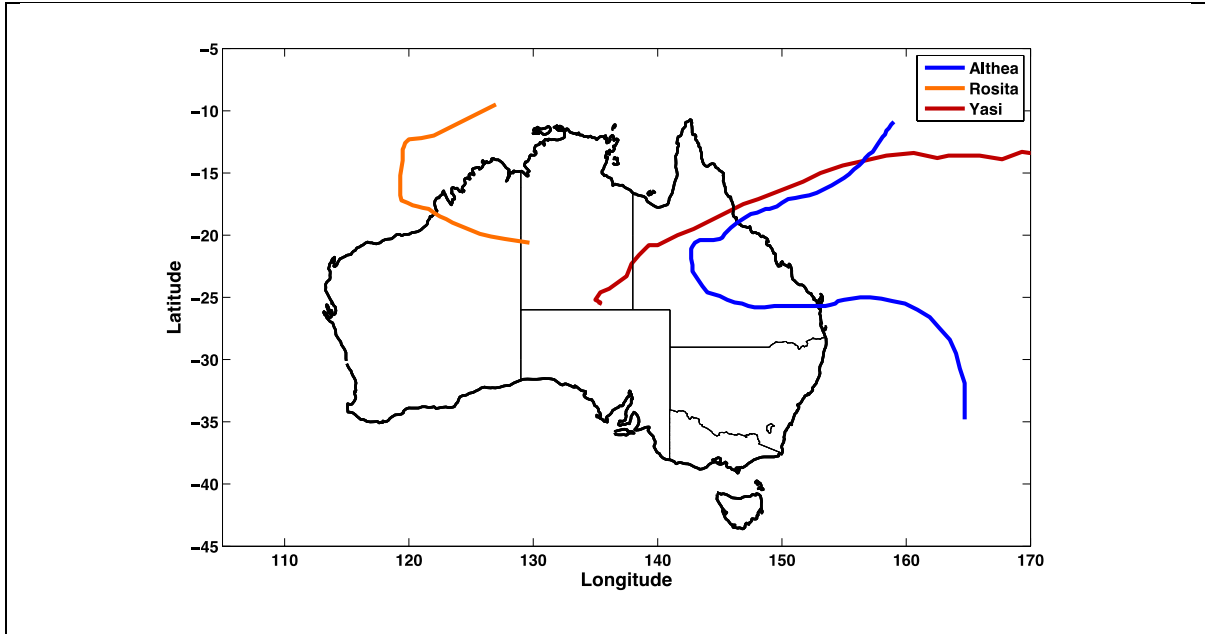


Figure 17: Comparisons between the measured (blue) and predicted (red) surge time-series at (a) Townsville for cyclone Althea and (b) Broome for cyclone Rosita.

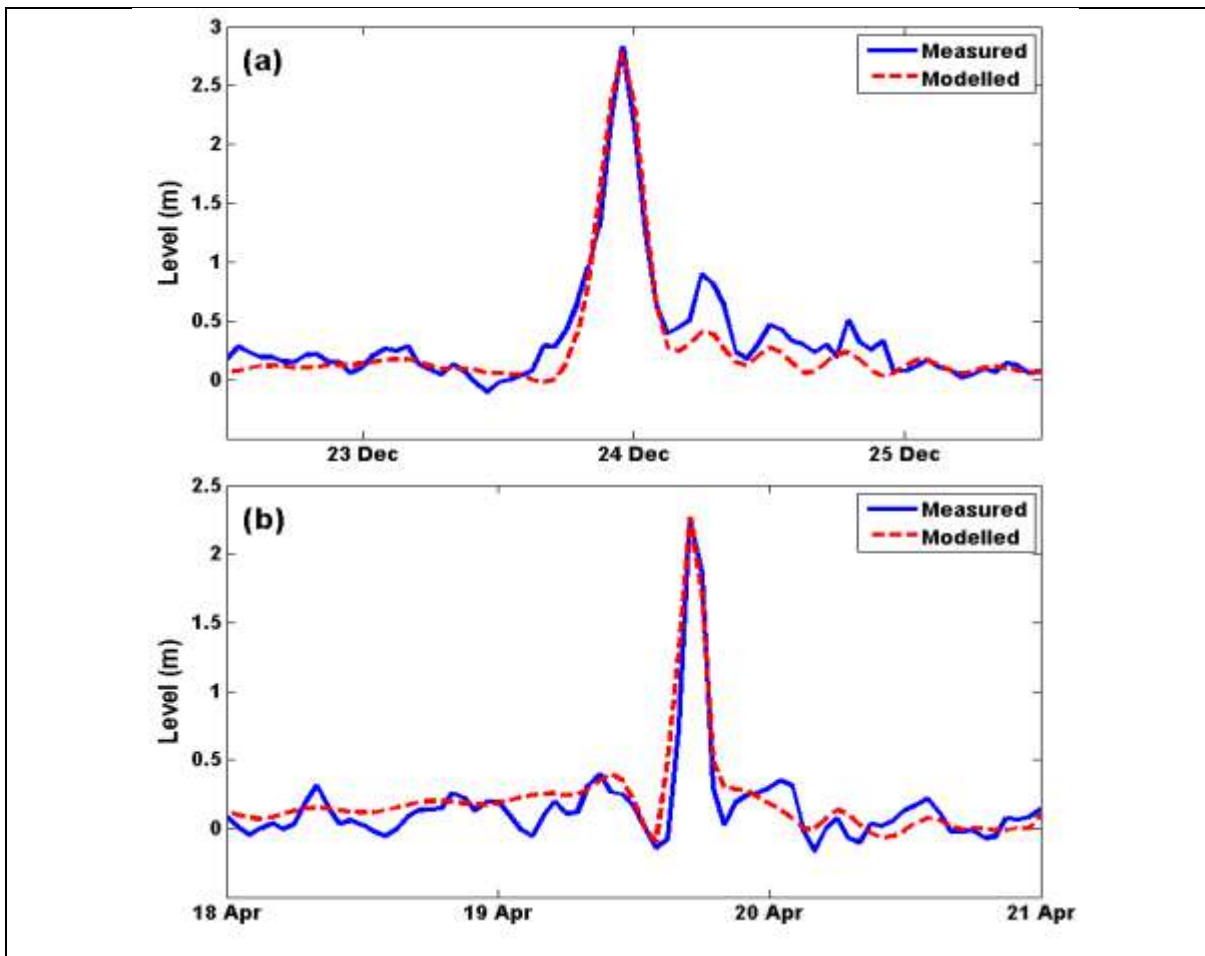


Figure 18: Comparisons between the measured (blue) and predicted (red) surge time-series for cyclone Yasi at four tide gauges in Queensland. Each time series has been arbitrarily offset for presentation purposes.

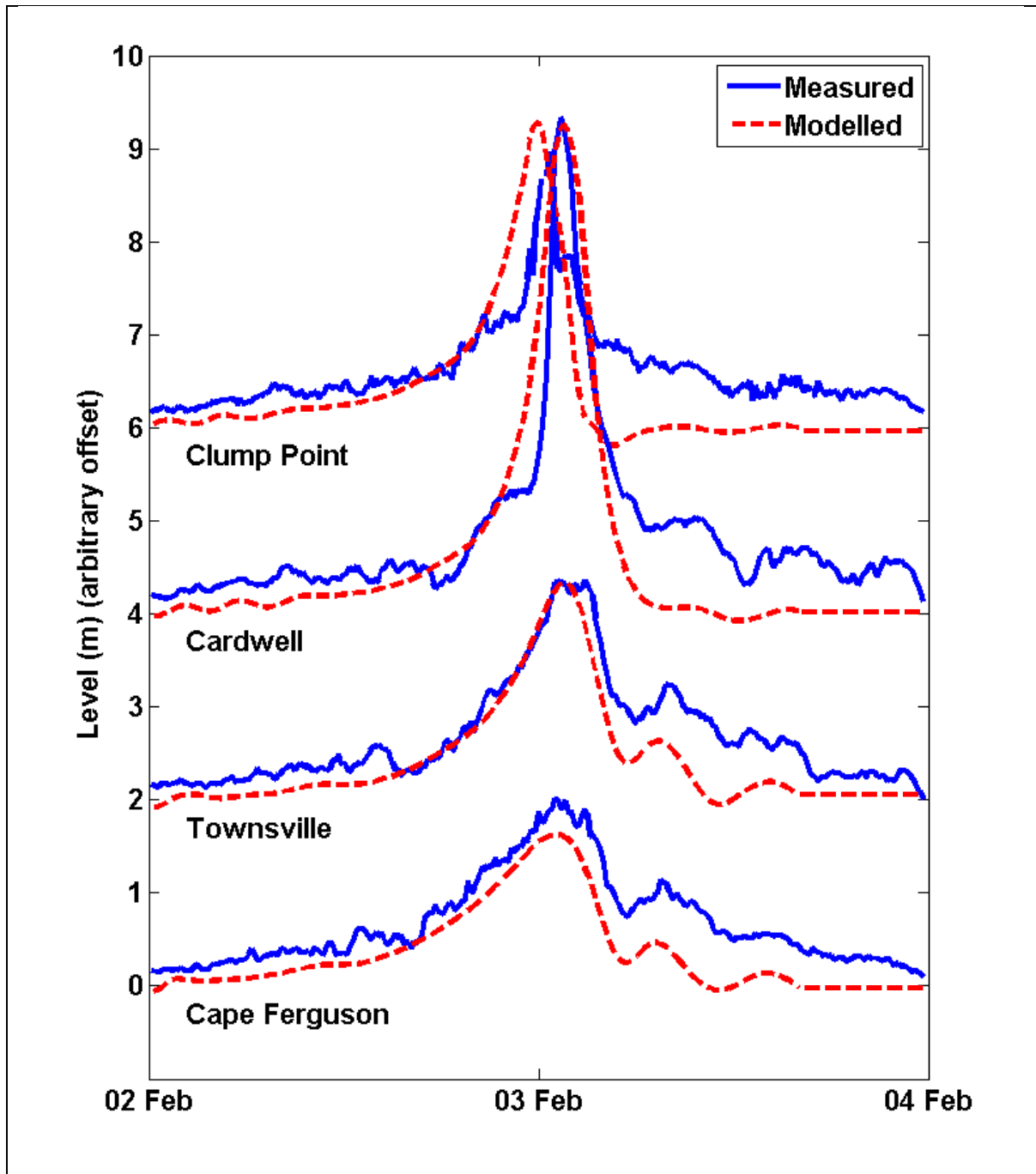


Figure 19: Tide-surge interaction at Townsville associated with tropical cyclone Rosita. (a) Total water levels for the four different tidal states; (b) surge levels for the four different tidal states and surge only simulation; (c) surge levels for the four different tidal states and surge only simulation, but re-adjusted for the time offset.

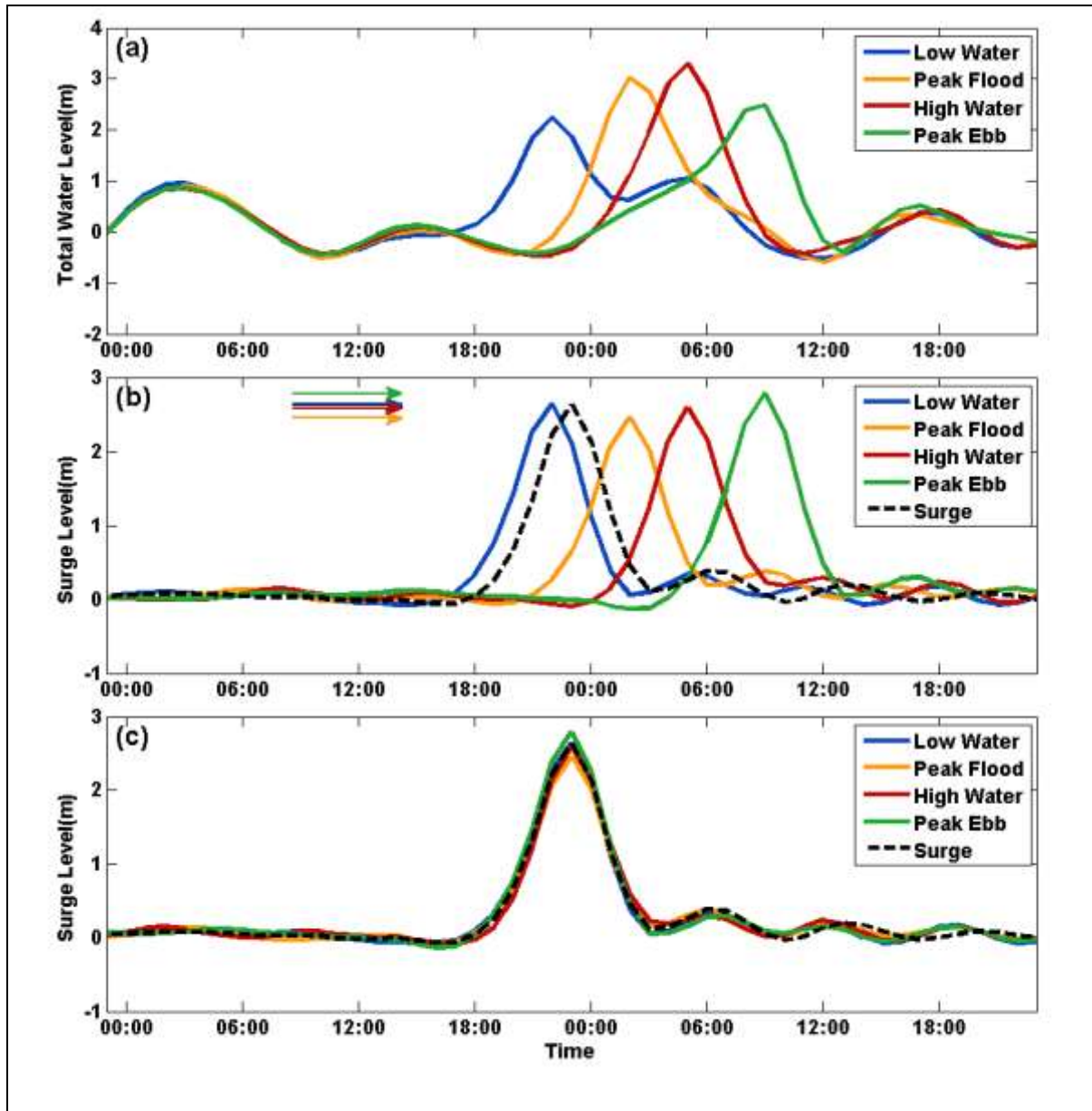


Figure 20: Tide-surge interaction at Broome associated with tropical cyclone Althea. (a) Total water levels for the four different tidal states; (b) surge levels for the four different tidal states and surge only simulation; (c) surge levels for the four different tidal states and surge only simulation, but re-adjusted for the time offset.

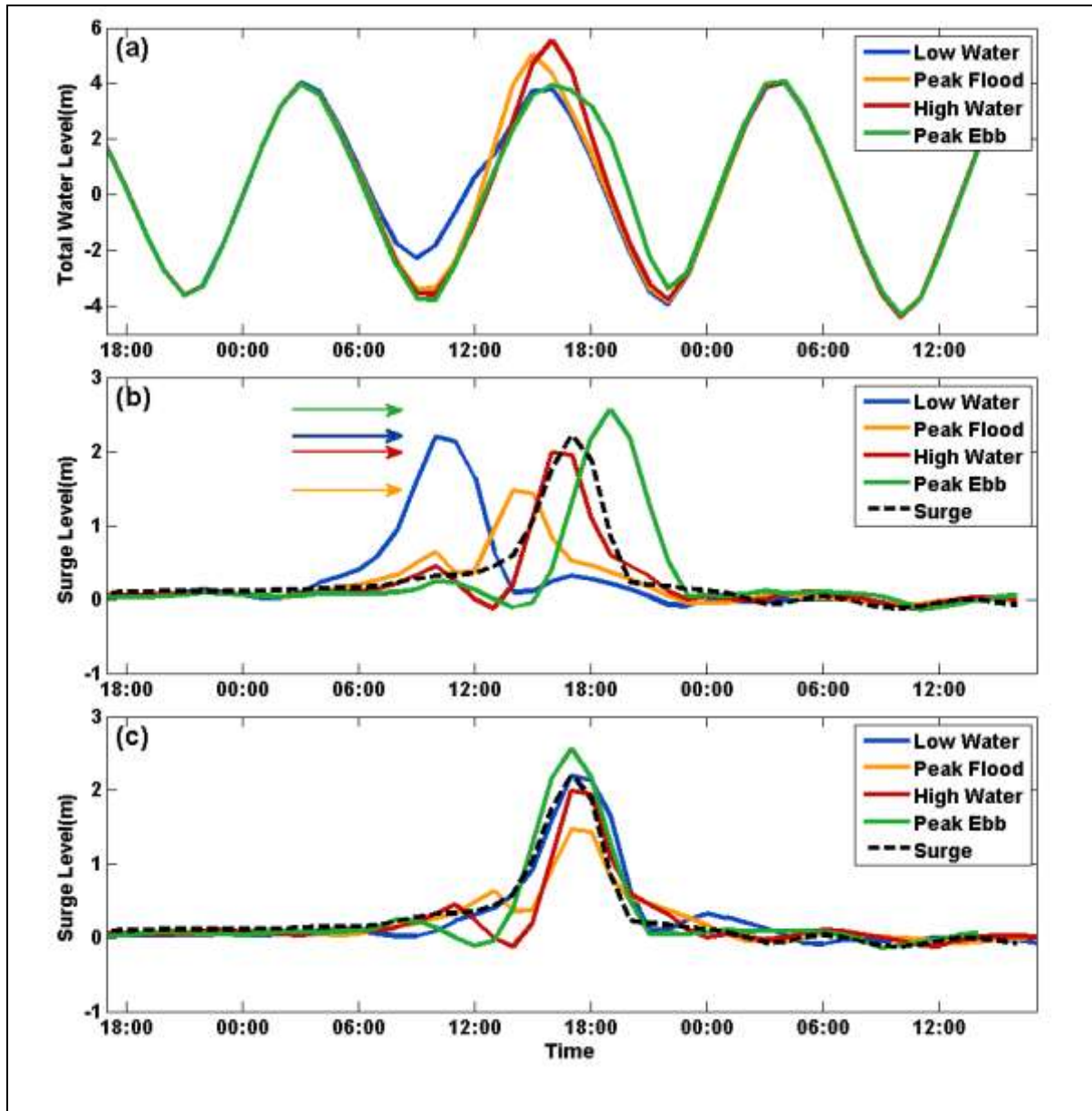


Figure 21: Synthetic tropical cyclone tracking (hatched) and genesis and tracking (cross-hatched) domains. Wind statistics validation locations also shown.

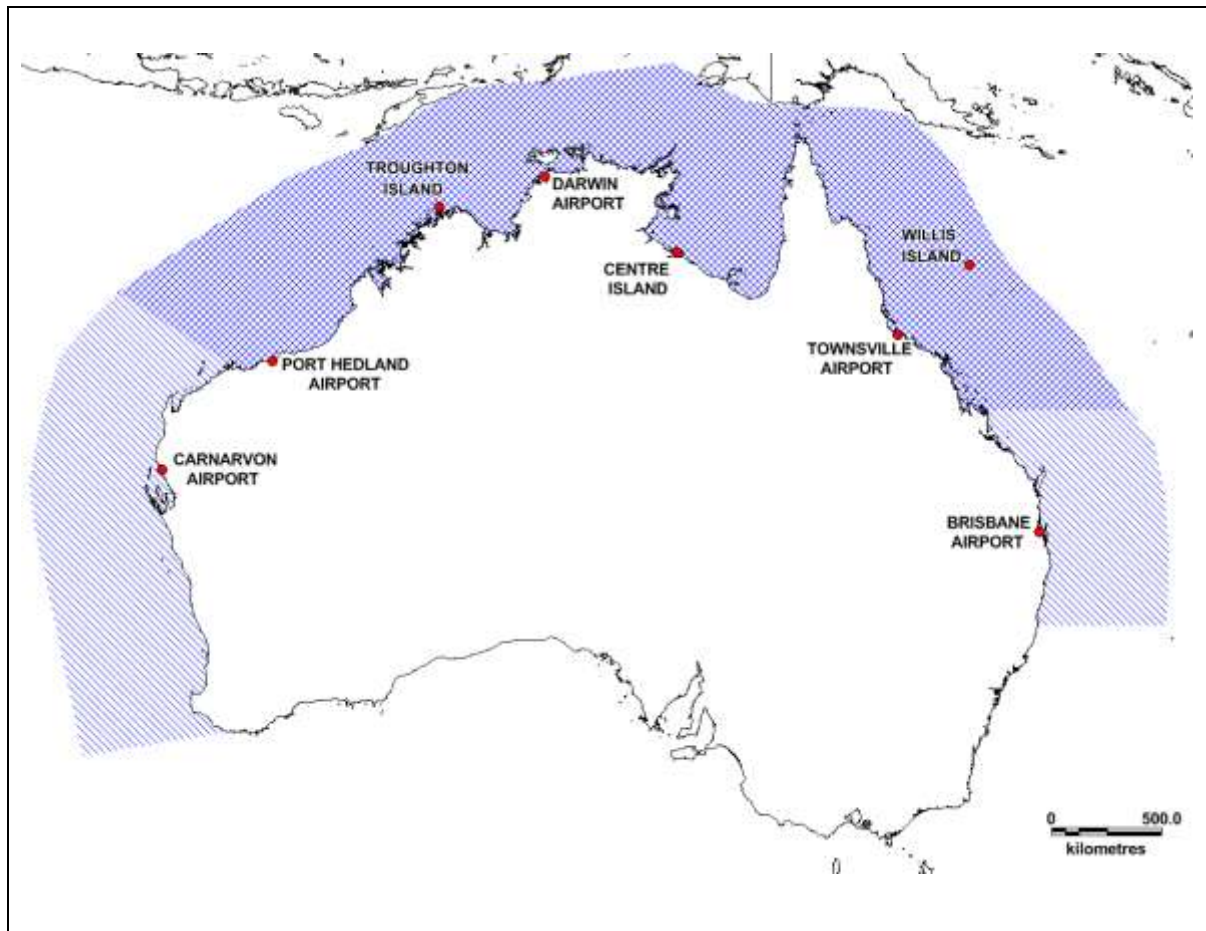


Figure 22: Measured (dot) and predicted (line) wind speed return period curves for 2010 at select locations around the Australian coastline. Local wind speed adjustments are applied to the predicted data.

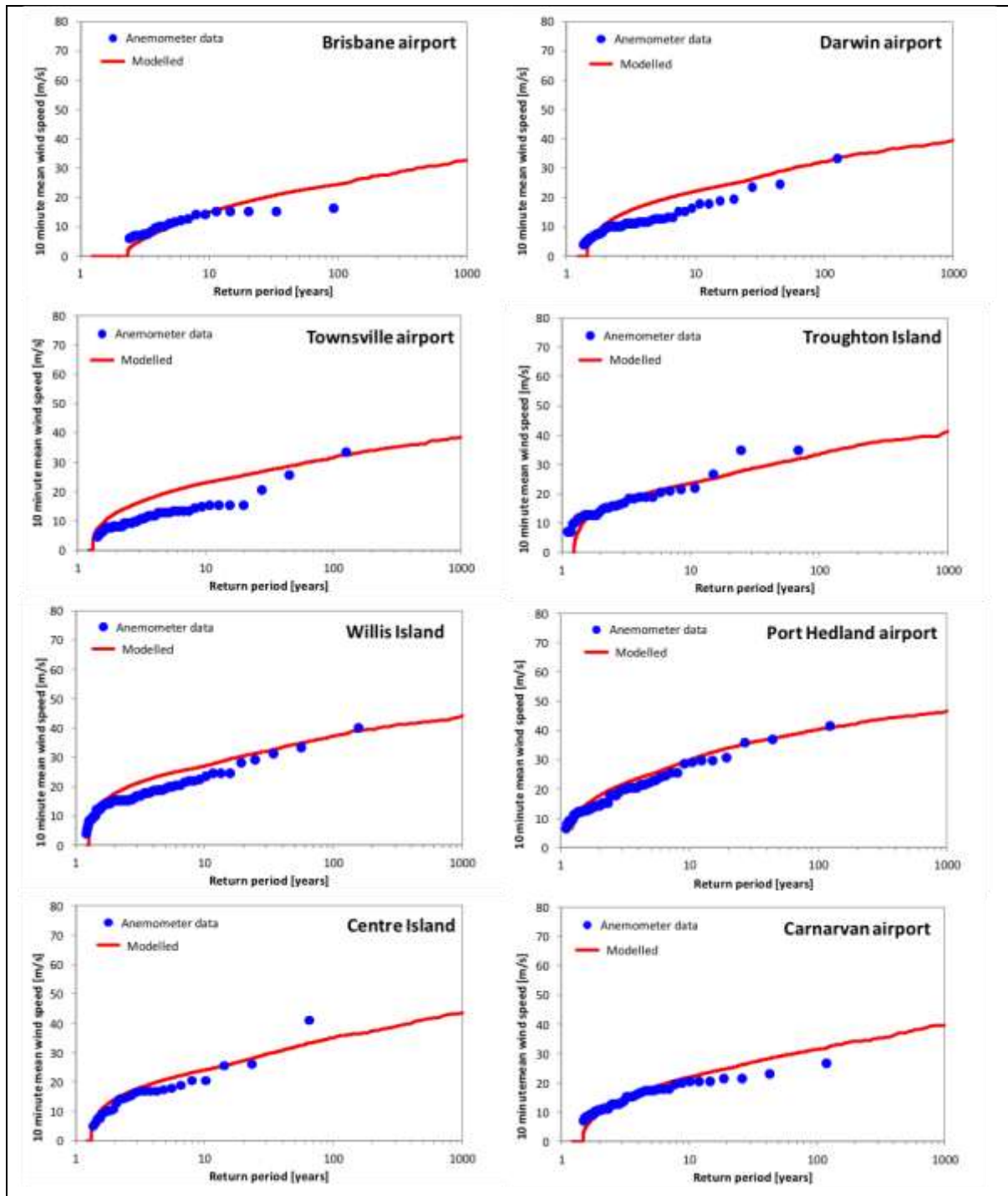


Figure 23: (a) Observed tropical cyclone tracks for the 39 year period between 1970 and 2008; (b) Synthetic tropical cyclone tracks for a 39-year period; and (c) Synthetic tropical cyclone tracks for a 1,000 year period.

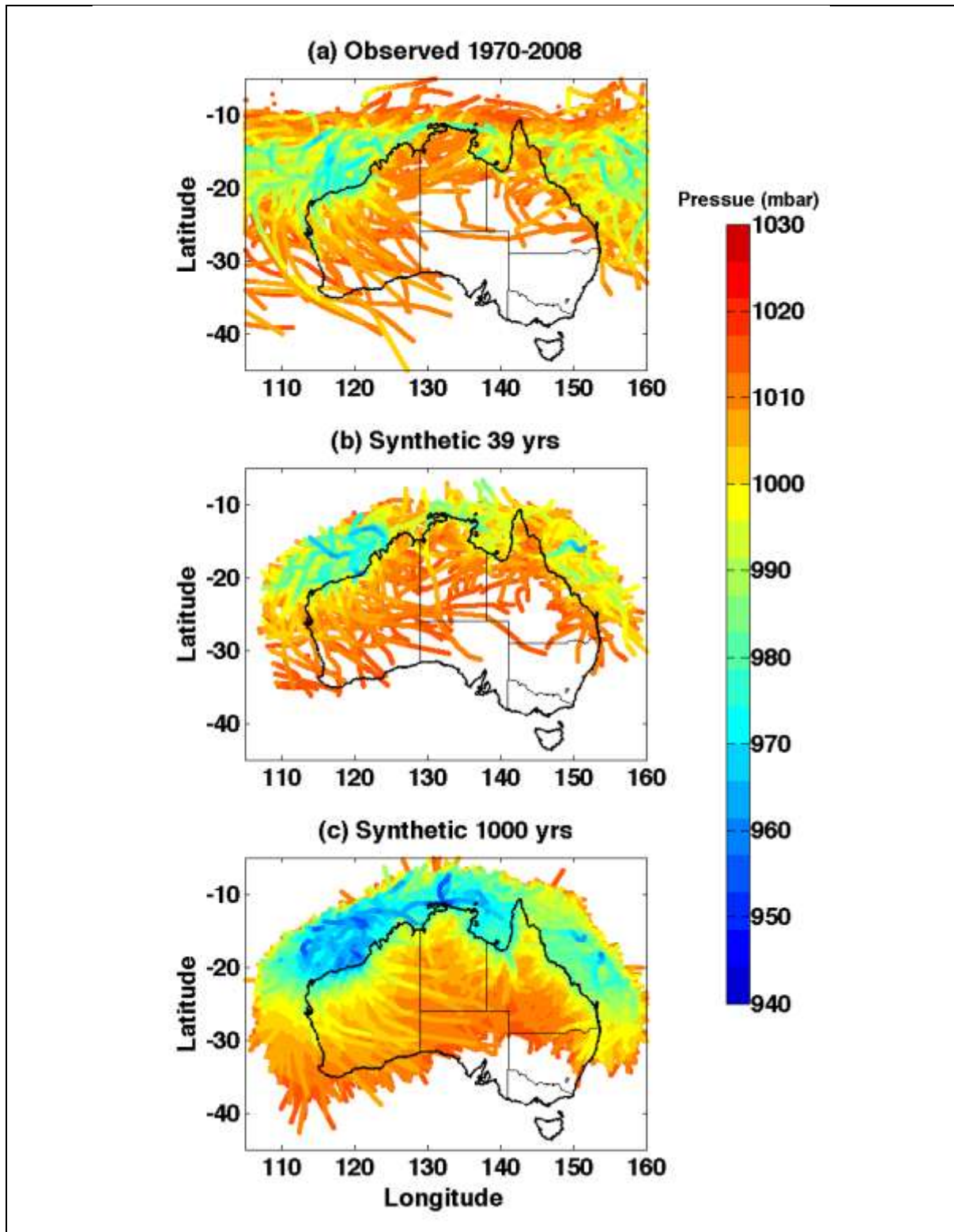


Figure 24: 1,000-year surge return levels for 2010 (relative to AHD) at the model coastal grid points estimated in (a) stage 1 and (b) stage 2 (tropical cyclones).

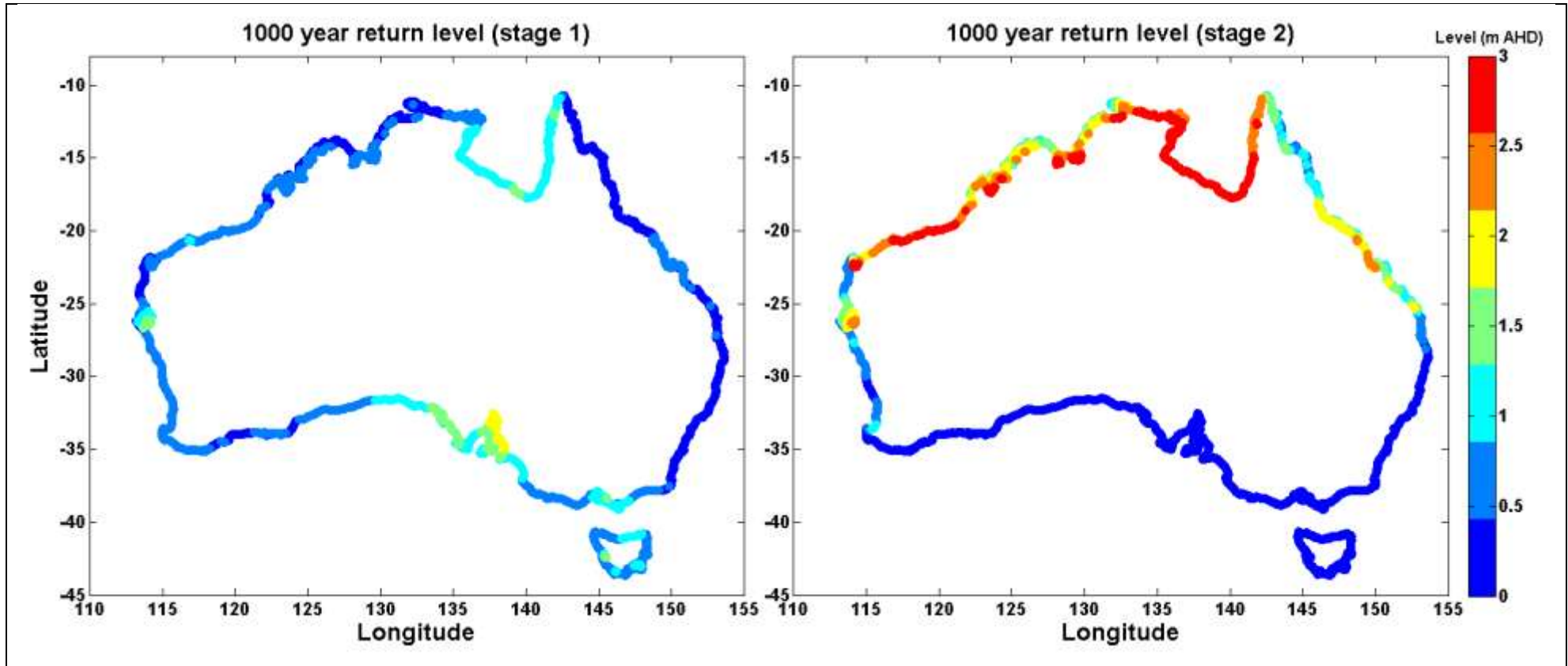


Figure 25: Return periods (years) at which the tropical cyclone generated surges are larger than the extra-tropical generated surges at the model coastal grid points.

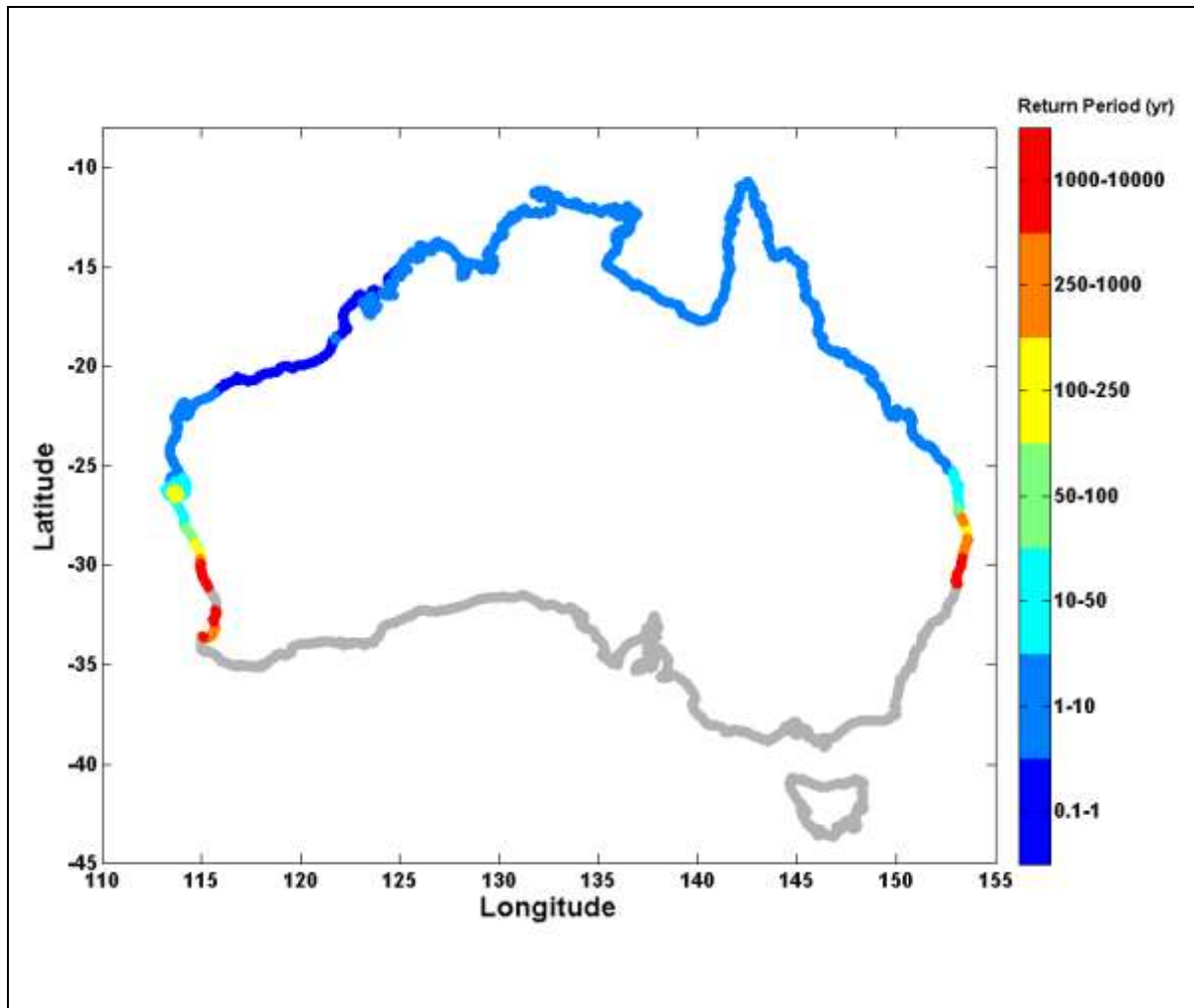


Figure 26: 1,000-year total water return levels for 2010 (relative to AHD) at the model coastal grid points estimated in (a) stage 1 and (b) stage 2 (i.e. tropical cyclones).

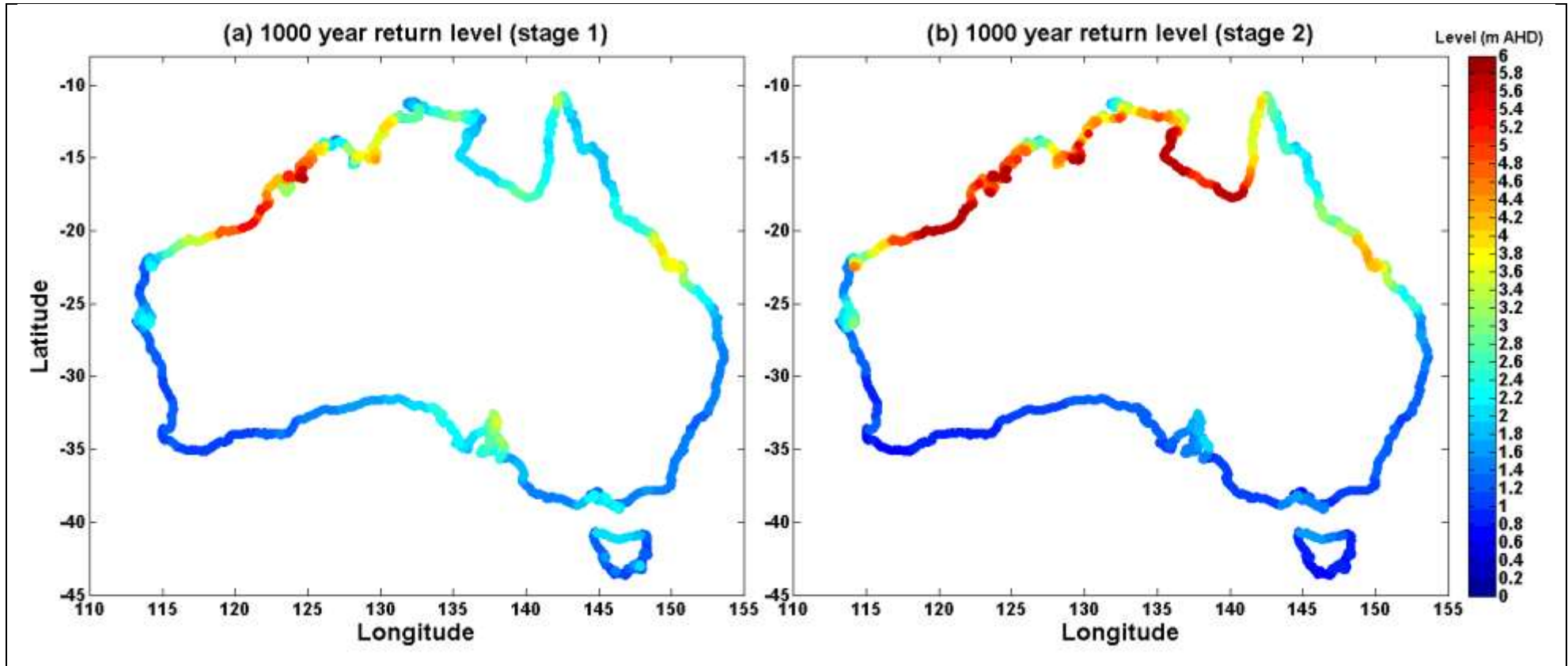


Figure 27: Comparison of the return period curves for 2010 (relative to AHD) for stage 1 (blue) and stage 2 (red) at the 30 validation sites.

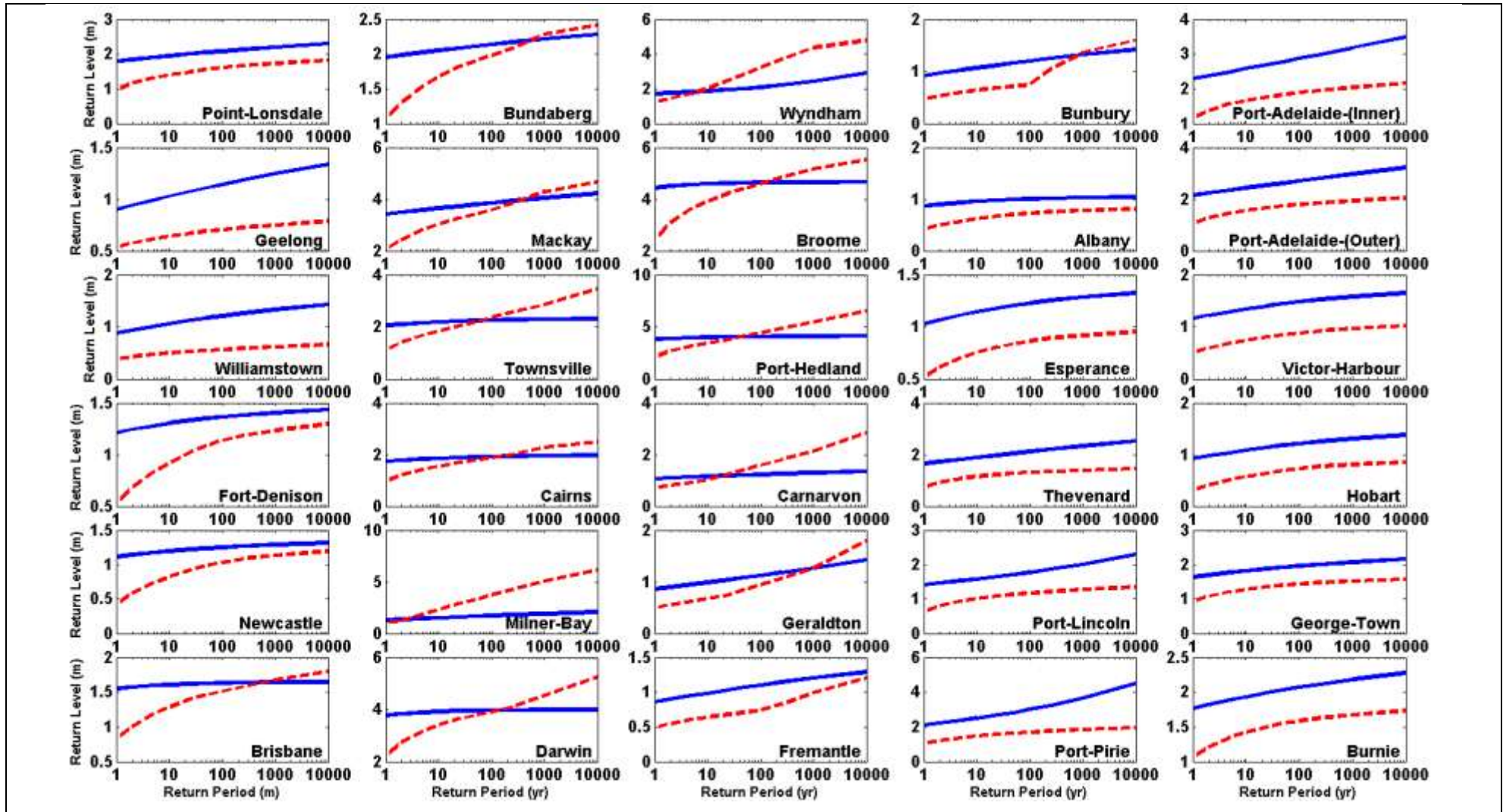


Figure 28: Return periods (years) at which the tropical cyclone generated total water levels are larger than the extra-tropical generated total water levels at the model coastal grid points.

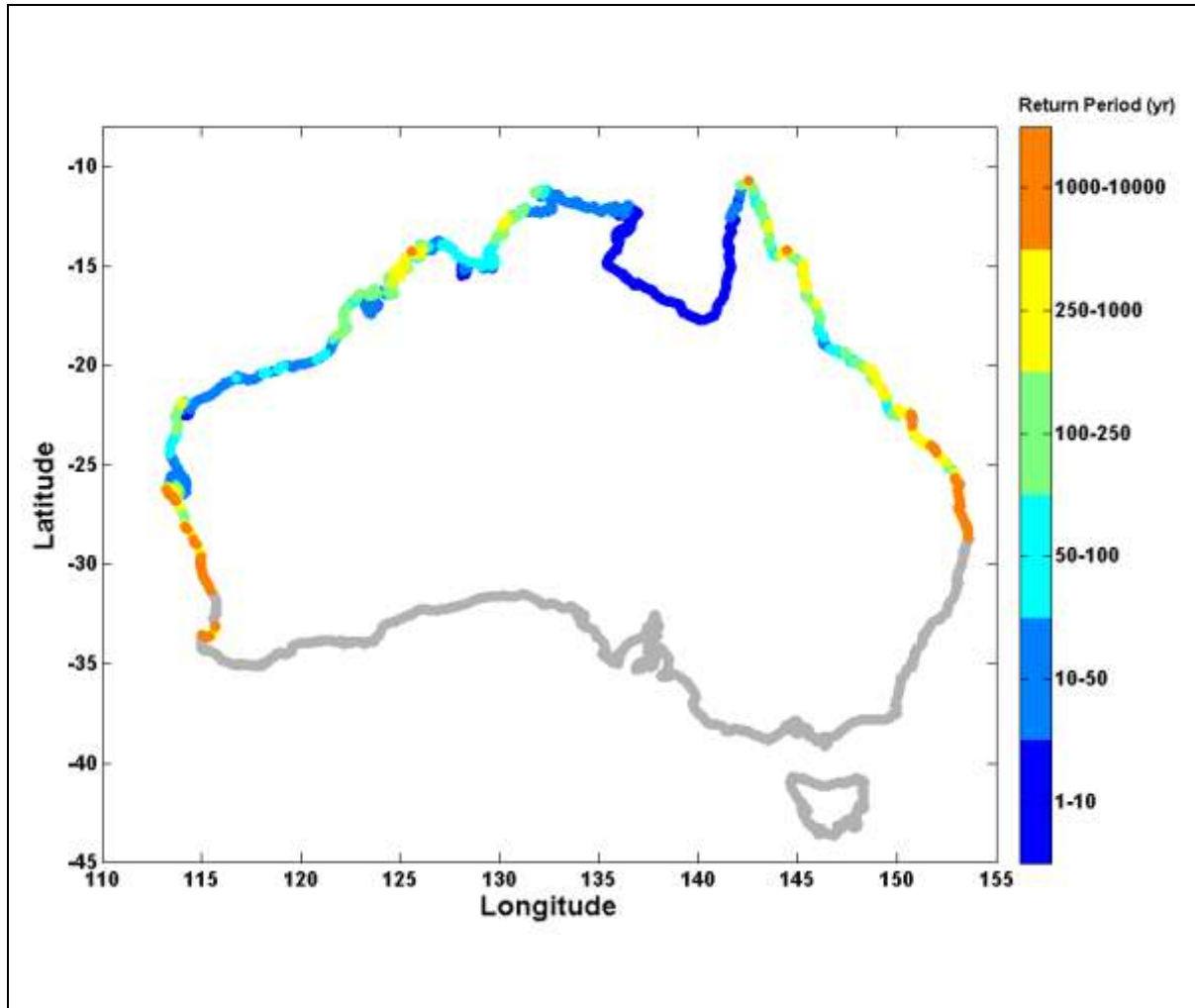
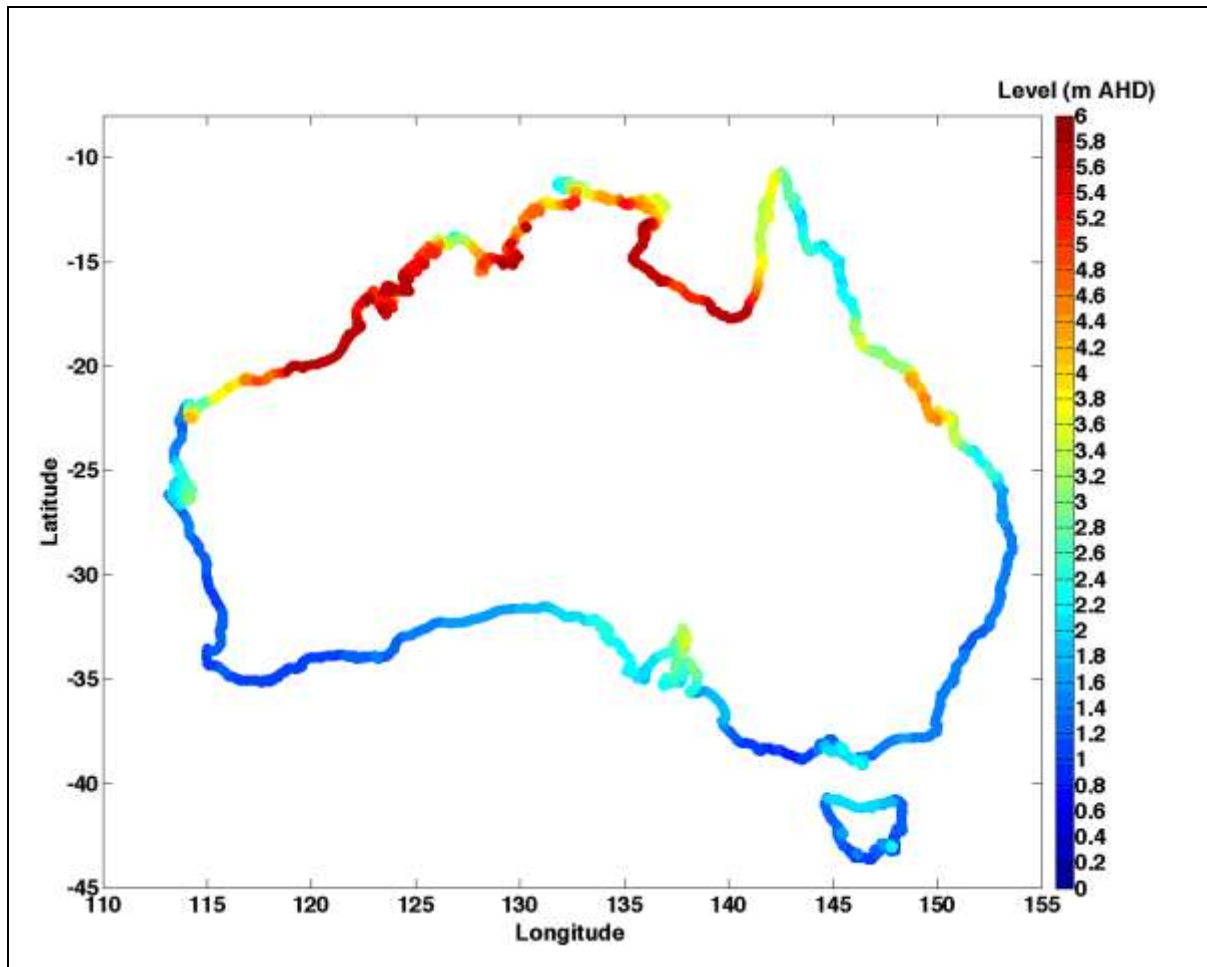


Figure 29: Combined (from stages 1 and stage 2) 1,000-year total water return levels for 2010 (relative to m AHD) at the model coastal grid points.





ANTARCTIC CLIMATE
& ECOSYSTEMS CRC

www.acecrc.org.au